Lightweight Solid Decks for Movable Bridges – Phase II

Final Report

FDOT Contract BDV29-977-11

Amir Mirmiran and Sahar Ghasemi

Department of Civil and Environmental Engineering
Florida International University
Miami, Florida

Kevin Mackie, Yulin Xiao and Munaf Al-Ramahee

Department of Civil, Environmental, and Construction Engineering
University of Central Florida
Orlando, Florida

Submitted to:

Mr. William Potter
Project Manager
Florida Department of Transportation, Research Center
2007 E. Paul Dirac Drive, Tallahassee, FL 32310

January 2016

DISCLAIMER

The opinions, findings, and conclusions expressed in this publication are those of the authors alone, and not necessarily those of the State of Florida Department of Transportation.

APPROXIMATE CONVERSIONS TO SI UNITS

SYMBOL	WHEN YOU KNOW	MULTIPLY BY	TO FIND	SYMBOL
LENGTH				
in	inches	25.4	millimeters	mm
ft	feet	0.305	meters	m
yd	yards	0.914	meters	m
mi	miles	1.61	kilometers	km

SYMBOL	WHEN YOU KNOW	MULTIPLY BY	TO FIND	SYMBOL
AREA				
in^2	square inches	645.2	square millimeters	mm^2
ft^2	square feet	0.093	square meters	m^2
yd^2	square yard	0.836	square meters	m^2
ac	acres	0.405	hectares	ha
mi^2	square miles	2.59	square kilometers	km^2

SYMBOL	WHEN YOU KNOW	MULTIPLY BY	TO FIND	SYMBOL
VOLUME				
fl oz	fluid ounces	29.57	milliliters	mL
gal	gallons	3.785	liters	L
ft^3	cubic feet	0.028	cubic meters	m^3
yd^3	cubic yards	0.765	cubic meters	m^3
NOTE: volumes greater than 1000 L shall be shown in m^3				

SYMBOL	WHEN YOU KNOW	MULTIPLY BY	TO FIND	SYMBOL
MASS				
oz	ounces	28.35	grams	g
lb	pounds	0.454	kilograms	kg
T	short tons (2000 lb)	0.907	mega grams (or "metric ton")	Mg (or "t")

SYMBOL	WHEN YOU KNOW	MULTIPLY BY	TO FIND	SYMBOL
TEMPERATURE (exact degrees)				
ºF	Fahrenheit	5 (F-32)/9 or (F-32)/1.8	Celsius	ºC
SYMBOL	**WHEN YOU KNOW**	**MULTIPLY BY**	**TO FIND**	**SYMBOL**
ILLUMINATION				
fc	foot-candles	10.76	lux	lx
fl	foot-Lamberts	3.426	candela/m^2	cd/m^2

SYMBOL	WHEN YOU KNOW	MULTIPLY BY	TO FIND	SYMBOL
FORCE and PRESSURE or STRESS				
lbf	pound force	4.45	newtons	N
kipf	kip force	4448.22	newtons	N
lbf/in^2	poundforce per square inch	6.89	kilopascals	kPa
$kipf/ft^2$	kip force per square foot	47.88	kilopascals	kPa
ksi	kip force per square inch	6,894.76	kilopascals	kPa

APPROXIMATE CONVERSIONS TO IMPERIAL UNITS

SYMBOL	WHEN YOU KNOW	MULTIPLY BY	TO FIND	SYMBOL
LENGTH				
mm	millimeters	0.039	inches	in
m	meters	3.28	feet	ft
m	meters	1.09	yards	yd
km	kilometers	0.621	miles	mi

SYMBOL	WHEN YOU KNOW	MULTIPLY BY	TO FIND	SYMBOL
AREA				
mm^2	square millimeters	0.0016	square inches	in^2
m^2	square meters	10.764	square feet	ft^2
m^2	square meters	1.195	square yards	yd^2
ha	hectares	2.47	acres	ac
km^2	square kilometers	0.386	square miles	mi^2

SYMBOL	WHEN YOU KNOW	MULTIPLY BY	TO FIND	SYMBOL
VOLUME				
mL	milliliters	0.034	fluid ounces	fl oz
L	liters	0.264	gallons	gal
m^3	cubic meters	35.314	cubic feet	ft^3

m^3	cubic meters	1.307	cubic yards	yd^3
SYMBOL	**WHEN YOU KNOW**	**MULTIPLY BY**	**TO FIND**	**SYMBOL**

MASS				
g	grams	0.035	ounces	oz
kg	kilograms	2.202	pounds	lb
Mg (or "t")	mega grams (or "metric ton")	1.103	short tons (2000 lb)	T
SYMBOL	**WHEN YOU KNOW**	**MULTIPLY BY**	**TO FIND**	**SYMBOL**
TEMPERATURE (exact degrees)				
^oC	Celsius	1.8C+32	Fahrenheit	^oF

SYMBOL	**WHEN YOU KNOW**	**MULTIPLY BY**	**TO FIND**	**SYMBOL**
ILLUMINATION				
lx	lux	0.0929	foot-candles	fc
cd/m^2	$candela/m^2$	0.2919	foot-Lamberts	fl

SYMBOL	**WHEN YOU KNOW**	**MULTIPLY BY**	**TO FIND**	**SYMBOL**
FORCE and PRESSURE or STRESS				
N	newtons	0.225	pound force	lbf
kPa	kilopascals	0.145	pound force per square inch	lbf/in^2

TECHNICAL REPORT DOCUMENTATION PAGE

1. Report No.	2. Government Accession No.	3. Recipient's Catalog No.
4. Title and Subtitle **Lightweight Solid Decks for Movable Bridges – Phase II**		5. Report Date January 2016 6. Performing Organization Code
7. Author(s) **Amir Mirmiran, Kevin Mackie, Sahar Ghasemi, Yulin Xiao, Munaf Al-Ramahee**		8. Performing Organization Report No.
9. Performing Organization Name and Address FIU, Department of Civil Engineering, 10555 W. Flagler Street, EC 3600, Miami, FL 33174 UCF, Department of Civil, Environmental, and Construction Engineering, 402 Engineering Building 2, Orlando, FL 32816		10. Work Unit No. (TRAIS) 11. Contract or Grant No. BDV29-977-11
12. Sponsoring Agency Name and Address The Florida Department of Transportation Research Center 2007 E. Paul Dirac Drive, Tallahassee, FL 32310		13. Type of Report and Period Covered Draft Final, September 2012-October 2015 14. Sponsoring Agency Code
15. Supplementary Notes		

16. Abstract

Movable bridges often include open grid steel deck for its light weight and ease of installation. These decks, however, suffer from poor rideability and high maintenance costs. The primary objective of this research project was to search for a new generation of lightweight solid decks that address these issues. Alternative deck systems, including ultra-high performance concrete (UHPC)-high-strength steel (HSS) deck, and UHPC-fiber reinforced polymer (FRP) deck, and UHPC-FRP hybrid system, were developed and studied in this research. The UHPC-HSS and UHPC-FRP deck system showed a great potential to serve as viable alternatives. Accordingly, this phase of the project covered all studies needed for their design and implementation. Also, suitability of a UHPC-FRP hybrid bridge deck system as an alternative to open-grid steel decks was evaluated. The study confirmed that the proposed deck with only 4-inch overall depth and a self-weight of 20.88 psf for the deck with HSS reinforcement and 18.79 psf for the deck system with CFRP reinforcement meets the strength requirements for a 4-ft. stringer spacing. Additional work is required to ensure the deck with CFRP reinforcement meets the displacement criteria. The deck is not susceptible to punching shear of its thin slab, and fails in a ductile manner. Load distribution among the ribs, whether calculated based on deflections or strains, is consistent for both types of reinforcement. In order to study the long-term behavior of the proposed decks under the effects of a moving wheel load, additional testing was carried out at the Accelerated Pavement Testing (APT) facility of the Florida Department of Transportation in Gainesville, FL. A hybrid section of UHPC and FRP was considered as another alternative in this research. Based on test results, the main failure mode was at the interface with the top UHPC plate. The hybrid system requires additional improvement.

17. Key Word	18. Distribution Statement
Movable bridge, Lightweight deck, Ultra-high performance concrete, High-strength steel, Fiber reinforced polymers.	No restriction.

19. Security Classif. (of this report)	20. Security Classif. (of this page)	21. No. of Pages	22. Price
Unclassified	Unclassified	166	

ACKNOWLEDGEMENTS

The authors would like to thank the Florida Department of Transportation (FDOT) for providing the funding for this project. Special thanks are also due to the project manager, Mr. William Potter, for his continued support and technical contributions to the project.

The authors would also like to take this opportunity and recognize Mr. Sam Fallaha, the initial project manager on this project.

Finally, the authors would like to acknowledge MMFX Technologies of Irvine, CA, and Lafarge North America for providing materials for this project and the Structural Composites Inc. of Melbourne, FL, for providing the FRP bridge deck for testing.

EXECUTIVE SUMMARY

The primary objective of this research project was to search for a new generation of lightweight solid decks that address current issues, such as poor rideability, maintenance cost, fatigue, high noise level, and bicycle safety. Alternative deck systems, including ultra-high performance concrete (UHPC)-high-strength steel (HSS) deck, UHPC-fiber reinforced polymer (FRP) deck, and UHPC-FRP hybrid system, were developed and studied in this research. The UHPC-HSS and UHPC-FRP deck system showed great potential to serve as viable alternatives. This phase of the project focused on studies needed for their design and implementation. Also, suitability of an UHPC-FRP hybrid bridge deck system as an alternative to open-grid steel decks was evaluated.

In the previous phases of this project (FDOT Contract No. BD015 RPWO #22), the UHPC-HSS deck in the form of a low-profile asymmetric waffle slab was experimentally investigated at both the component and system levels. The deck was shown to be a structurally viable alternative, yet its overall weight, including haunches and connections, exceeded the weight limits for deck replacement on some existing movable bridges. The purpose of this study was to optimize the design of the proposed UHPC-HSS deck system to meet the weight limits for existing movable bridges. The size and reinforcement of the proposed deck were modified in two phases, and eight specimens with single or multiple ribs were tested in simple or two-span configurations.

In the other part of the research, a UHPC-FRP bridge deck system was developed and studied. In this system, an ultra-lightweight low profile waffle slab of UHPC reinforced with carbon fiber reinforced polymer (CFRP) bars was investigated. A total of ten specimens at two different overall depths, with single or multiple ribs and in simple or two-span configuration, were tested in two consecutive phases in this study. The study confirmed that the proposed deck with only 4-inch overall depth and a self-weight of 20.88 psf for the deck with HSS reinforcement and 18.79 psf for the deck system with CFRP reinforcement meets the strength requirements for a 4-ft. stringer spacing. Additional work is required to ensure the deck with CFRP reinforcement meets the displacement criteria. The deck is not susceptible to punching shear of its thin slab, and fails in a ductile manner. Load distribution among the ribs, whether calculated based on deflections or strains, is consistent for both types of reinforcement. In order to study the long term behavior of the proposed decks under a moving wheel load, additional testing was carried out using the Heavy Vehicle Simulator (HVS) at the Accelerated Pavement Testing (APT) facility of the Florida Department of Transportation in Gainesville, FL. Also tested at this facility, was a full-depth FRP deck product made by Structural Composites Inc. of Melbourne, FL.

A hybrid section of UHPC and FRP was considered as another alternative in this research. The composite, or hybrid, system is infused with low viscosity resin using vacuum-assisted resin transfer molding (VARTM) to get a high quality system with better adhesion and fiber volume content than would be achieved using typical wet layup. The method is typically suitable for manufacturing of carbon and glass fiber composites, and it is commonly used by professional manufacturers for the production of any fiber body panels such as for boats and automobiles. In the first phase of the tests, six hybrid specimens were tested. Another six hybrid specimens with two different lengths were made and tested. According to the test results, the main failure mode was the interface failure and delamination of the top UHPC plate. It started within the unsupported length and then propagates to the other locations until cracking the top UHPC plate.

TABLE OF CONTENTS

LIST OF TABLES

LIST OF FIGURES

Chapter-1

Introduction

1.1. Problem Statement

Currently, most of the movable bridges use open grid steel decks (Figure 1.1). There are major concerns with these types of decks, such as poor rideability, susceptibility to fatigue, and high noise levels and maintenance cost.

Besides, traditional deck systems and construction methods usually lead to prolonged periods of traffic delays, limiting options for transportation agencies to replace or widen a bridge, especially in urban areas. A new generation of lightweight decks with solid riding surface are sought to address these issues, while staying within the weight limit of 21 lb/ft^2 for a movable bridge with a stringer spacing of 4 to 6 ft., which is the prevailing configuration of the movable bridges with steel open grid decks.

Accordingly, three alternative deck systems were developed and studied in the first phase of this research project (Mirmiran et al., 2009). The three deck systems included SAPA aluminum deck by SAPA Group of Sweden, ultra-high performance concrete (UHPC)-high-strength steel (HSS) deck, and UHPC-fiber-reinforced polymer (FRP) tube deck.

Although detailed experimental and analytical evaluation of the UHPC-HSS deck system indicated its viability to serve as an alternative to conventional open steel grid decks, the deck weight exceeded the weight limitation of 21 lb/ft^2. On the other hand, more studies were deemed necessary to improve the design of SAPA aluminum deck and UHPC-FRP tube deck.

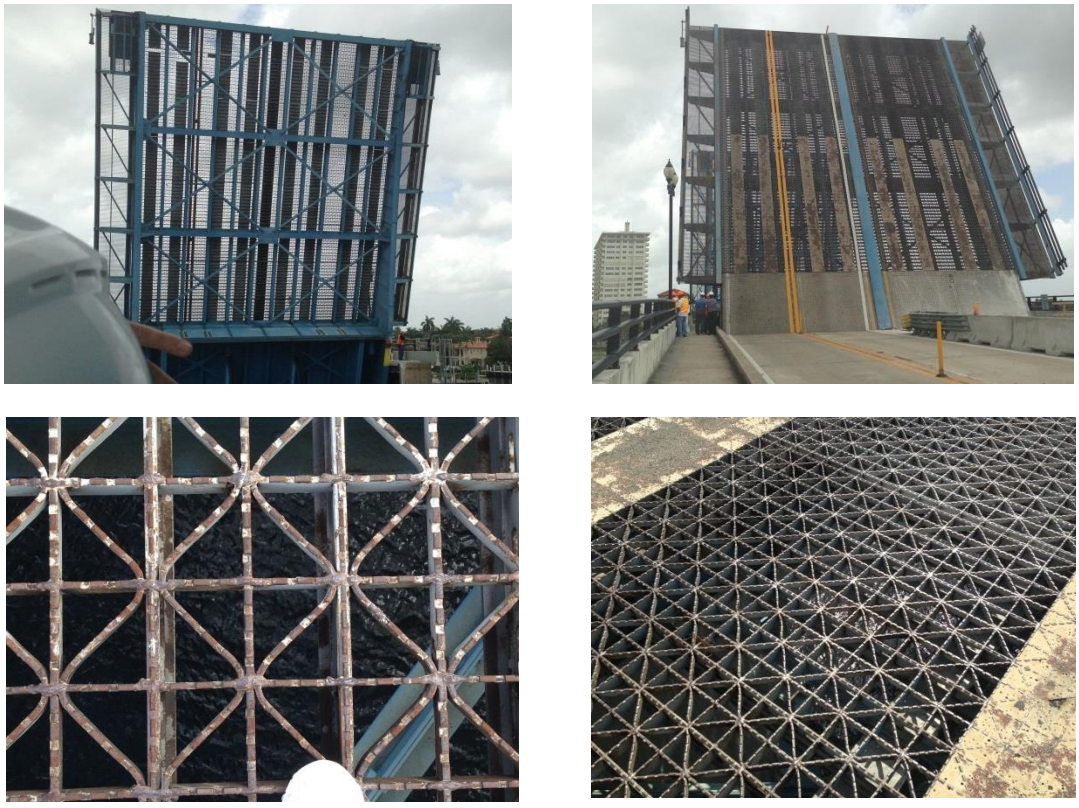

Figure 1.1 Open Steel Grid Deck (Las Olas Bridge, Fort Lauderdale, FL)

1.2. Research Objectives and Approach

The primary objective of this project was to develop lightweight deck system alternatives for movable bridges. The three different deck systems that were developed and studied are:

1- UHPC-HSS Deck System:

The goal was to optimize the design of proposed UHPC-HSS deck system, which was studied in the first phase of the project (Mirmiran et al., 2009), to meet the weight limits for existing movable bridges. The size and reinforcement of the proposed deck were modified in two phases, and a number of specimens with single or multiple ribs were tested in simple or two-span configurations.

2- UHPC-FRP Deck System:

Fiber reinforced polymer (FRP) is another advanced material with high strength-to-weight ratio and excellent corrosion resistance. A novel deck system was developed as an ultra-lightweight low profile waffle slab of UHPC reinforced with carbon fiber reinforced polymer (CFRP) bars. A number of specimens at two different overall depths, with single

or multiple ribs, and in simple or two-span configurations were tested in two consecutive phases in this study.

3- UHPC-FRP Hybrid Deck System:

A UHPC-FRP hybrid system is potentially a viable alternative to regular decks due to its extremely light weight. The proposed deck system includes UHPC as the upper layer for compression resistance, CFRP distributed on the bottom layer for tension resistance, and GFRP as shear reinforcement is optimal. The composite, or hybrid, system is infused with low viscosity resin using VARTM to get a high quality system with better adhesion and fiber volume content than would be achieved using typical wet layup.

1.3. Report Organization

This report is comprised of six chapters. This first chapter serves as an introduction, mainly describing the problem statement, research objectives, and research approach. Chapter 2 covers the experimental work related to UHPC-HSS deck, including component-level and system-level tests along with finite element modeling. Chapter 3 focuses on the experimental work related to UHPC-CFRP deck as well as ancillary tests for developing and enhancing anchorage system as well as finite element modeling. The experimental work related to UHPC-FRP Hybrid deck is presented in Chapter 4. The accelerated pavement testing of the FRP hybrid deck made by Structural Composites Inc. is provided in Chapter 5. Chapter 6 includes summary and conclusions for the project, as well as recommendations for future research.

Chapter-2

A Super Lightweight UHPC-HSS Deck Panel for Movable Bridges

2.1. Introduction

Movable bridges often include open grid steel deck for its light weight and ease of installation. However, inherent problems with these decks include poor rideability, susceptibility to fatigue, and high noise levels and maintenance cost (Mirmiran et al., 2009 and 2012). A new generation of lightweight decks with solid riding surface are sought to address these issues, while staying within the weight limit of 21 psf for a movable bridge with a stringer spacing of 4 ft. (Saleem, 2011). With applications well beyond movable bridges, such lightweight decks are expected to include advanced construction materials, e.g., ultra-high performance concrete (UHPC) and high-strength steel (HSS).

UHPC, first developed in France in the 1990's (Keierleber et. al., 2007), consists of high-strength cementitious materials, steel fibers, ground quartz, and super plasticizer (Habel et al., 2006, Graybeal, 2007). UHPC has less permeability, creep and shrinkage as compared to conventional concrete (Graybeal, 2006), while it also features compressive strengths above 21 ksi, elastic moduli over 6,500 ksi, usable tensile strengths in excess of 0.7 ksi, and high durability and damage tolerance (Graybeal, 2005, Ahlborn et al., 2008). UHPC is also shown as a suitable pavement overlay (Graybeal and Hartmann, 2003), and has recently been applied in several bridges in the U.S., Canada, Europe and Asia (Blais and Couture, 1999, Hajar et al., 2004, and Graybeal, 2011).

HSS rebars offer another advanced option in bridge construction (Rizkalla et al., 2006), with almost 25% higher yield strength, six times more corrosion resistance and two times slower corrosion rate than conventional steel. These exceptional properties can lead to less reinforcement, longer service life and lower life-cycle costs (Kahl, 2007).

Saleem et al. (Saleem, 2011 and 2012) developed a novel bridge deck system, utilizing UHPC in the form of a low-profile solid waffle slab reinforced with HSS rebars, and an asymmetric arrangement of primary and secondary ribs, respectively perpendicular and parallel to traffic. The feasibility of the proposed system was shown through a number of experiments with single and multiple ribs, and in simple or two-span configurations. Although the weight of each panel was reasonably low as 32.37 psf, the total weight of the deck system including haunches and

accessories turned out to exceed the weight limits for existing movable bridges. Therefore, the main objective of this study was to improve the proposed UHPC-HSS deck system by reducing its weight below 21 psf, while still meeting the strength and ductility demands.

2.2. Experimental Work

2.2.1. Test Matrix

Table 1 presents the test matrix for two groups of UHPC-HSS deck specimens tested in two consecutive phases. The specimen names in the table include number of primary ribs (1 or 4), number of spans (1 or 2), overall depth (5, 4½, or 4 in.), and the duplicate number in the case of identical specimens. In Phase 1, both section geometry and reinforcement were modified from those tested by Saleem (2011), which are also shown as Phase 0 for comparison. The overall section depth, slab thickness, and the width of the primary rib were each reduced by ½ in., while the spacing of the primary ribs was increased by 3 in. The reinforcement was also reduced from No.4 to No.3 in the slab and from No.7 to No.5 in the rib. Two identical 4½ in. deep single-rib simple-span specimens were tested in this phase (Figure 2.1).

The specimens in Phase 1 weighed 33% less than those of Saleem (2011). The weight was calculated with 4½ in. wide solid block to support the deck on each stringer. Test results, as will be presented later, still showed excess capacity over demand. Hence, the section was further optimized in Phase 2, reducing its depth by another ½ in. (Figure 2.1) and lowering its weight to only 20.26 psf. In this phase, one single-rib simple-span specimen was tested, along with a single-rib two-span specimen and a multi-rib simple-span specimen (Figures 2.1 and 2.2). The two-span and multi-rib specimens were utilized to investigate the continuity behavior of the deck, its punching shear behavior, and load distribution among the ribs.

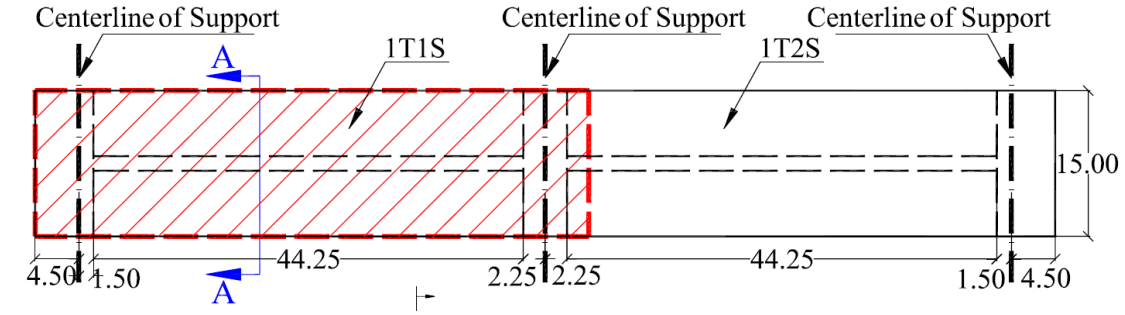

Plan View

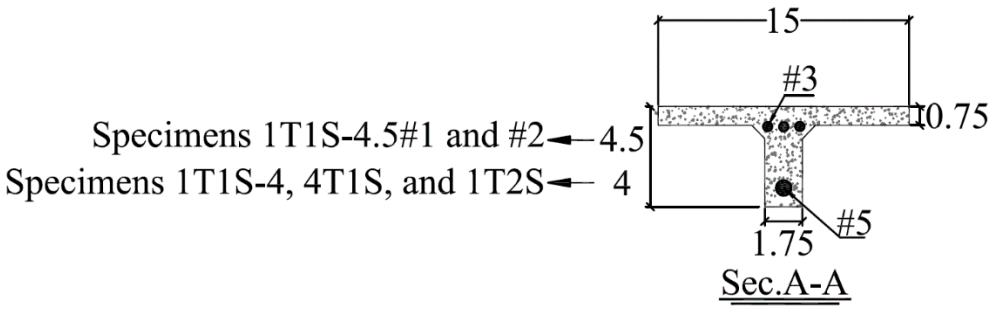

All dimensions are in inches.

Figure 2.1 Schematics of Single-Rib, Simple-Span, or Two-Span Specimens

Table 2.1 Test Matrix

Phase	Specimen Name	Overall Depth (in.)	Rib Spacing (in.)	Slab Thickness (in.)	Unit Weight (psf)	28-Day UHPC Compressive Strength (ksi)	Flexural Reinforcement	
							Slab	Primary Rib
0*	1T1S-5#1	5	12	1¼	32.37	18	No. 4	No. 7
	1T1S-5#2					27		
	4T1S-5					26		
	1T2S-5					22		
1	1T1S-4½#1	4½	15	¾	21.72	24	No. 3	No. 5
	1T1S-4½#2					24		
2	1T1S-4	4	15	¾	20.26	27		
	4T1S					27		
	1T2S					25		

* Taken from Saleem (2011).

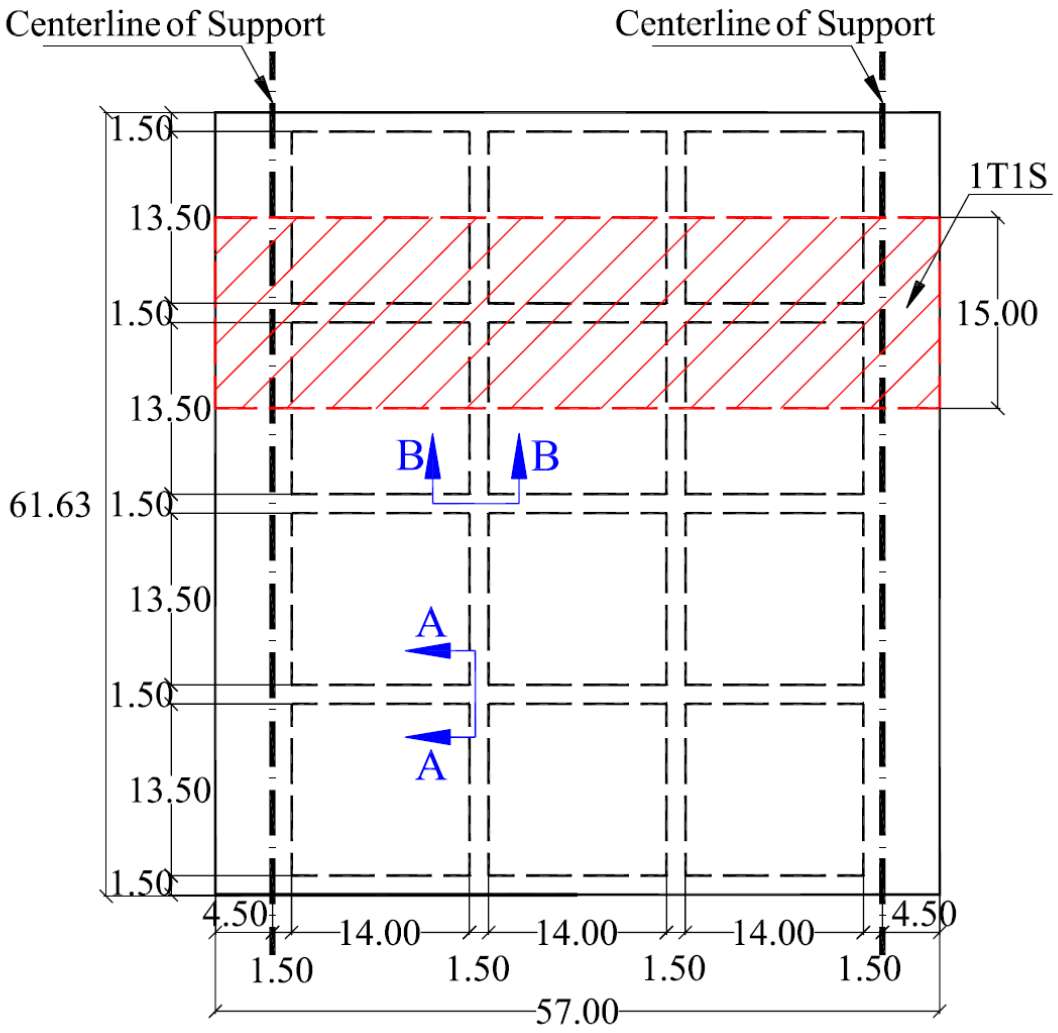

Plan View

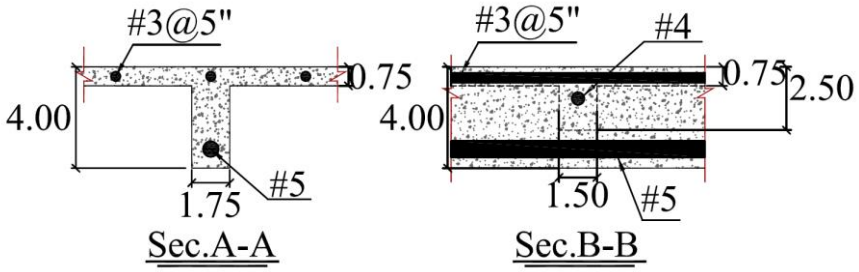

*****All measurements are in inch.

Figure 2.2 Schematics of Multi-Rib Simple-Span Specimen

2.2.2. Specimen Preparation and Material Properties

Formwork was made using Styrofoam and timber (Figure 2.3). HSS rebars made by HSS Technologies of Irvine, CA, were used as primary reinforcement with yield strength of 100 ksi, as reported by the manufacturer. Rebars in primary ribs were all anchored using 180^{o} hook at both ends. Transverse ribs included a No. 4 rebar. Only the multi-rib specimen featured transverse ribs to help with load distribution among its ribs, and to assess the punching shear behavior of the deck.

a)

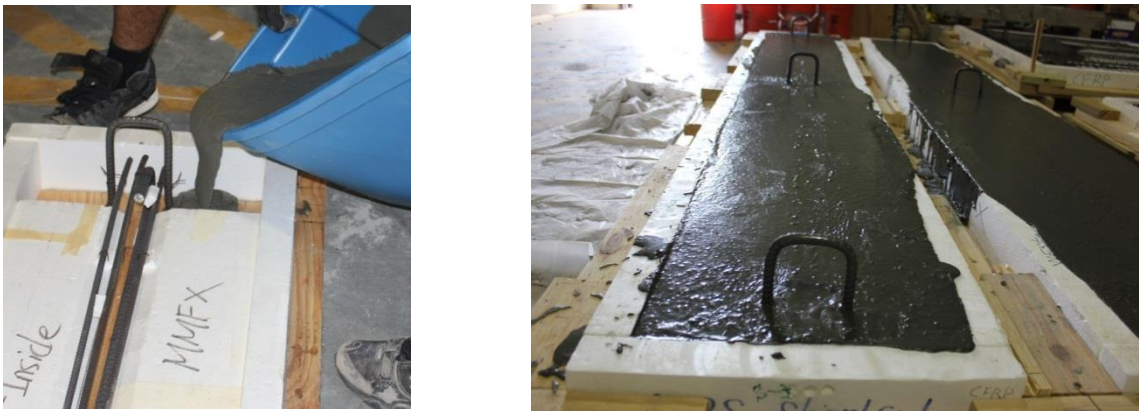

b)

Figure 2.3 Specimen Preparation: (a) Formwork, and (b) Casting

Ductal®, a commercially available UHPC product, made by Lafarge North America, was used in this study. It is composed of premix powder (cement, silica fume, ground quartz and sand), water, superplasticizer, and 2% metallic fibers by volume. The fibers were ½ in. long with a tensile strength of 406 ksi. Six different batches of UHPC were mixed for casting the specimens (Figure 2.3). All specimens were air cured in the laboratory for a period of 28 days. Two

companion 4 in. × 8 in. cylinders were used to measure the average 28-day compressive strength of each batch, as reported in Table 2.1.

2.2.3. Test Setup and Instrumentation

A 10 in. × 20 in. steel plate was used to simulate the prescribed dual tire wheel load of an HS20 truck. The simple-span specimens were subjected to a single load at mid-span (Figures 2.4a and 2.6a), whereas the two-span specimen was under two equal loads applied simultaneously in the middle of both spans (Figure 2.9a). At the conclusion of its flexure test, the multi-rib specimen was further tested using the same load patch to determine the punching shear capacity of its thin slab (Figure 2.8a). Several strain gauges were used to monitor responses of HSS rebars and UHPC at critical points. String pots were used to measure deflections at strategic locations. Loading was applied using a 230-kip capacity hydraulic actuator, at an average rate of 0.03 in./min. The data were recorded at a frequency of 1 Hz, and tests were stopped at 30% load drop, unless preceded by a clear sign of failure due to significant deflection, which may make the specimens unbalanced.

2.2.4. Test Results and Discussion

Table 2.2 presents a summary of test results. Also shown in the table are the required live load demands calculated using the equivalent strip method and the deck slab design table for each group of specimens based on the specimen width, load factors, multiple presence factors, dynamic load allowance, and the loading configuration. The table shows the over-capacity for each specimen as well as over-capacity per unit weight of the deck panel. The optimized specimens have comparable over-capacity per unit weight as those of Saleem (2011), demonstrating the effectiveness of the new design. The table also shows measured deflections for each specimen at the levels of service and ultimate loads. The ratio of these two deflection levels indirectly suggests a reasonable ductility for each deck specimen.

Figure 2.4 shows the test setup, failure mode, and load-deflection responses of single-rib simple-span specimens. Failure was initiated by minor web shear cracks near supports. Minor flexural cracks were also present near mid-span, but did not seem to have an impact on the failure. As the load increased, shear cracks propagated towards the slab near the loading plate. These cracks gradually widened, leading to eventual failure and a significant load drop, much the same as those observed by Saleem (2011). Figure 2.4c shows the load-deflection responses of the three specimens tested in this study, as well as the two deeper specimens tested by Saleem (2011). Deflections are averages of three recorded values (D1-D3) at mid-span, as shown in the figure inset. The ultimate and service demand loads are also shown, as described earlier. Given its smaller section and reduced reinforcement, while the capacity of Specimen 1T1S-4 is about half of those tested by Saleem (2011), it is still twice its expected demand.

Table 2.2 Summary of the Test

Phase	Specimen Name & Graph Label	Service Load Deflection (in.)	Ultimate Deflection (in.)	Ultimate Load (kip)	Demand Load (kip)	Capacity/ Demand	Capacity/ Demand per Unit Weight
0*	1T1S-5#1	0.06	0.98	40.02	8.21	4.9	0.15
	1T1S-5#2	0.1	0.98	46.99		5.7	0.18
	4T1S-5	0.19	0.79	84.98	34.17	2.5	0.08
	1T2S-5	0.9	1.26	55.08	12.52	4.4	0.14
1	1T1S-4½#1	0.1	0.83	27.65	10.25	2.7	0.12
	1T1S-4½#2	0.14	0.87	24.73		2.4	0.11
2	1T1S-4	0.15	0.91	22.71		2.2	0.11
	4T1S-4	0.18	0.87	51.48	42.04	1.2	0.06
	1T2S-4	0.07	0.87	44.96	15.65	2.9	0.14

* Taken from Saleem (2011)

(a)

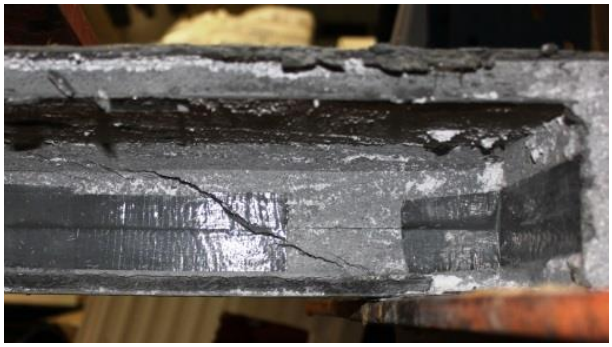

(b)

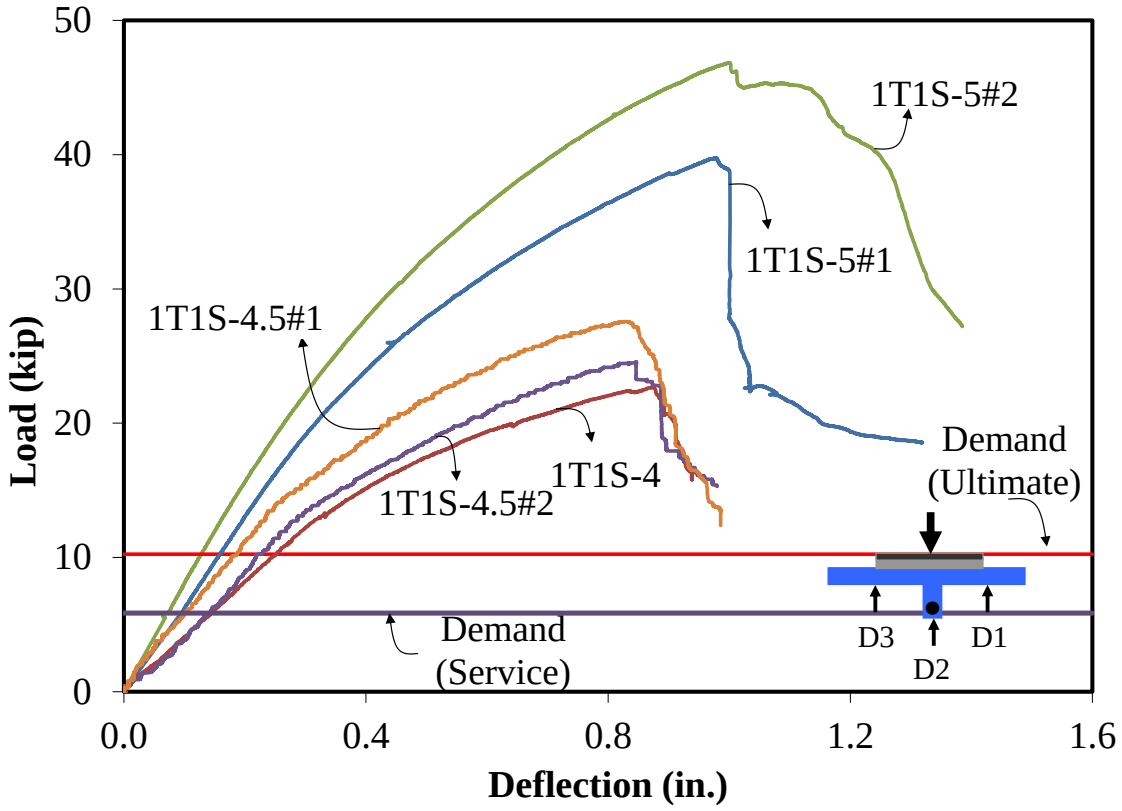

(c)

Figure 2.4 Flexure Tests of Specimens 1T1S: (a) Test Setup, (b) Failure Mode, and (c) Load-Deflection Responses (Note: Curves 1T1S-5#1 and #2 from Saleem, 2011)

Figure 2.5 shows load-strain responses for Specimens 1T1S-4.5#1 and 1T1S-4, based on strain gauges attached at the mid-span to the rebar in the primary rib. Although yielding of rebar in both specimens occurs at a level much higher than the service load demand, it may generally be construed as a good indication of a fairly ductile behavior. It should be noted that in the face of dominant shear cracks, Xia et al. (2011) have demonstrated that the ductile behavior of these decks is more representative of the fiber pull-out mechanism in UHPC and the dowel action of the HSS bars rather than traditional yielding of steel reinforcement.

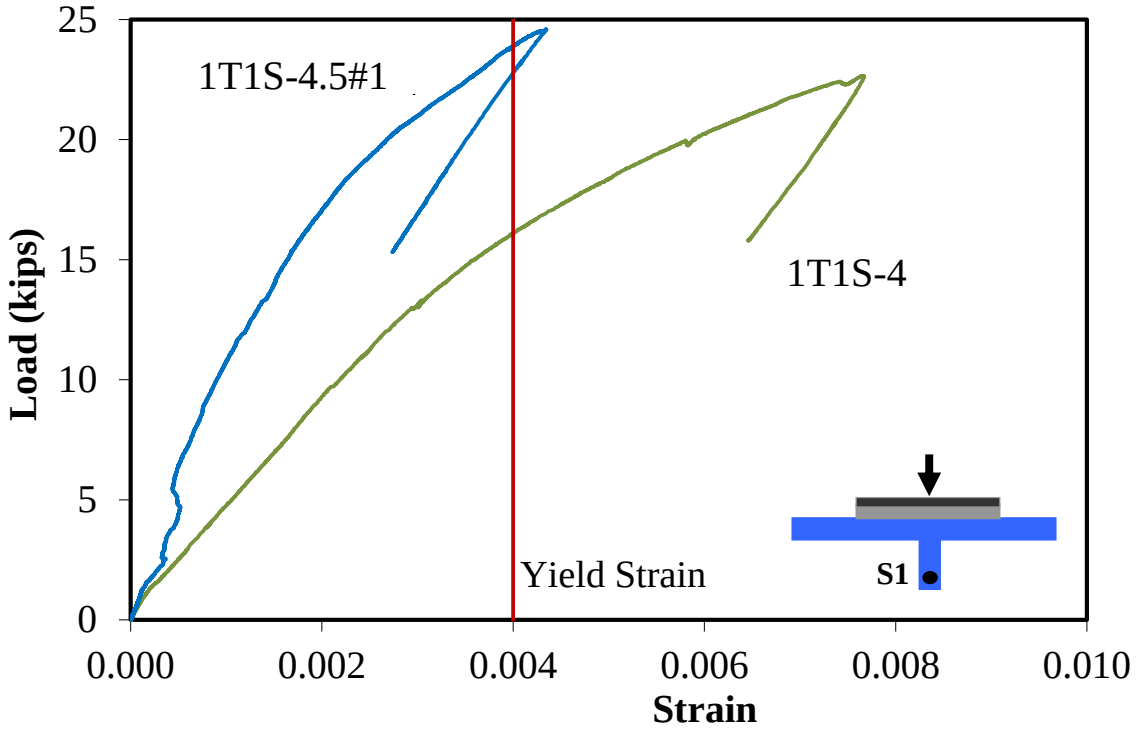

Figure 2.5 Load-Strain Response of Rebars in Specimens 1T1S

Several strain gauges were used to monitor the strain in UHPC. Results are presented in Appendix A.

2.2.4.1 Panel Action

Figure 2.6 shows the test setup, failure mode and load-deflection responses of the multi-rib simple-span specimen. Deflections are three recorded values (D1-D3) at mid-span, as shown in the figure inset. The failure mode was generally similar to that of single-rib simple-span specimens, in that it initiated with diagonal shear cracks near the supports, albeit mainly in the interior ribs. With the increase of the load, shear cracks grew both in width and length, especially in the center rib, leading to the failure accompanied by a considerable load drop.

As shown in Figure 2.6c, Specimen 4T1S showed an almost linear response up to about twice the service load deflection, while exhibiting a plastic behavior thereafter until failure. In comparison to the single-rib specimens (Figure 2.4c), the presence of multiple ribs helped increase the ductility of the proposed deck panel significantly through a considerable plastic deformation. This confirms earlier findings that failure of the proposed UHPC-HSS deck panel system is clearly ductile, despite the presence of dominant shear cracks.

For comparison, Figure 2.6c also includes the load-deflection response curves for the deeper specimen tested by Saleem (2011). Although specimen 4T1S-4 has a 20% shallower section and 28% less reinforcement, its capacity is about 60% of Specimen 4T1S-5, it still exceeds its expected demand by at least 22%.

Load distribution among the ribs may be calculated based on mid-span deflections of each rib or mid-span strains in HSS bar in each rib. Using either approach, the load distribution among the ribs is found as 33% for the center rib and 22% and 11% for the next two ribs. These factors are quite similar to those reported by Saleem et al. (2011).

(a)

(b)

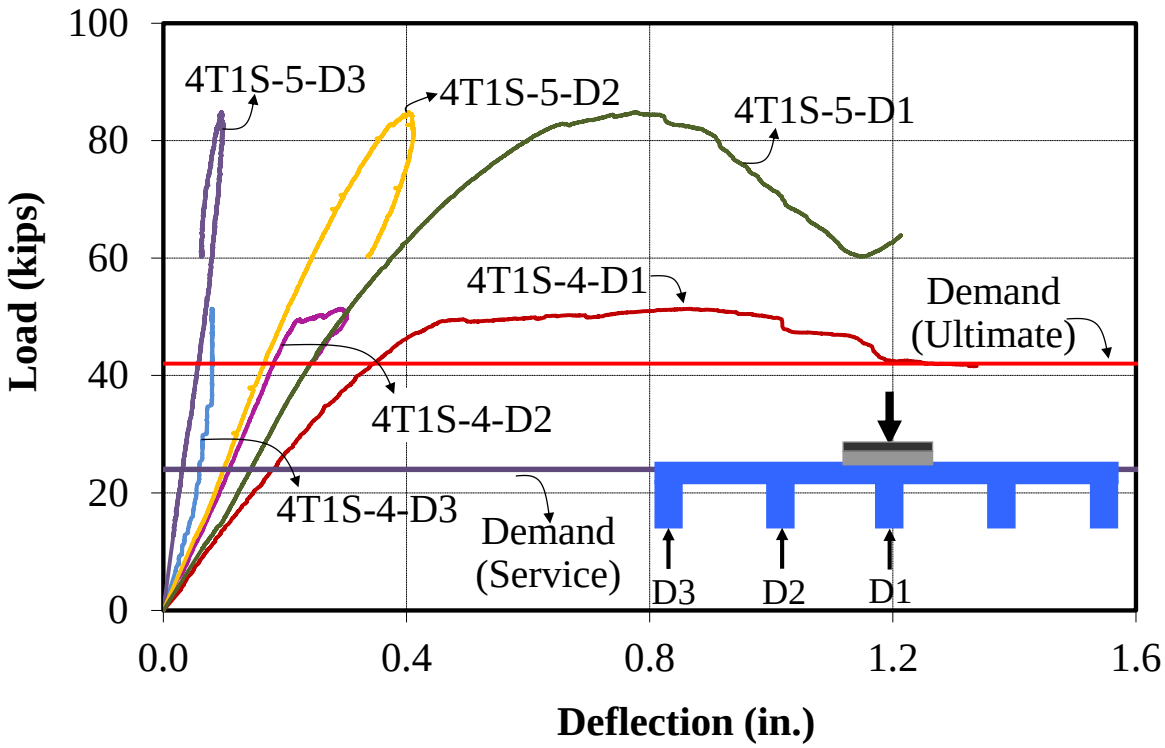

(c)

Figure 2.6 Tests of Specimens 4T1S: (a) Test Setup, (b) Failure Mode, and (c) Load-Deflection Responses (Note: Curves 4T1S-5-D1, D2, and D3 from Saleem, 2011)

Figure 2.7 shows load-strain responses for Specimen 4T1S-4 based on the strain gauges attached to the rebars in each of the primary ribs at the mid-span. The strain gauge in the exterior rib was damaged before reaching the ultimate load. Of the other four, the largest strain occurred in the rebar of the center rib, although it was still below the yield limit. As discussed earlier, one should note the sizeable displacement-based ductility of the deck system (Figure 2.6a); despite the apparent shear failure and the relatively low strain levels in the flexural reinforcement.

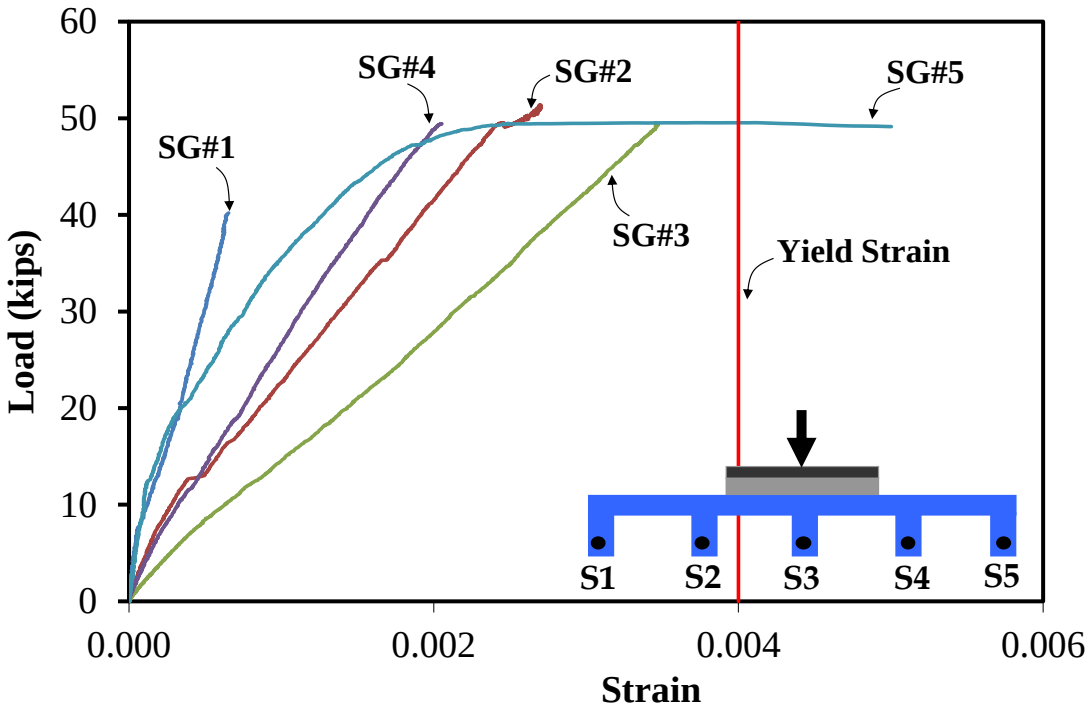

Figure 2.7 Load-Strain Response of Rebars in Specimen 4T1S-4

2.2.4.2 Punching Shear Behavior

Figure 2.8a shows the reserved punching shear test carried out on an exterior panel of Specimen 4T1S-4 at the conclusion of its flexural test described above. The load was applied using the same loading plate on the slab between the first two ribs. Figure 2.8b shows the failure governed by major cracks in the primary ribs adjacent to the loading patch. No sign of punching shear, however, was observed on the top of the slab around the loading plate. Figure 2.8c shows the load-deflection responses. As shown in the figure inset, the deflections (D1-D3) were recorded at mid-span, under the loading patch and the two adjacent ribs. A sizeable deflection of 0.6 in. was measured in the middle of the panel right under the loading patch at the ultimate load of 42.49 kips. The ultimate load was about 17% lower than that observed in the first flexure test of the specimen. Clearly, the asymmetric loading did not allow full contribution of other ribs. The test was stopped after the load dropped to 37.32 kips due to excessive damage in the exterior rib.

Harris and Roberts-Wollmann (2005) proposed a modification to ACI equation for concrete breakout strength to predict the punching shear capacity of thin UHPC slabs

$$V_c = 0.38\, f_{ten} \frac{[(3h + a) \times (3h + b)] - (a \times b)}{\sqrt{h}} \qquad (2.1)$$

where f_{ten} = tensile strength of UHPC, h = thickness of the UHPC slab, and a and b = dimensions of the loading plate. Using a tensile strength of 1.1 ksi for a 10 in. × 20 in. loading plate, the punching shear capacity of the ¾ in. slab is calculated as 6.97 kips, which is substantially lower than its experimentally measured capacity of 42.49 kips. This explains why no sign of punching shear was observed in the slab, clearly because the spacing of the primary ribs prevents a punching shear failure of the slab, and instead promotes one-way shear failure of primary ribs.

(a) (b)

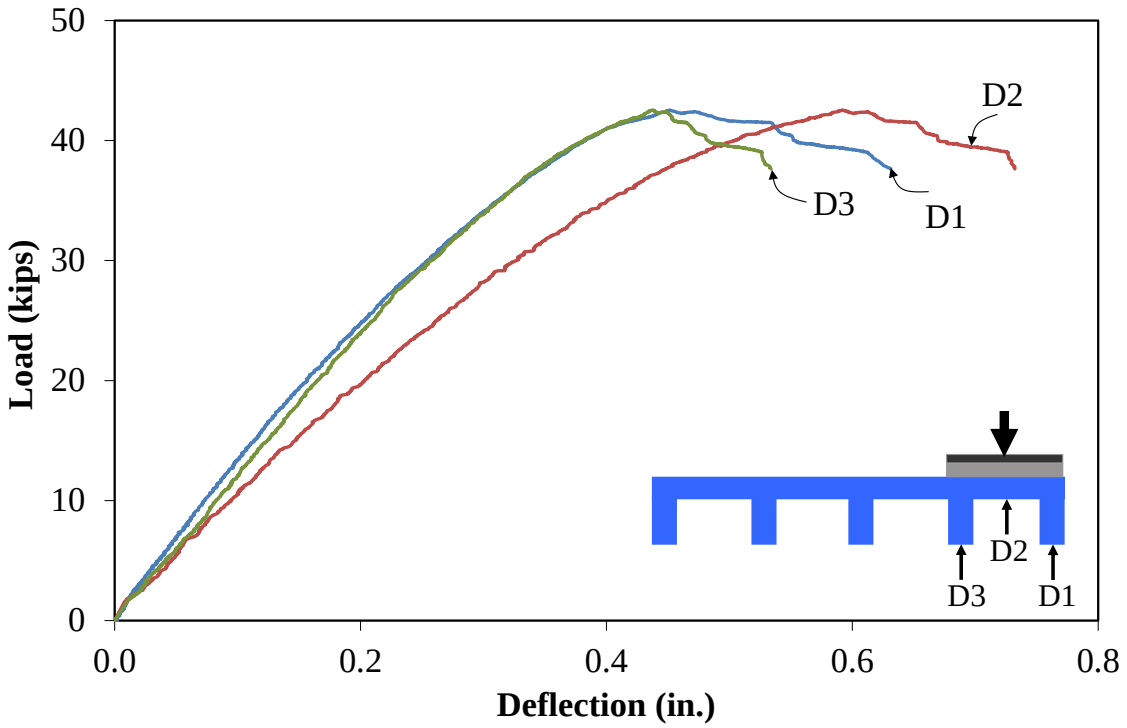

(c)

Figure 2.8 Punching Shear Test of Specimen 4T1S: (a) Test Setup, (b) Failure Mode, and (c) Load-Deflection Responses

2.2.4.3 Continuity Effects

The effects of continuity and negative moments were investigated using the single-rib two-span Specimen 1T2S. Figure 2.9 shows the test setup, deflected shape, and the failure mode, where diagonal cracks initiated near an exterior support in one span and propagated to the slab leading to the eventual failure. Minor shear cracks were also present in the other span, while some flexural cracks were observed on top of the slab over the interior support.

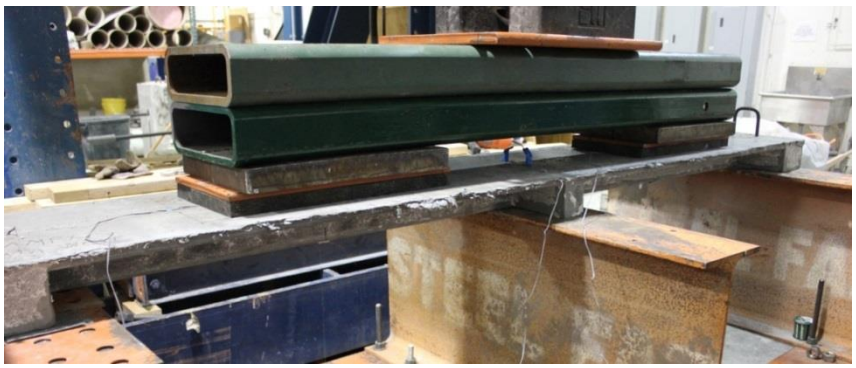

(a)

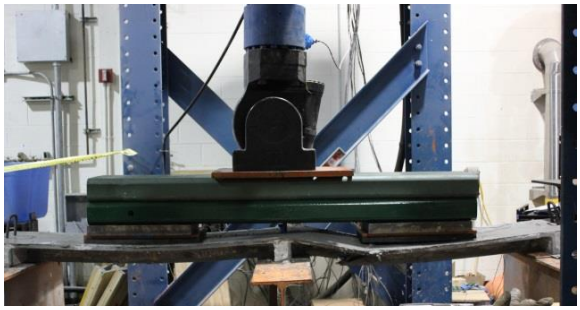

(b)

(c)

Figure 2.9 Flexure Tests of Specimen 1T2S: (a) Test Setup, (b) Deflected Shape, and (c) Failure Mode

Figure 2.10 shows the load-deflection response for the two measured mid-span displacements. Also shown for comparison are the load-deflection response curves for the deeper specimen tested by Saleem (2011). The comparison shows that although the new design has led to 18% reduction in the ultimate load, the capacity is still close to three times that of the expected demand, while the weight has been reduced by 37%. It is equally important to note the apparent high displacement-based ductility of the deck.

From the perspective of serviceability, the specimen showed a deflection of 0.07 in. at the service demand of 8.92 Kips. This corresponds to L/697, where L = center to center spacing of

stringers, i.e., 4ft. Noting the continuity effect of typical decks spanning over multiple stringers, one can calculate a correction factor of 0.74 comparing the deflections of two-span and five-span decks under two wheel loads. As such, the corrected deflection of the proposed deck turns out to be L/942, which clearly meets the deflection limit of L/800. Further testing of multi-span decks can help confirm this finding.

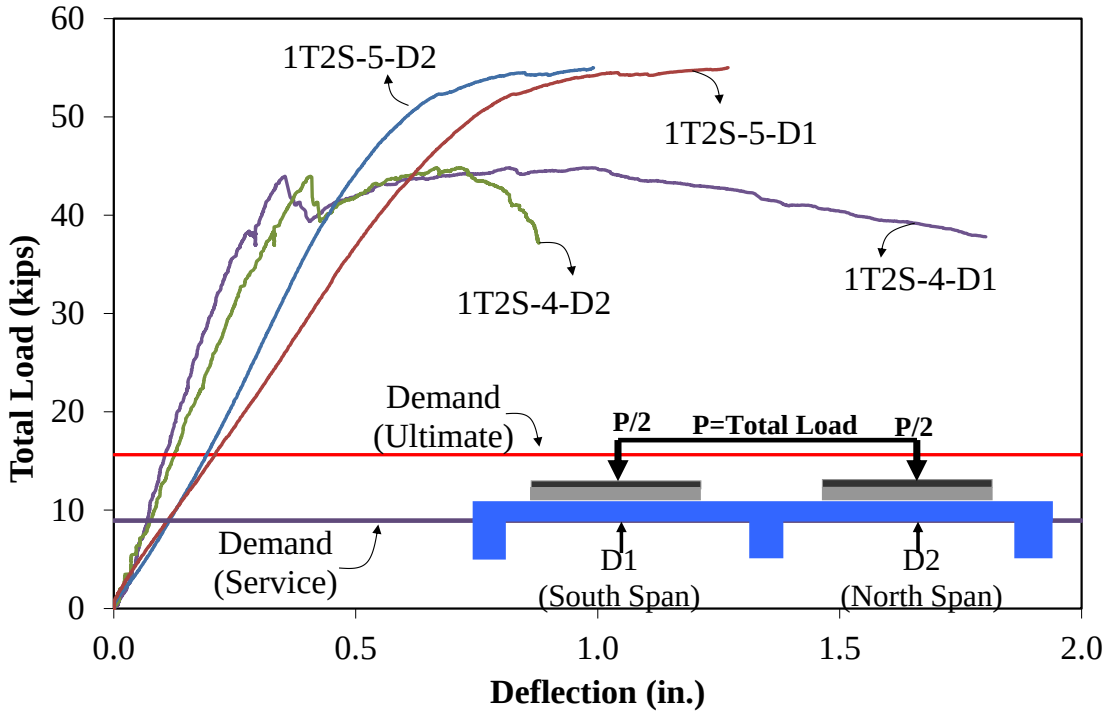

Figure 2.10 Load-Deflection Responses of Specimens 1T2S (Note: Curves 1T2S-127-D1 & D2 from Saleem, 2011)

Figure 2.11 shows the load-strain response of Specimen 1T2S, based on its measured rebar strains at both mid-spans. Similar to the load-displacement response, the strain in the north span was higher than that at the other span (which may be due to several factors including the alignment of the loading beam), where the gauge was damaged before reaching the ultimate load. As discussed earlier, the load-deflection behavior of the specimen was very ductile, while the rebar clearly did not reach its yield strain in either span.

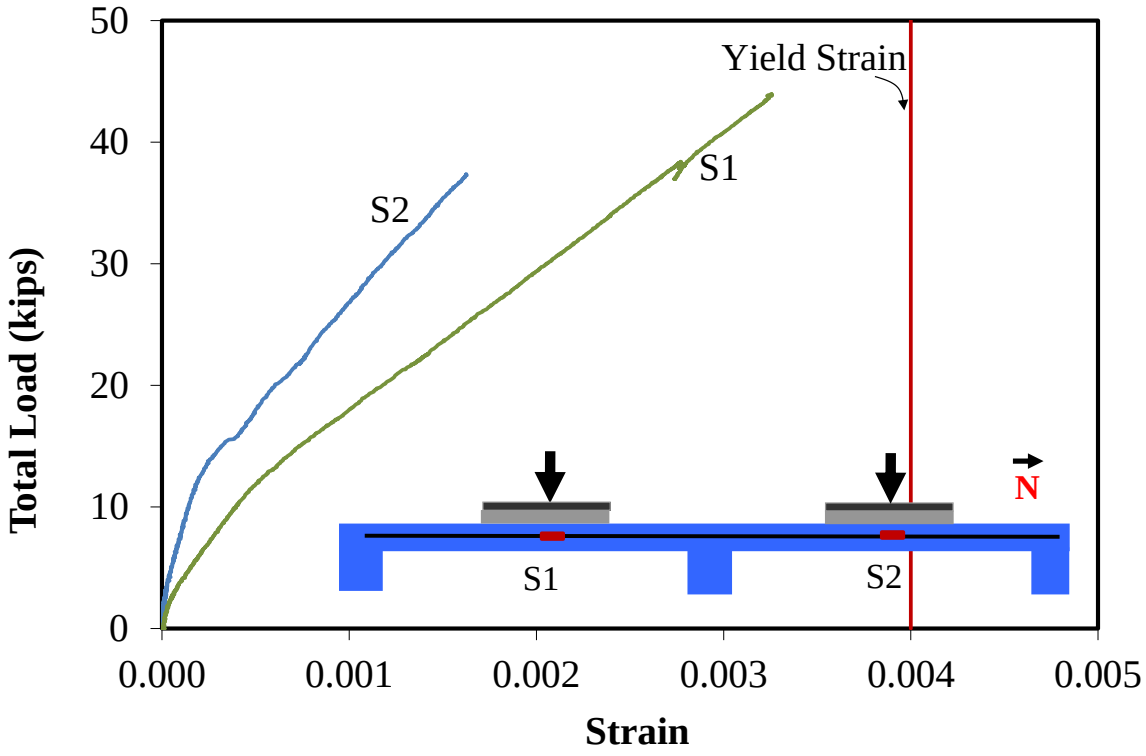

Figure 2.11 Load-Deflection Responses of Specimens 1T2S (Note: Curves 1T2S-127-D1 & D2 from Saleem, 2011)

2.3. Finite Element Modeling

2.3.1. General Modeling

The finite element analysis was performed using MSC.Marc® 2010, a commercial software with nonlinear abilities. This study consisted of the analyses of 48 in. long center-to-center single-rib T-model (1T1S) as well as the multi-span, and multi-rib models (1T2S, 4T1S) utilizing HSS as main reinforcement. A wheel load pattern was applied to the models and the load increased monotonically to obtain the strength and displacement at the end of the analysis. The wheel load was assumed to be uniformly distributed within the 20 in. tire patch on the center of the span for 1T1S and 4T1S and in the center of the two spans in the case of 1T2S. The UHPC material was simulated with 8-node hexahedral elements. Both the top and bottom HSS rebars were modeled using two-node beam elements to enable explicit treatment of nonlinearity and flexural stiffness of the bars. The bond between ultra-high performance concrete and rebar is found to be critical on ultimate load capacity and failure modes. Therefore, two- dimensional four-node elements with cohesive zone properties were used in the finite element program to simulate the bond between the two materials as shown in Figure 2.12. Two different types of interface properties were used in the analysis. The strong interface (End interface layer) is used to simulate the bond at the beam ends due to the existence of the rebar hooks, if applicable. The weak interface

(Middle interface layer) is used to simulate shear transfer between the rebar and concrete along the interior of the beam spans.

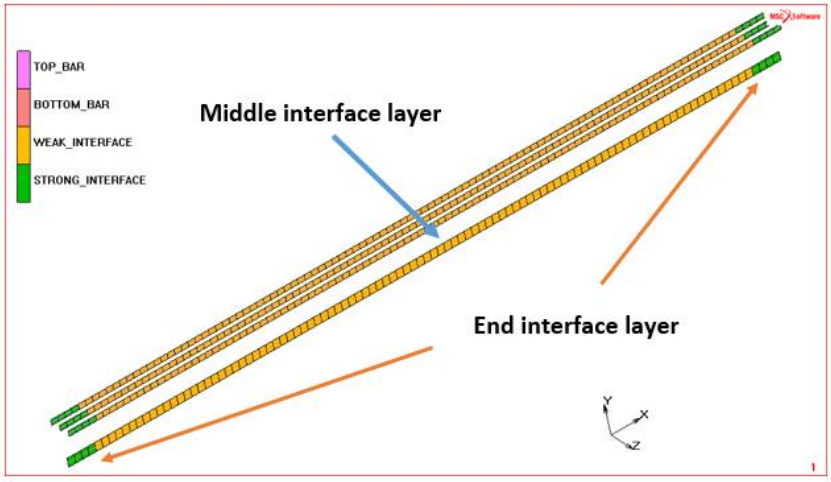

Figure 2.12 Interface Configuration

For tensile properties of UHPC, the softening material model built in MSC.Marc was used as shown in Figure 2.13. The input parameters for the material model are shown in Table 2.3. The comparison of the principal stress to the cracking stress that predefined in the software as shown in Table 2.3 was used to judge the cracking. After cracking, the material was treated as orthotropic material. A typical equivalent plastic strain curve was used to define stress-strain behavior of HSS rebar, as shown in Figure 2.14, based on manufacturer's data. Cohesive materials were used to model the interface element, as shown in Figure 2.15 with a bilinear bond-slip curve, and the material properties shown in Table 2.4, including cohesive energy (G_c), critical opening displacement (v_c), and maximum opening displacement (v_m), beyond which traction is reduced to zero. The interface parameters were calibrated to model the weak and strong interface configurations using the straight bar (no hook) and 180° hook 1T1S tests from Saleem et al. (ACI 2011 paper), respectively.

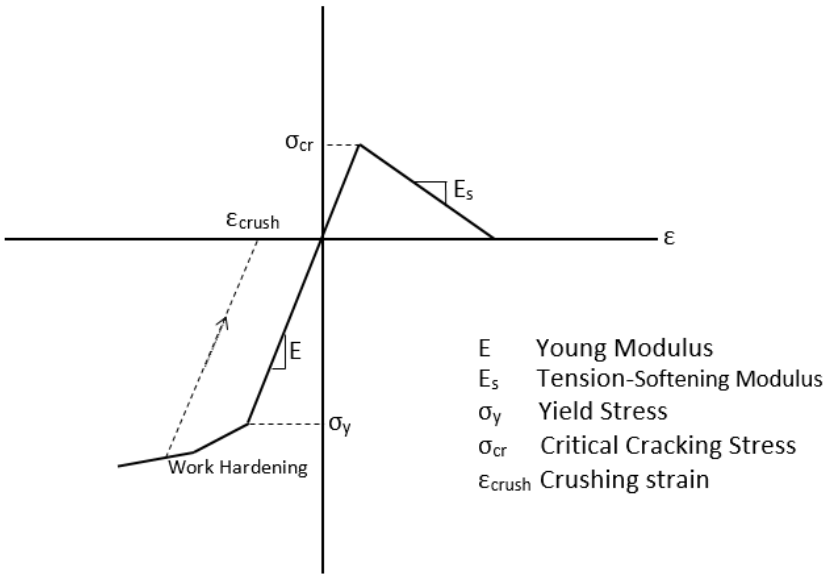

Figure 2.13 Low Tension Material Curve

Table 2.3 UHPC Material Properties

Parameter	**Definition**	**Typical Value**
E	Modulus of Elasticity	7000 ksi
ν	Poisson Ratio	0.17
E_s	Softening Modulus	50 ksi
f_t	Crack Stress	1 ksi
ε_{crush}	Plastic Strain	0.0032
γ_{shear}	Shear retention factor	0.1

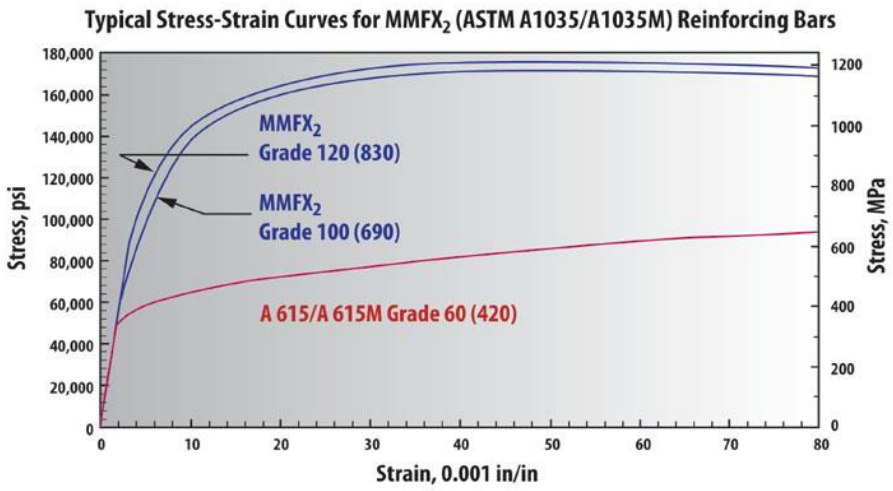

Figure 2.14 Stress-Strain Curve for HSS (Manufacturer Website: www.mmfx.com)

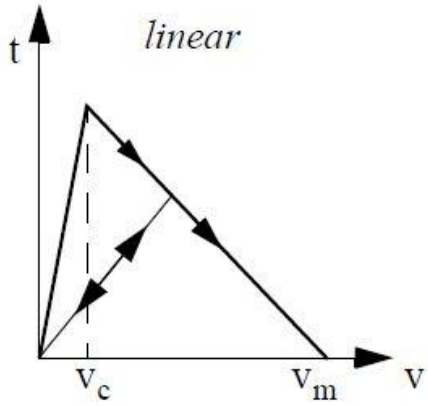

Figure 2.15 Interface Element Model

Table 2.4 Interface Element Parameters

Section	**Strong Interface**			**Weak Interface**		
	G_c	V_c	V_m	G_c	V_c	V_m
HSS	35	0.15	0.25	0.08	0.01	0.02

2.3.2. Modeling and Results for 1T1S Section

The mesh and the geometry of 1T1S for HSS as main reinforcement are shown in Figure 2.16. Full deck was modeled to avoid the stress concentration along the boundaries that results from the symmetry. As mentioned before, two types of interface element were used to model the connection between the rebar and concrete element. The interface at the support was assumed to be very strong to simulate the hook condition for the HSS bar. The stress distribution, comparison of load-displacement curve, and the comparison of load-strain response for the HSS are shown in Figures 2.17, 2.18, and 2.19, respectively. It can be noticed that the finite element results showed a good agreement with the tests result.

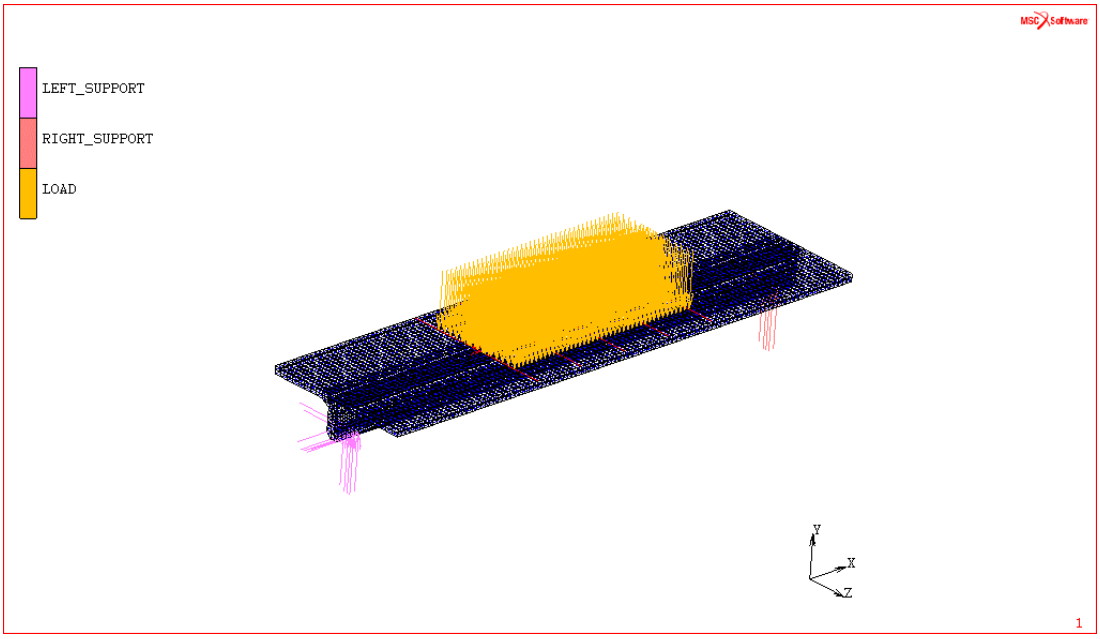

Figure 2.16 Discretized Model for Specimen 1T1S

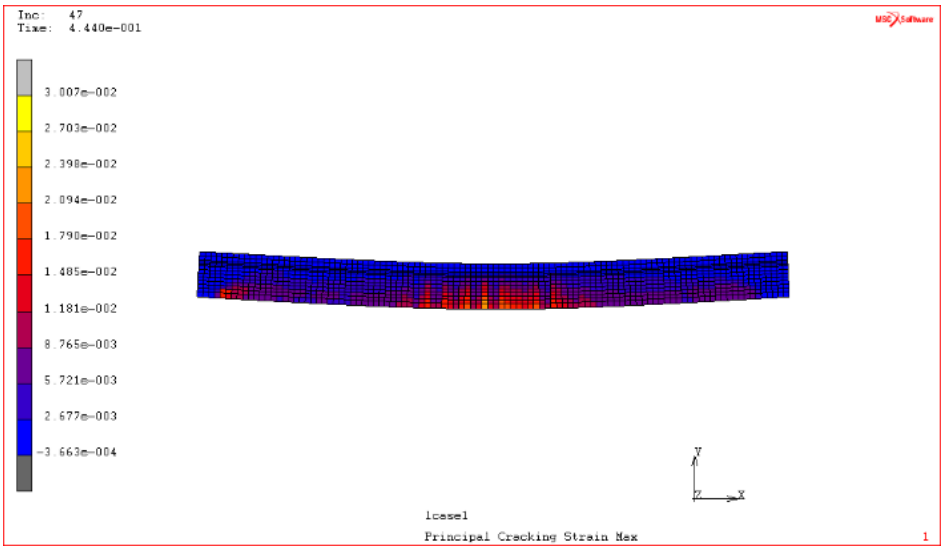

Figure 2.17 Stress Distribution of Specimen 1T1S at Peak Load

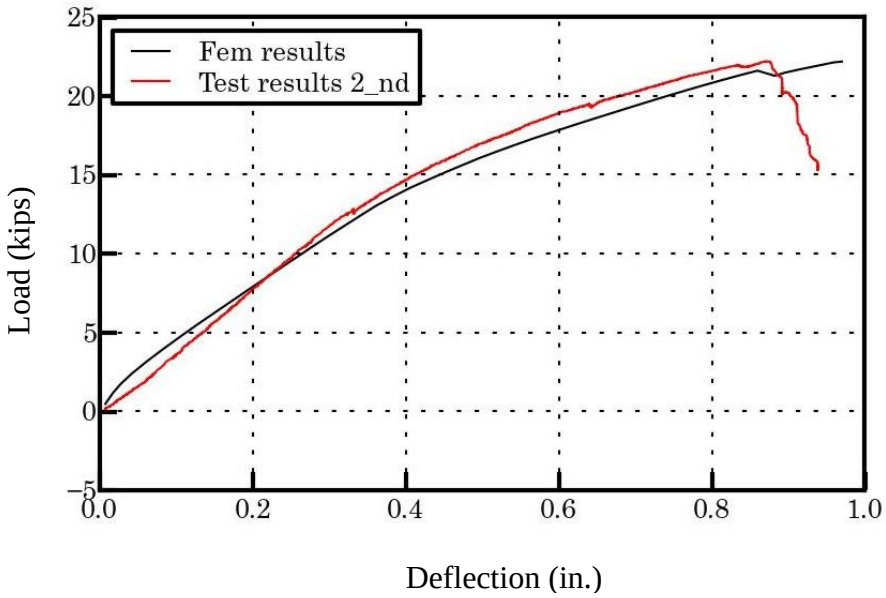

Figure 2.18 Load-Deflection Responses for Specimen 1T1S

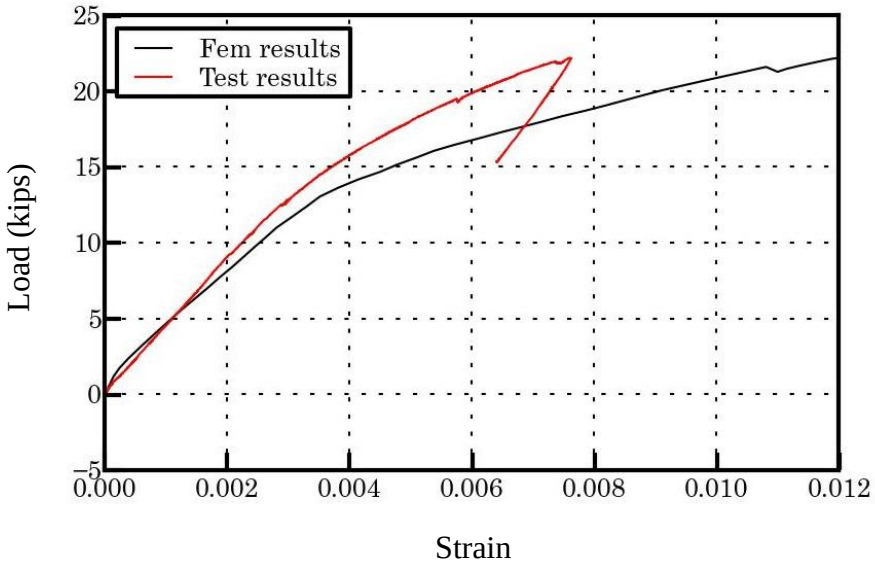

Figure 2.19 Load-Strain Responses for Bars at Mid-Span

2.3.3. Modeling and Results for 1T2S Section

The finite element model for the 1T2S deck with the boundaries is shown in Figure 2.20. The load-deflection and load-strain response curves are shown in Figures 2.21 and 2.22, respectively. From these figures, it can be seen that the model captured the initial stiffness for the deck; however, it overestimated the load capacity for both options.

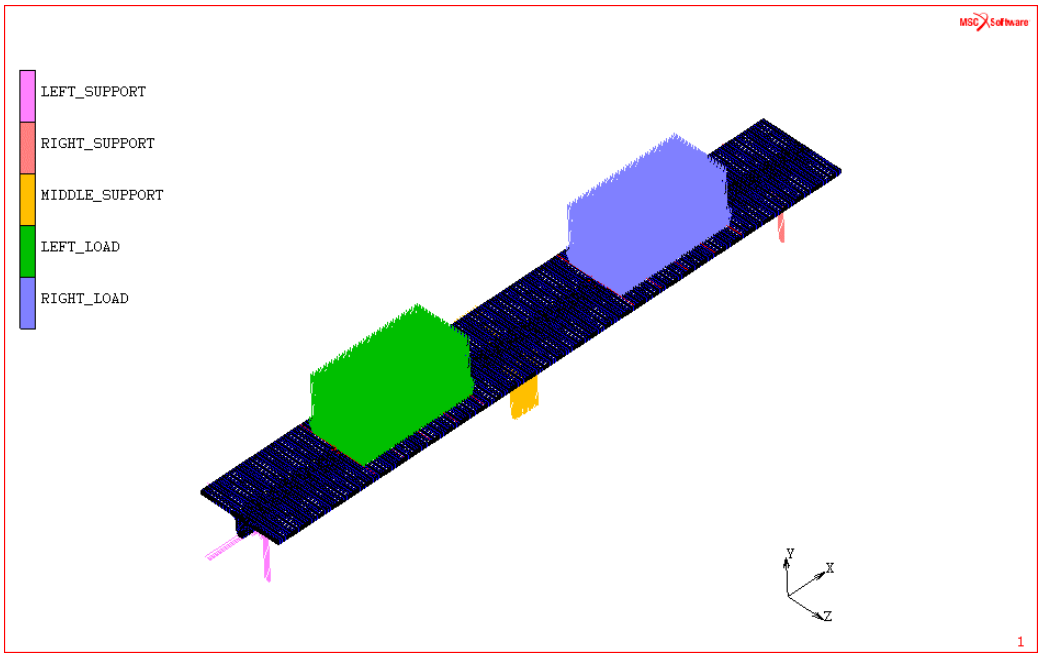

Figure 2.20 FEM Model for Specimen 1T2S

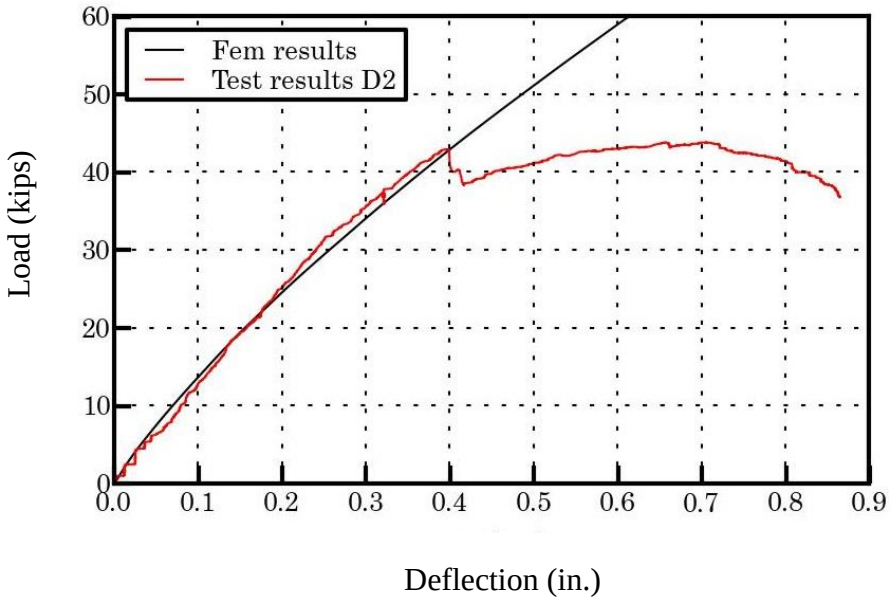

Figure 2.21 Load-Deflection Responses for Specimen 1T2S

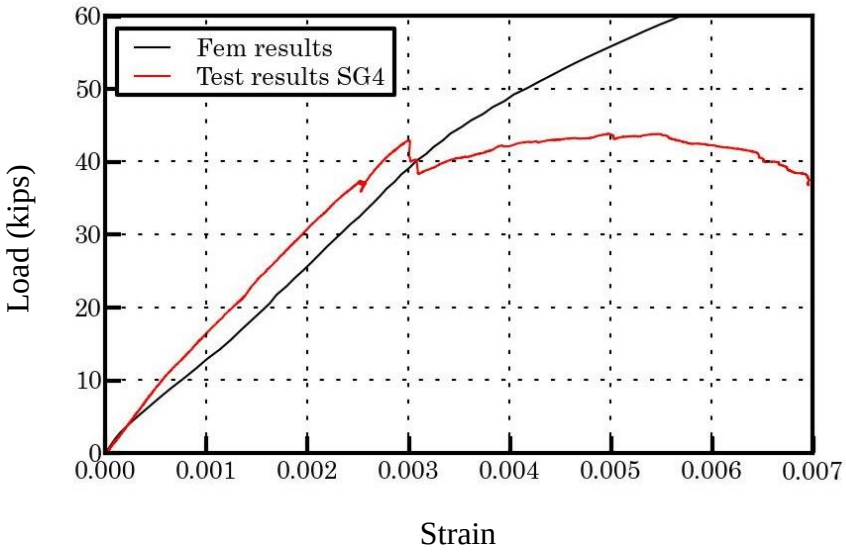

Figure 2.22 Load-Strain Responses for Bars at the Middle of First Span

2.3.4. Modeling and Results for 4T1S Section

The finite element model for the 4T1S deck with the boundaries is shown in Figure 2.23. Transverse ribs with #4 bars at a distance one third of the total length from both ends are used to avoid the punching shear failure as showing in Figure 2.24. The load-displacement and load-strain response curves are shown in Figures 2.25 and 2.26.

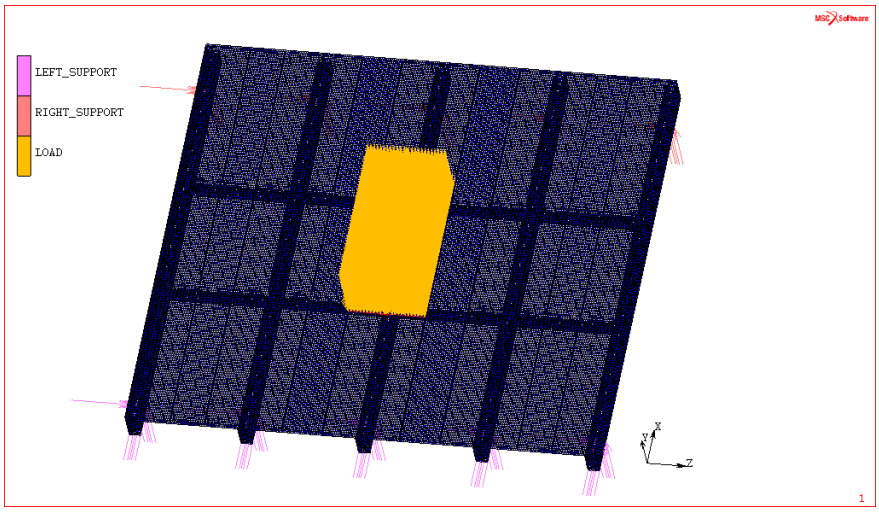

Figure 2.23 FEM Model for Specimen 4T1S

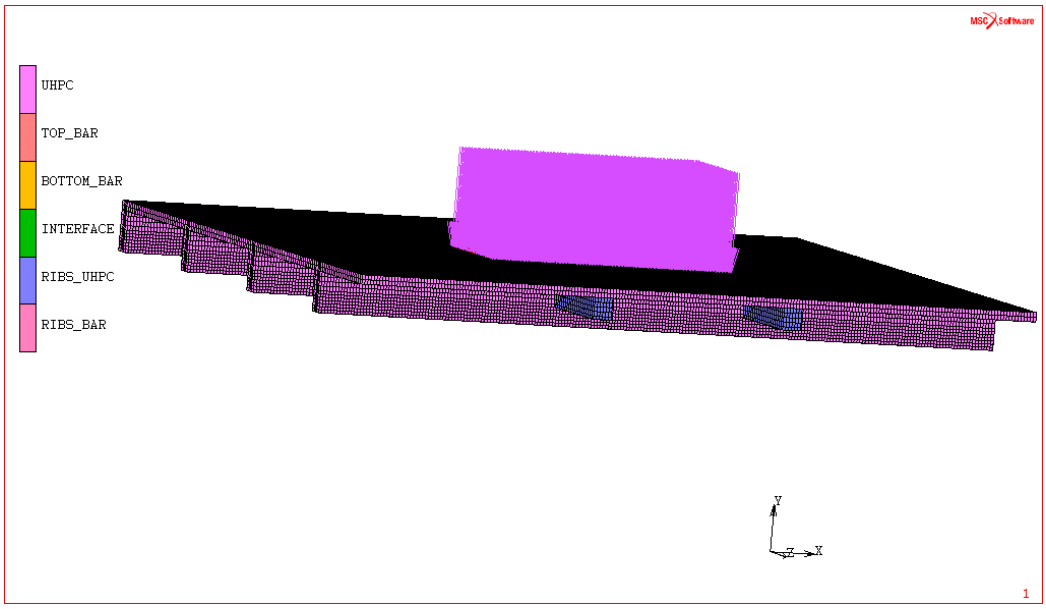

Figure 2.24 Location of the Ribs

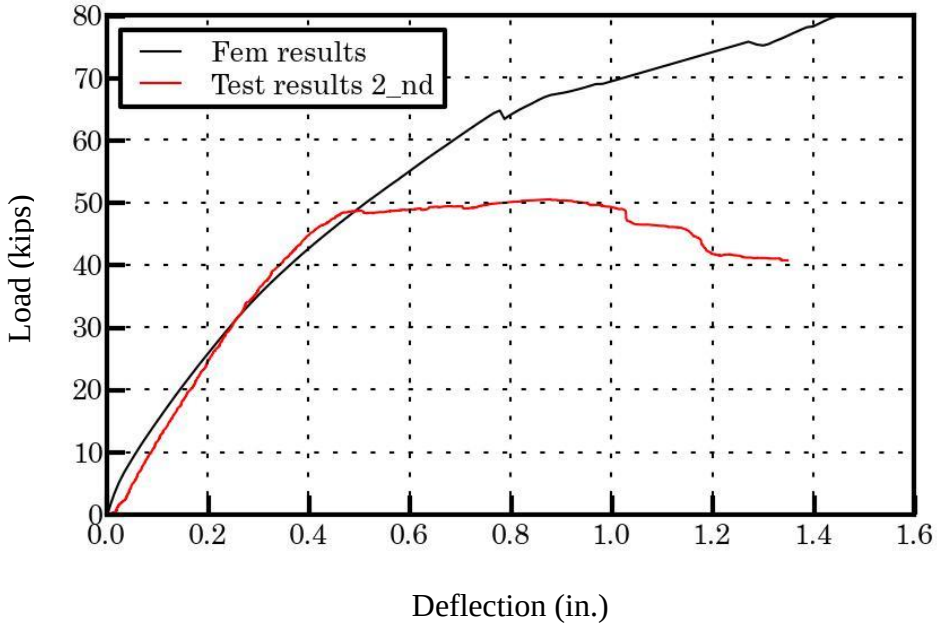

Figure 2.25 Load-Deflection Responses for Specimen 4T1S

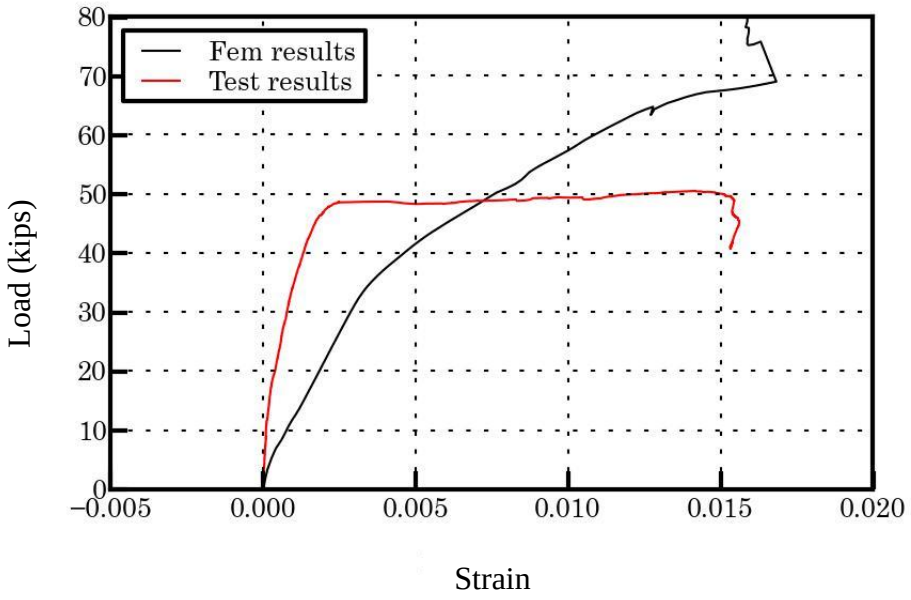

Figure 2.26 Load-Strain Responses for Mid-Span Bars for Specimens 4T1S

In summary, all deck configurations were modeled and the finite element analysis was performed to compare the displacement and strain results from the experiments with the outcomes of finite element analysis to examine the ability of the model to predict the overall and component-level behavior of the decks. The results generally showed a good agreement for UHPC-HSS specimens between the experimental and analytical results especially for the 1T1S deck in the linear behavior range. Moreover, the model captured the initial stiffness for the 1T2S and 4T1S although it overestimated the ultimate load.

2.4. Accelerated Pavement Testing of Waffle Bridge Deck

Based on static testing conducted in the lab, the UHPC waffle deck system has shown great promise as a viable alternative to open grid steel decks. In order to evaluate the long-term performance of the UHPC deck panels under field conditions, it was decided to test the system at the Accelerated Pavement Testing (APT) facility in Gainesville under the Heavy Vehicle Simulator (HVS). Four lightweight bridge deck panels and their connections to each other and the stringers were tested at the APT facility.

2.5. Experimental Work

Due to the geometry and configuration of the testing pit, the depth of the deck section needed to be 5 inches, which is different from the optimized depth of 4 inches as described in previous chapters. In order to have a better understanding of the behavior of the section with a 5-inch depth under HVS loading, six laboratory specimens were built for the purpose of sizing through static tests with single and multiple ribs in simple and double span configurations. The results of recent tests were then compared to those of previous tests, as described in the following sections.

2.5.1. Test Matrix and Specimen Preparation

Table 2.5 shows the test matrix for this study. The specimen names include number of ribs (T), number of spans (S), specimen depth and sample number (if more than one). All specimens have the same depth of 5 inch, but in three different configurations, single-rib simple-span, single-rib two-span, and multi-rib simple-span (see Figures 2.1 and 2.2). The multi-rib specimen featured 2¾-inch-deep transverse ribs to help with load distribution among primary ribs. For comparison, the table also shows all UHPC waffle deck specimens with HSS reinforcement tested in all previous studies (Saleem et al. 2011, Ghasemi et al., 2015).

2.5.2. Test Setup and Instrumentation

The test setup and instrumentation is similar to Sections 2.2.2 and 2.2.3 while the span length was 5 ft. for the APT tests.

2.5.3. Test Results and Discussion

Table 2.6 shows a summary of test results for the current studies along with the results from prior experiments on the UHPC waffle decks with HSS (Saleem et al. 2011, and Ghasemi et al., 2015). The table shows the required live load demand for each group of specimens, along with capacity/demand ratio and capacity/demand per unit weight of the deck panel for each specimen. In the following sections, test results for each group of specimens are presented.

Table 2.5 Test Matrix

Group	Specimen Name	Test Phase	Overall Depth (in.)	Rib Spacing (in.)	Slab Thickness (in.)	Unit Weight (psf)	28-Day UHPC Compressive Strength (ksi)	Flexural Reinforcement	
								Slab	Primary Rib
UHPC-HSS									
HSS-3	1T1S-5	3	5	15	¾	26.13	22	No. 3	No. 6
	4T1S-5	3	5	15	¾		23	No. 3	No. 6
	1T2S-5	3	5	15	¾		22	No. 3	No. 6
UHPC-HSS									
HSS-0[1]	1T1S-5#1	0	5	12	1¼	32.37	18	No. 4	No. 7
	1T1S-5#2	0					27		
	4T1S-5	0					26		
	1T2S-5	0					22		
HSS-1	1T1S-4½#1	1	4½	15	¾	21.72	24	No. 3	No. 5
	1T1S-4½#2	1					24		
HSS-2	1T1S-4	2	4	15	¾	20.26	27		
	4T1S	2					27		
	1T2S	2					25		

[1] Taken from Saleem et al. (2011).

Table 2.6 Summary of Test Results

Group	Specimen Name	Graph Labels	Overall Depth (in.)	Service Load Deflection (in.)	Ultimate Deflection (in.)	Ultimate Load (kip)	Demand Load (kip)	Capacity/ Demand	Capacity/ Demand per Unit Weight
UHPC-HSS									
HSS-3	1T1S-5	HSS-5#3	5	0.076	1.71	23.07	8.14	2.83	0.11
	4T1S-5	HSS-5#3		0.21	0.93	55.59	52.13	1.07	0.04
	1T2S-5	HSS-5#3		0.084	1.20	35.45	17.45	2.03	0.08
UHPC-HSS									
HSS-0[1]	1T1S-5#1	HSS-5#1	5	0.06	0.98	40.02	8.21	4.9	0.15
	1T1S-5#2	HSS-5#2		0.1	0.98	46.99		5.7	0.18
	4T1S-5	HSS-5#1		0.19	0.79	84.98	34.17	2.5	0.08
	1T2S-5	HSS-5#1		0.9	1.26	55.08	12.52	4.4	0.14
HSS-1	1T1S-4½#1	HSS-4½#1	4½	0.1	0.83	27.65	10.25	2.7	0.12
	1T1S-4½#1	HSS-4½#2		0.14	0.87	24.73		2.4	0.11
HSS-2	1T1S-4	HSS-4	4	0.15	0.91	22.71		2.2	0.11
	4T1S-4	HSS-4		0.18	0.87	51.48	42.04	1.2	0.06
	1T2S-4	HSS-4		0.07	0.87	44.96	15.65	2.9	0.14

[1] Taken from Saleem et al. (2011).

2.5.3.1 Flexural Behavior

Similar to Section 2.2.4, the flexural behavior of Specimens 1T1S was assessed. Figure 2.27 shows the test setup, failure mode, and load-deflection responses of single-rib simple-span for UHPC-HSS specimen. Similar to previous experiments, failure was initiated by minor web shear cracks near supports. Minor flexural cracks were also present near mid-span without having any impact on the overall failure. Shear cracks gradually widened as testing progressed, eventually leading to a load drop and failure of the deck panel.

Figure 2.28 shows the load-deflection responses of the single-rib simple-span specimen compared to all previous specimens of the current research projects. The load capacity is normalized to the corresponding ultimate demand load for each specimen according to the data presented in Table 2.6. As seen in the figure, in all of the specimens, the capacity exceeded the ultimate demand load. The 5-inch deep specimens seem to be more flexible as compared to their counterparts in previous phases. This may be attributed to the larger clear span of 5-ft., in contrast to the 4-ft. span in previous phases. Having design information of all previous phases, the panels were resized to meet the 5 ft. span requirements, accordingly. Although the overall depth was also changed proportionally, not all thicknesses were sized for the larger span.

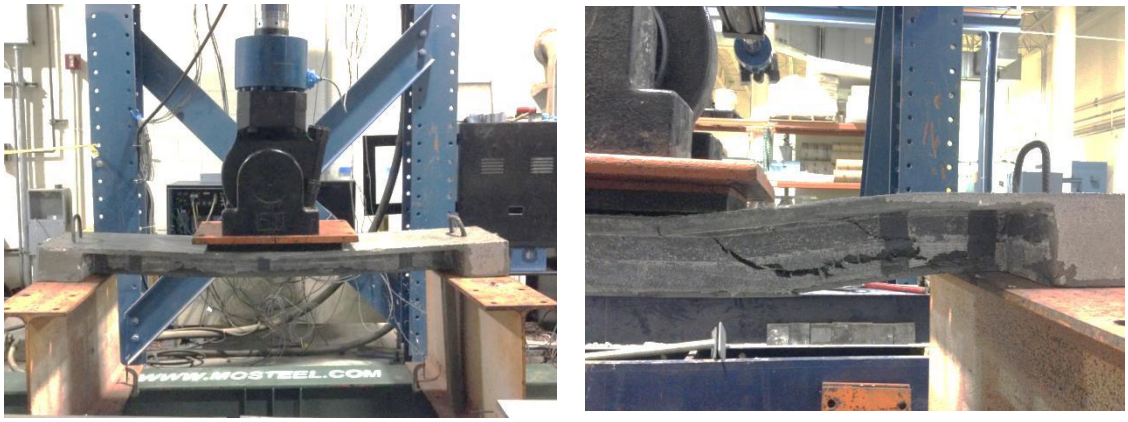

(a) (b)

Figure 2.27 Flexure Test and Failure Mode of Specimens 1T1S-HSS, (a) Deflected Shape of Specimen 1T1S, and (b) Beam Shear Crack

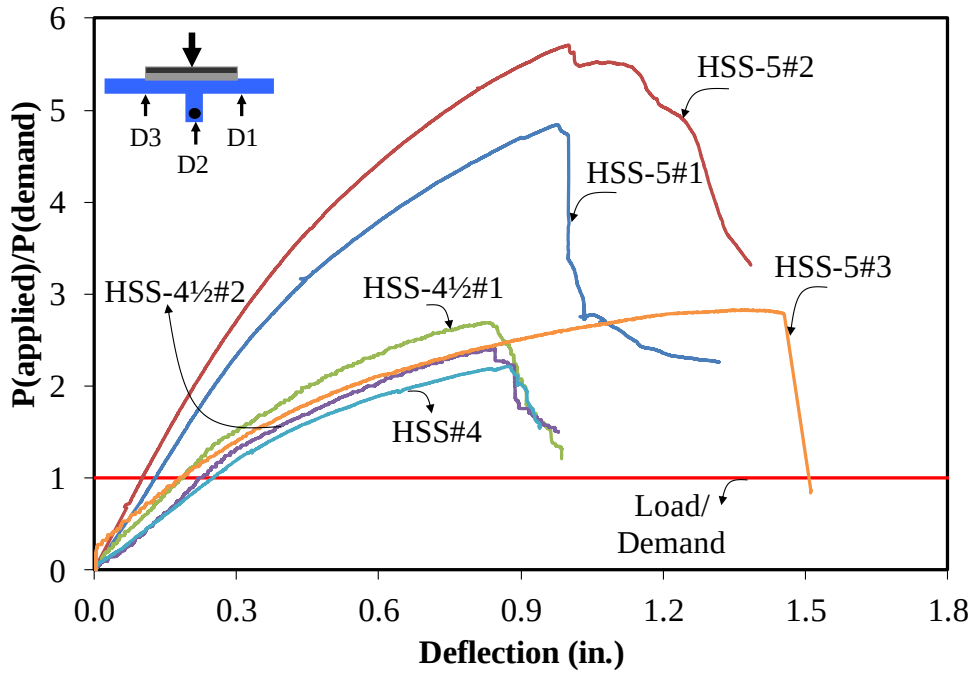

Figure 2.28 Load-Deflection Responses of All Specimens 1T1S

Figure 2.29 shows the load-strain responses for all specimens with HSS reinforcement. As expected, there is similarity between the results of this phase and those of previous phases.

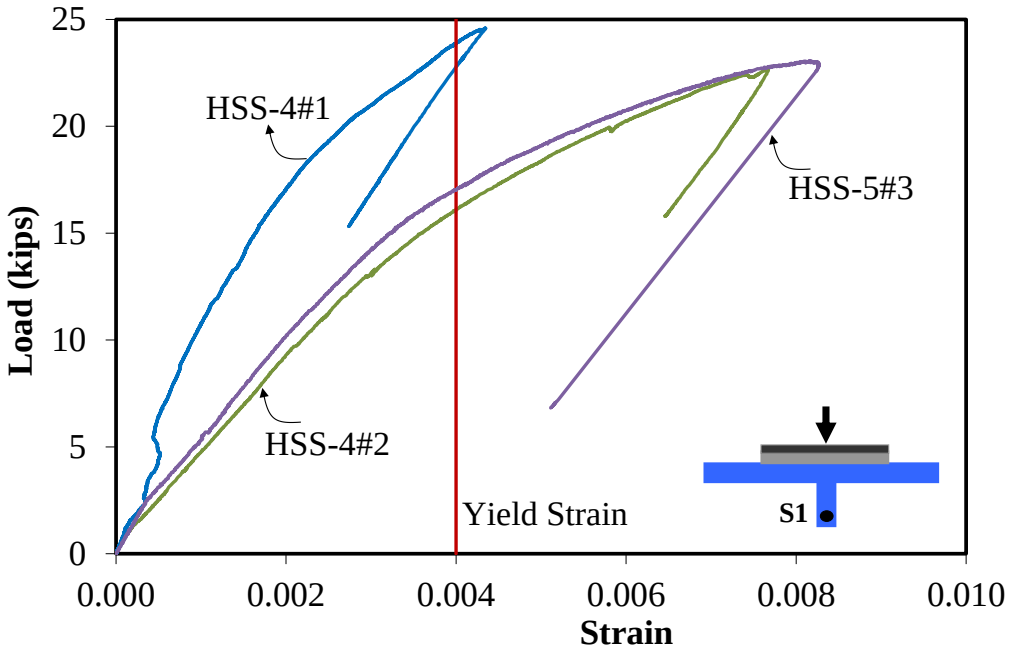

Figure 2.29 Strain Responses of HSS Bars in Specimens 1T1S

Additional strain gauges were attached to the top surface of the UHPC deck and to the web in order to capture the strain in the UHPC. The results are shown in Appendix A.

2.5.3.2 Panel Action

Performance of Specimens 4T1S was evaluated similar to Sections 2.2.4.1. Figure 2.30 shows the top and bottom views of the multi-rib simple-span Specimen 4T1S after its flexural test for Specimen 4T1S-HSS. The failure mode was similar to that observed for single-rib specimens of this phase and the previous multi-ribs simple-span specimens.

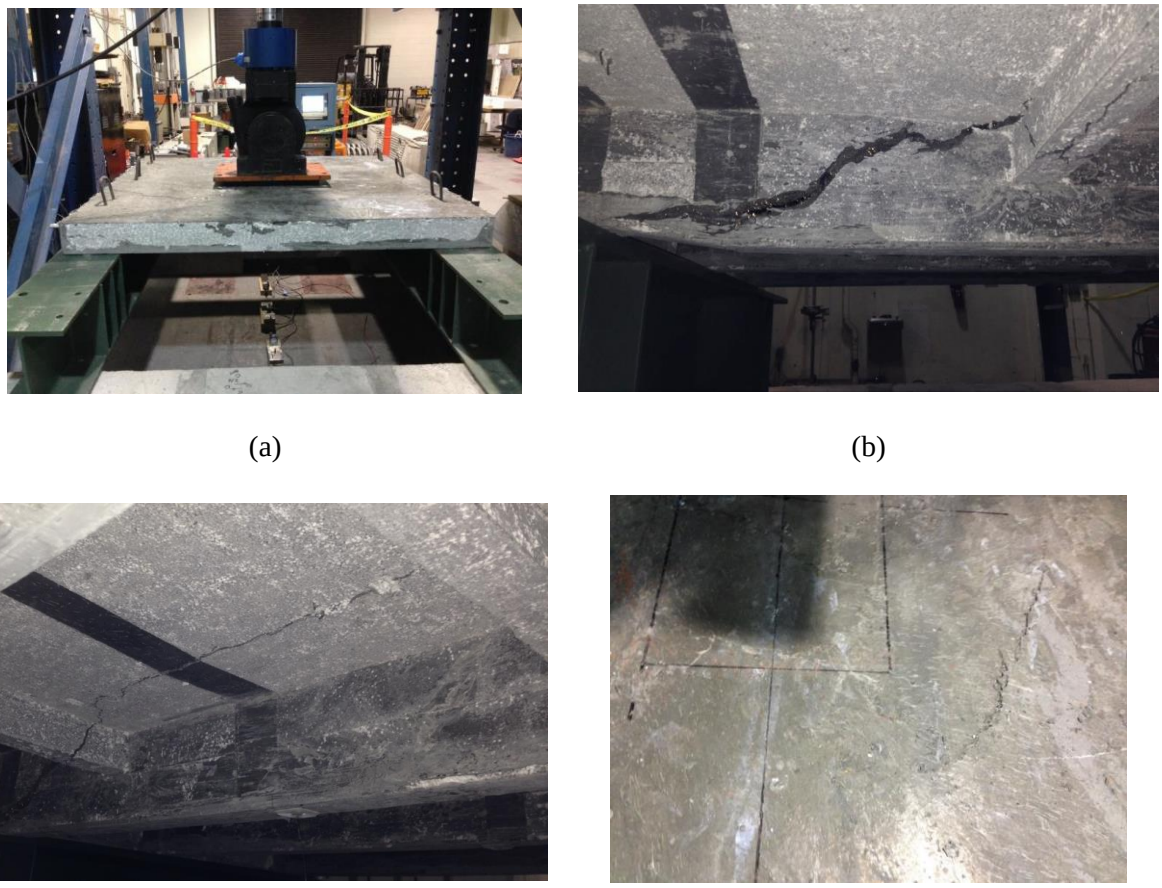

(a) (b)

(c) (d)

Figure 2.30 Flexure Test and Failure Mode of Specimens 4T1S-HSS, (a) Test Setup, (b) Beam Shear Crack, (c) Cracks on the Slab, and (d) Cracks on the Top Slab

For comparison, Figure 2.31 shows the response curves under each rib for current Specimens 4T1S along with all previous specimens. Only the load-deflection response of the middle rib (D3) is shown in the figure for all specimens.

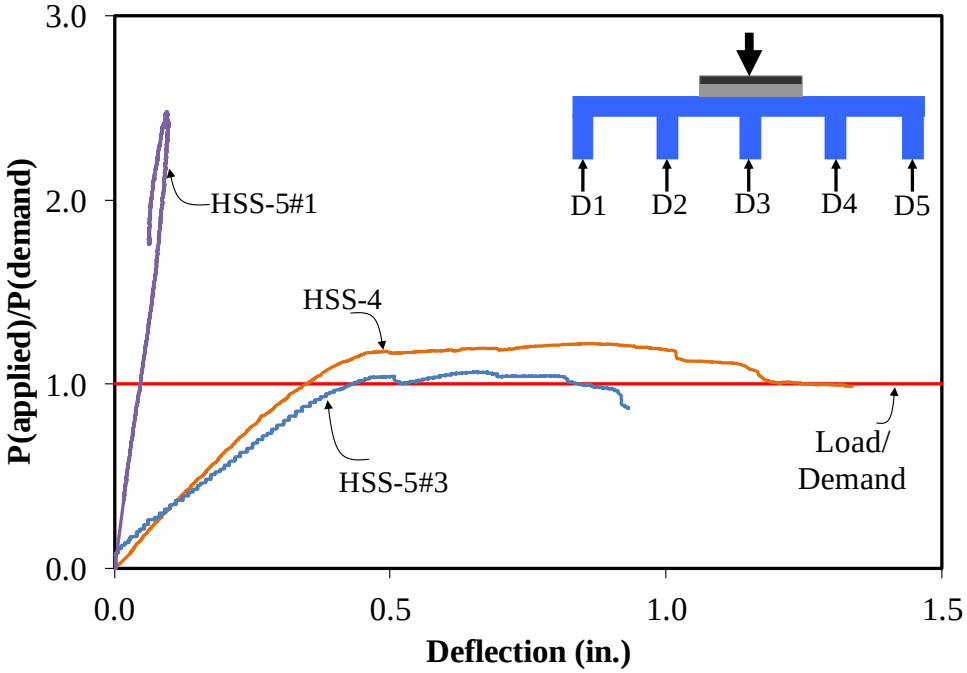

Figure 2.31 Load-Deflection Responses of All Specimens 4T1S

Figure 2.32 shows load-strain responses for all Specimens 4T1S with HSS reinforcement based on strain gauges attached at the mid-span to the rebar in the primary rib. The results are considerably similar to previous phases.

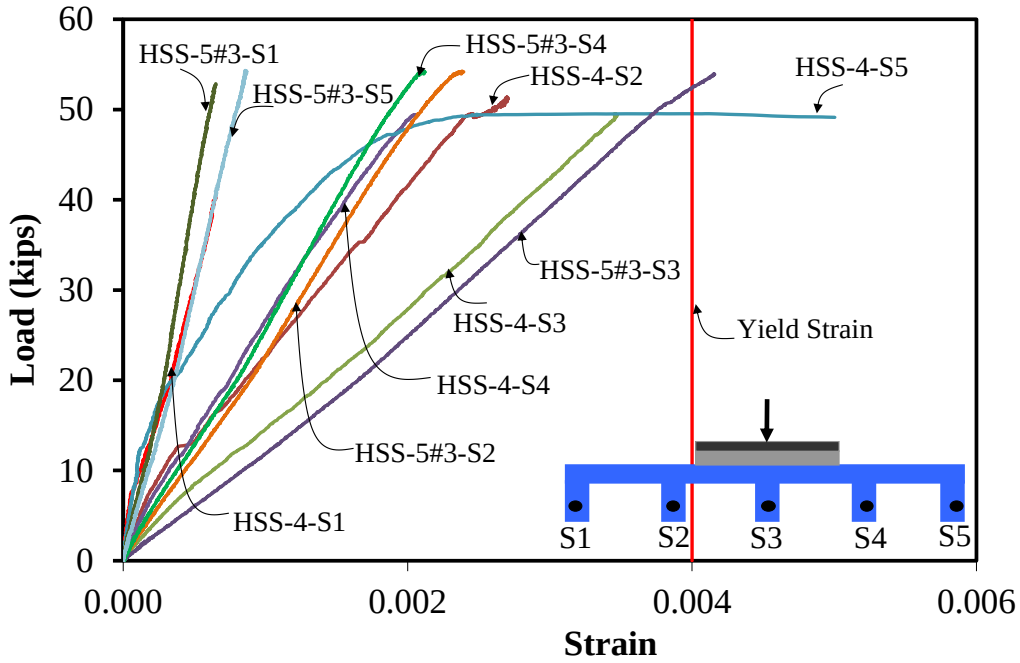

Figure 2.32 Load-Strain Responses of All Specimens 4T1S-HSS

2.5.3.3 Punching Shear Behavior

Similar to Section 2.2.4.2 the punching shear behavior of the Specimens 4T1S was assessed on the same specimen 4T1S after flexural tests. Figure 2.33 shows the punching shear test carried out on exterior panel of Specimen 4T1S-HSS. The load-deflection response of the punching shear test is presented in Figure 2.34.

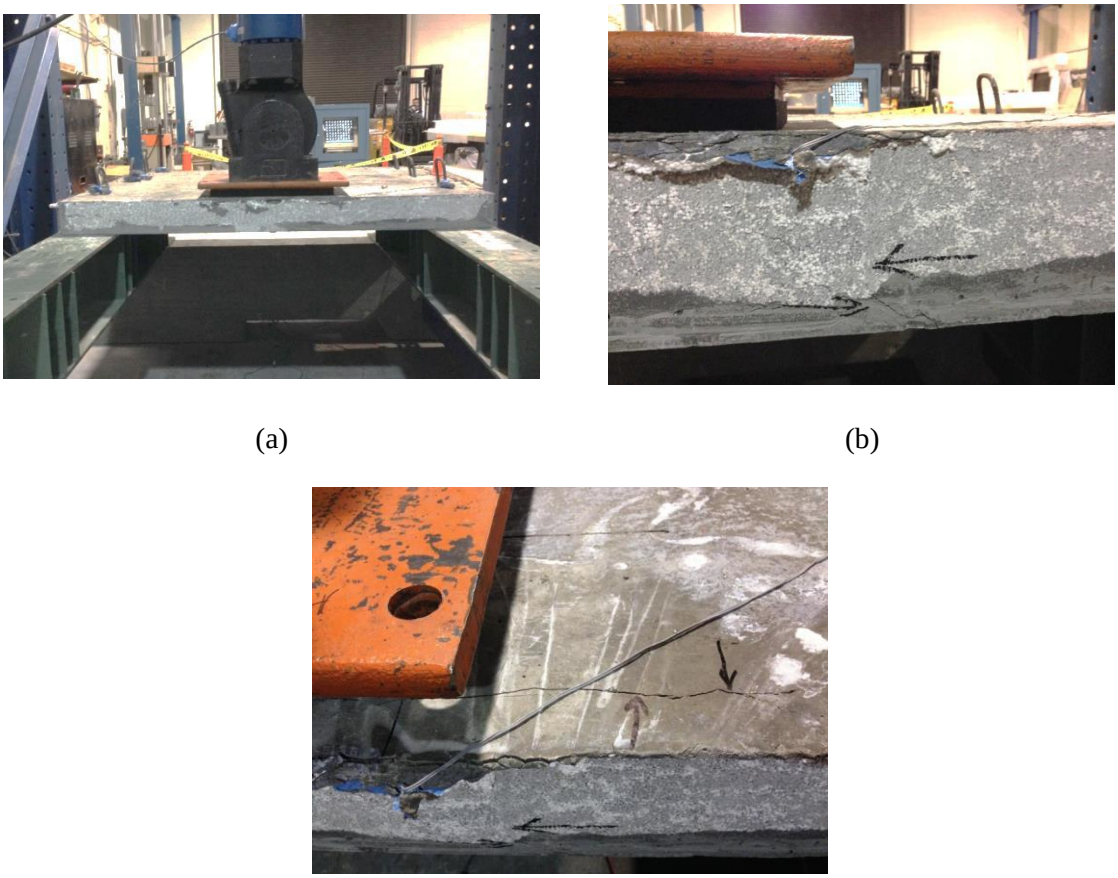

(a) (b)

(c)

Figure 2.33 Punching Shear Test of Specimen 4T1S: (a) Test Setup, (b) Beam Shear Crack, and (c) Cracks on the Top of the Slab

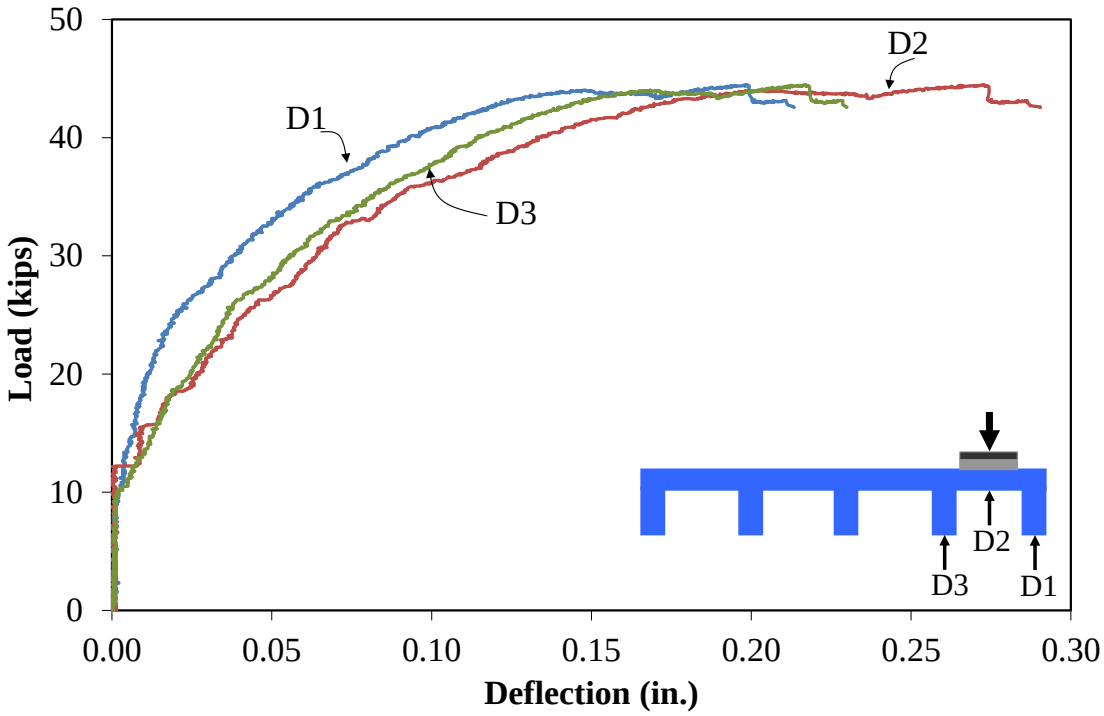

Figure 2.34 Load-Deflection Responses of Specimen 4T1S-HSS

2.5.3.4 Continuity Effects

The effects of continuity and negative moments were investigated using the single-rib two-span Specimen 1T2S. Figure 4.15 shows the test setup, deflected shape and the failure mode, where diagonal cracks initiated near an exterior support in one span, and propagated to the slab leading to the eventual failure for Specimen 1T2S-HSS. Minor shear cracks were also present in the other span, while some flexural cracks were observed on top of the slab over the interior support. Major flexural cracks on interior support at the face of the northern span of the specimens occurred (see Figure 2.35.d).

(a)

(b) (c)

Figure 2.35 Flexure Tests of Specimen 1T2S-HSS: (a) Test Setup, (b) Deflected Shape, and (c) Failure Mode

For comparison, Figure 2.36 shows the two mid-spans response curves for Specimens 1T2S along with all previous specimens. The responses are normalized based on the load capacity. All specimens meet the ultimate demand load capacity.

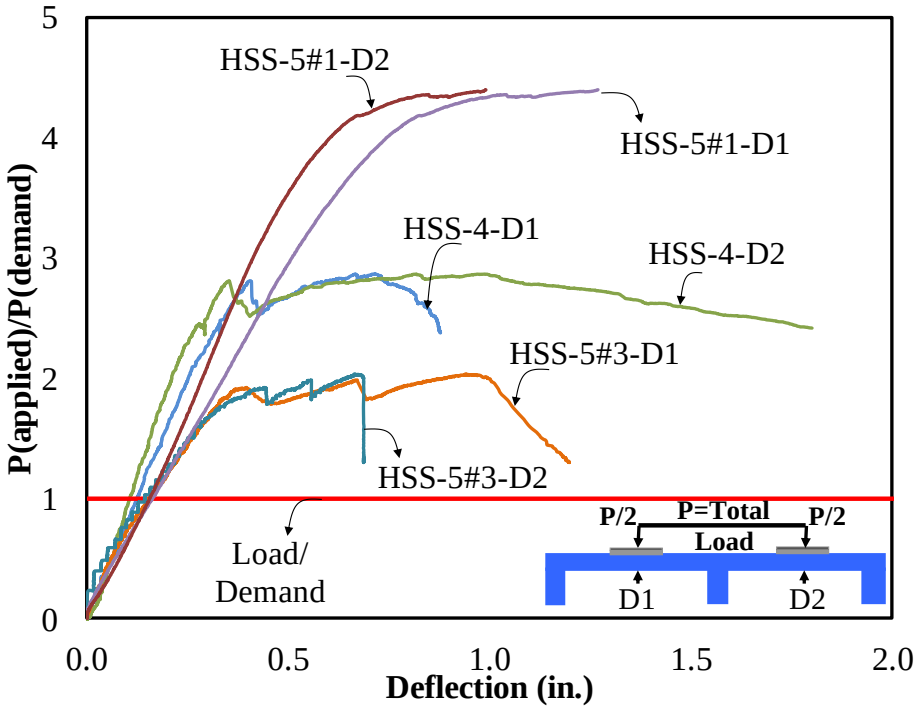

Figure 2.36 Load-Strain Responses of All Specimens 1T2S

Figure 2.37 shows load-strain responses for all Specimens 1T2S with HSS reinforcement based on strain gauges attached at the mid-span to the rebar in the middle of the primary ribs. Contrary to previous specimens with HSS reinforcement, the main bar in the span with maximum deflection approached the yield limit.

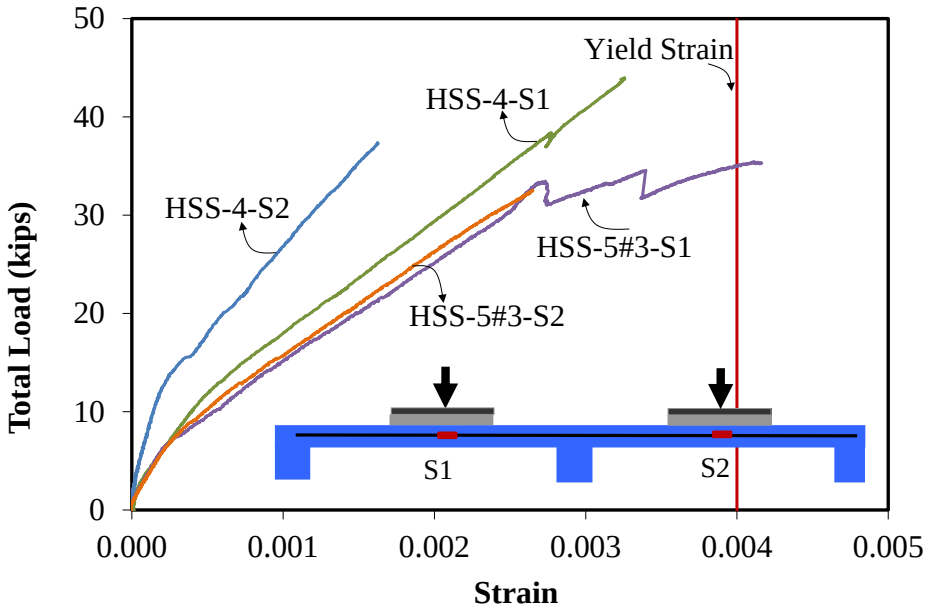

Figure 2.37 Load-Strain Responses of All Specimens 1T2S-HSS

2.5.4. Accelerated Pavement Testing under Heavy Vehicle System

According to Figures 2.33 (b) and 2.33 (c) the punching shear cracks occurred on the slab for Specimens 4T1S-HSS. Therefore, for the final slabs which will be tested under HVS, the thickness of the slab and the amount of reinforcement were both increased. The increase in the amount of reinforcement was due to keeping the same reinforcement ratio as compared to previous phases of the research. The increase accordingly affected the weight of the panel as stated in Table 2.5.

In the following pages, the overall testing diagram and the arrangement of the four deck panels including two panels of UHPC with HSS reinforcement and two panels of UHPC with CFRP reinforcement along with the schematic details of each deck system are presented. Figure 2.38 shows the test setup and layout plan of the waffle decks. As seen in this figure, the bridge deck consists of four deck panels sitting on two support beams of W10×39. All panels have a depth of 5 in. and a transverse length of 6 ft., with center-to-center spacing of the stringers as 5 ft. and a panel width of 5 ft. in the direction of traffic. The dimensions and components of the panels are illustrated in Figures 2.39 to 2.40.

Figure 2.47 shows the connections between the panels containing three different types of details based on the type of the reinforcement of each panel. Figure 2.48 shows the loading plan. As seen in the figure, a 9-kip wheel (due to the constraints of the equipment) was applied to the decks. The machine speed was 6ft/sec. and the data was recorded at 100 Hz frequency. Figure 2.49 shows the location of the block-outs, representing the connections between waffle deck panels and the supporting stringers. The loading path of the wheel is shown in Figure 2.50.

The instrumentation plans are shown in Figures 2.51 and 2.52. As seen in Figure 2.51, three types of string pots were planned to measure the deflections at critical locations, including mid-span deflections, joint deflections, and global deflection of the bridge, as well as transverse deflections. The locations of strain gauges are shown in Figure 2.52. The strain gauges were placed at the mid-span of the bar in the middle rib, where maximum positive moments were intended to occur, and locations under top and bottom flanges of the supporting stringers at mid-span.

The research team faced some issues during the construction such as leveling the panels on the stringers and maintaining sufficient covers for reinforcement in the thin slab.

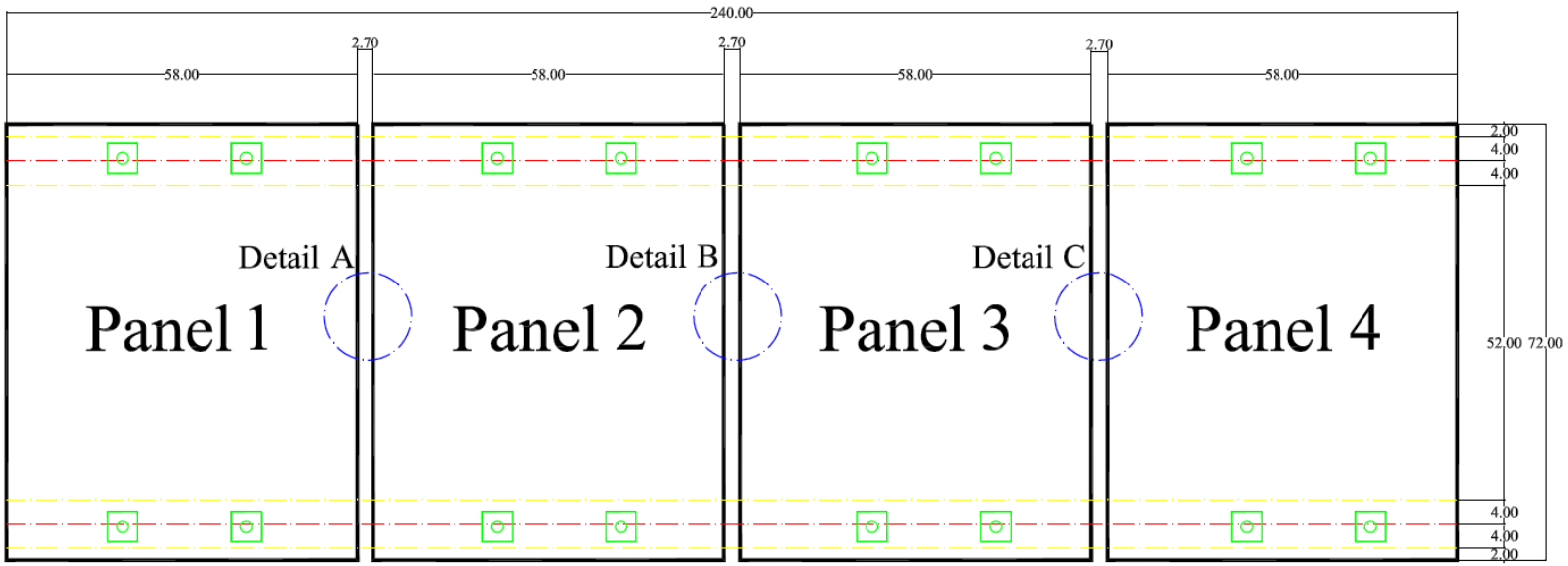

Figure 2.38 Panels Layout

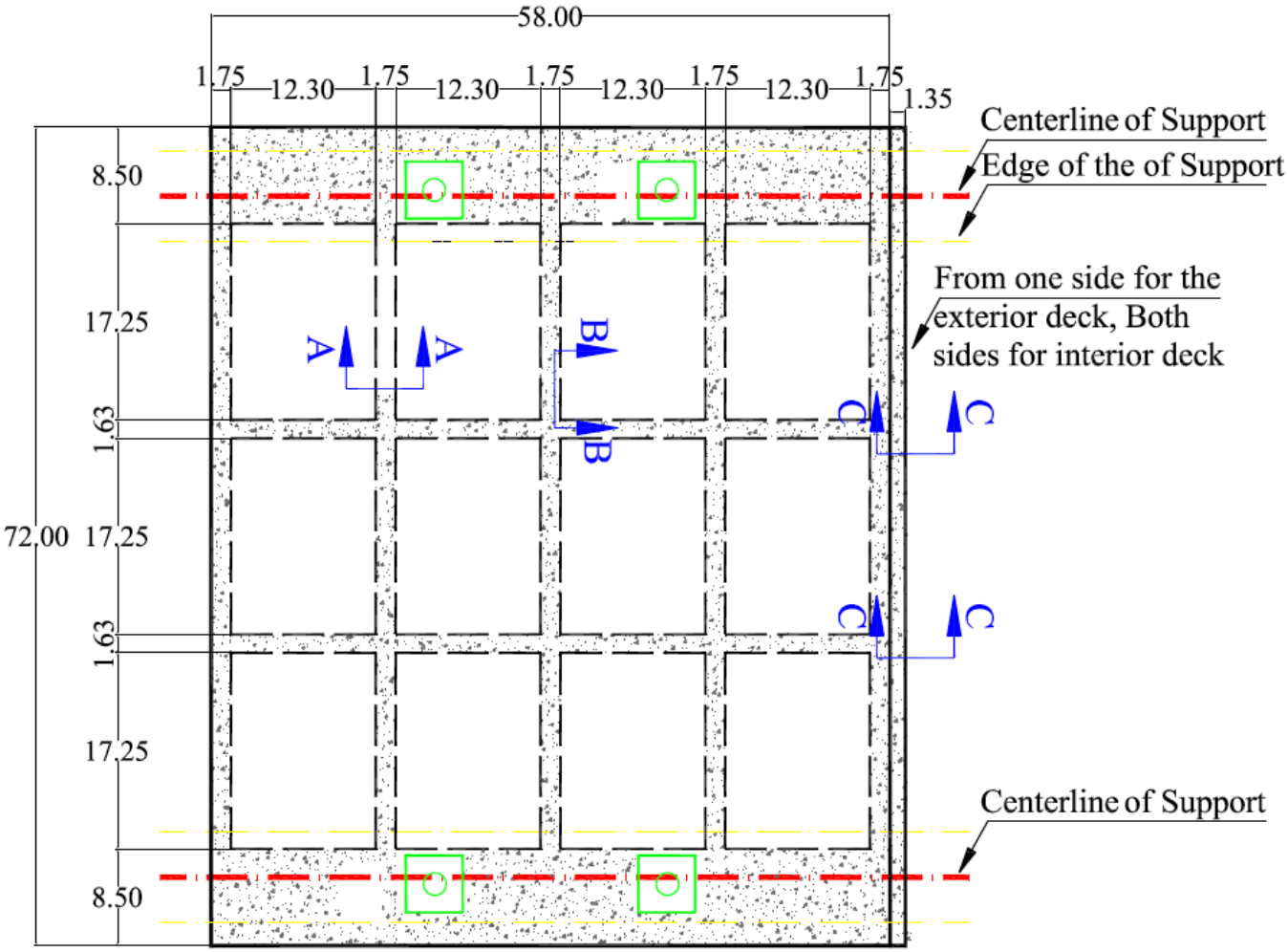

Figure 2.39 Panel 1 (UHPC-HSS)

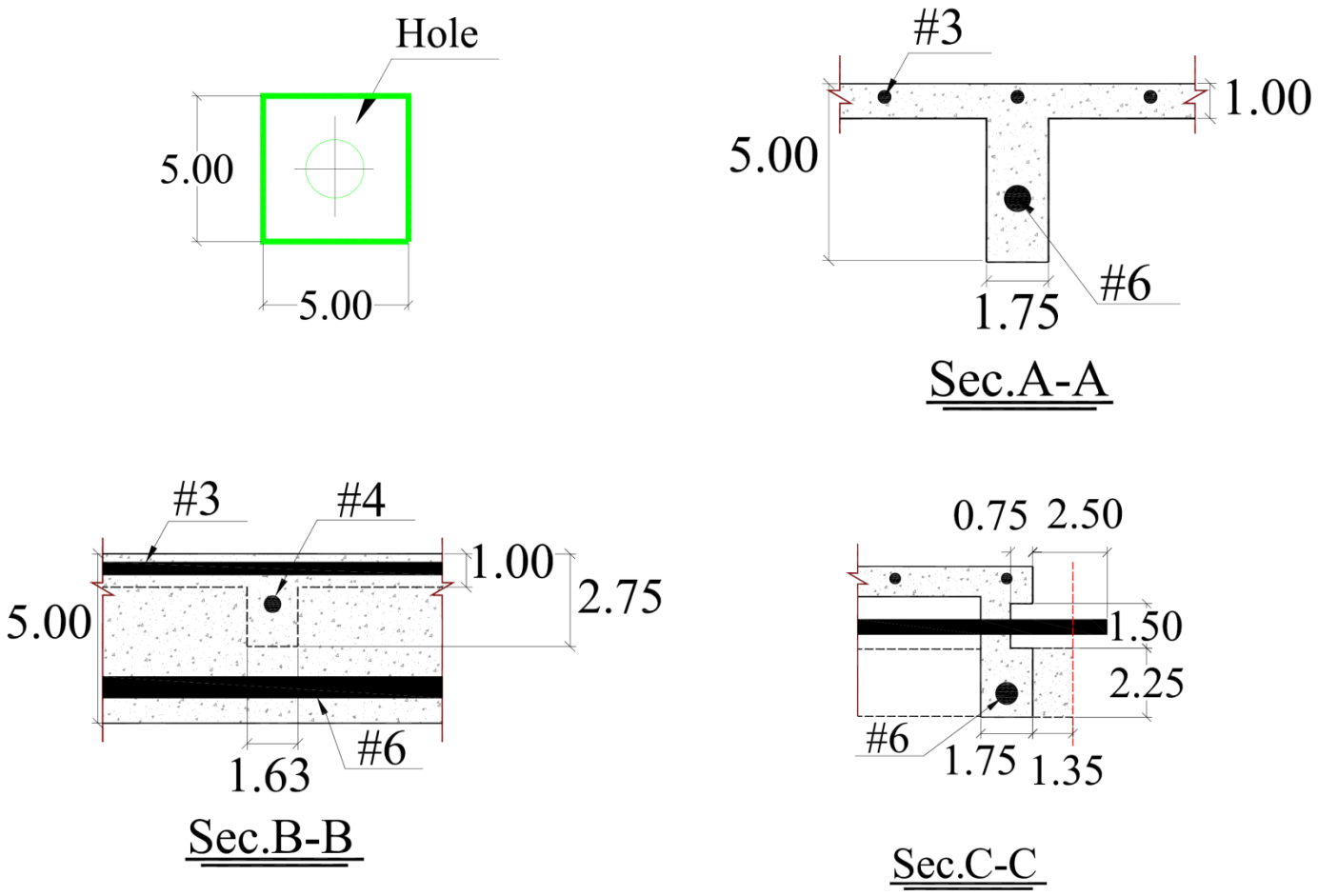

Figure 2.40 Detail of Panel 1 (UHPC-HSS)

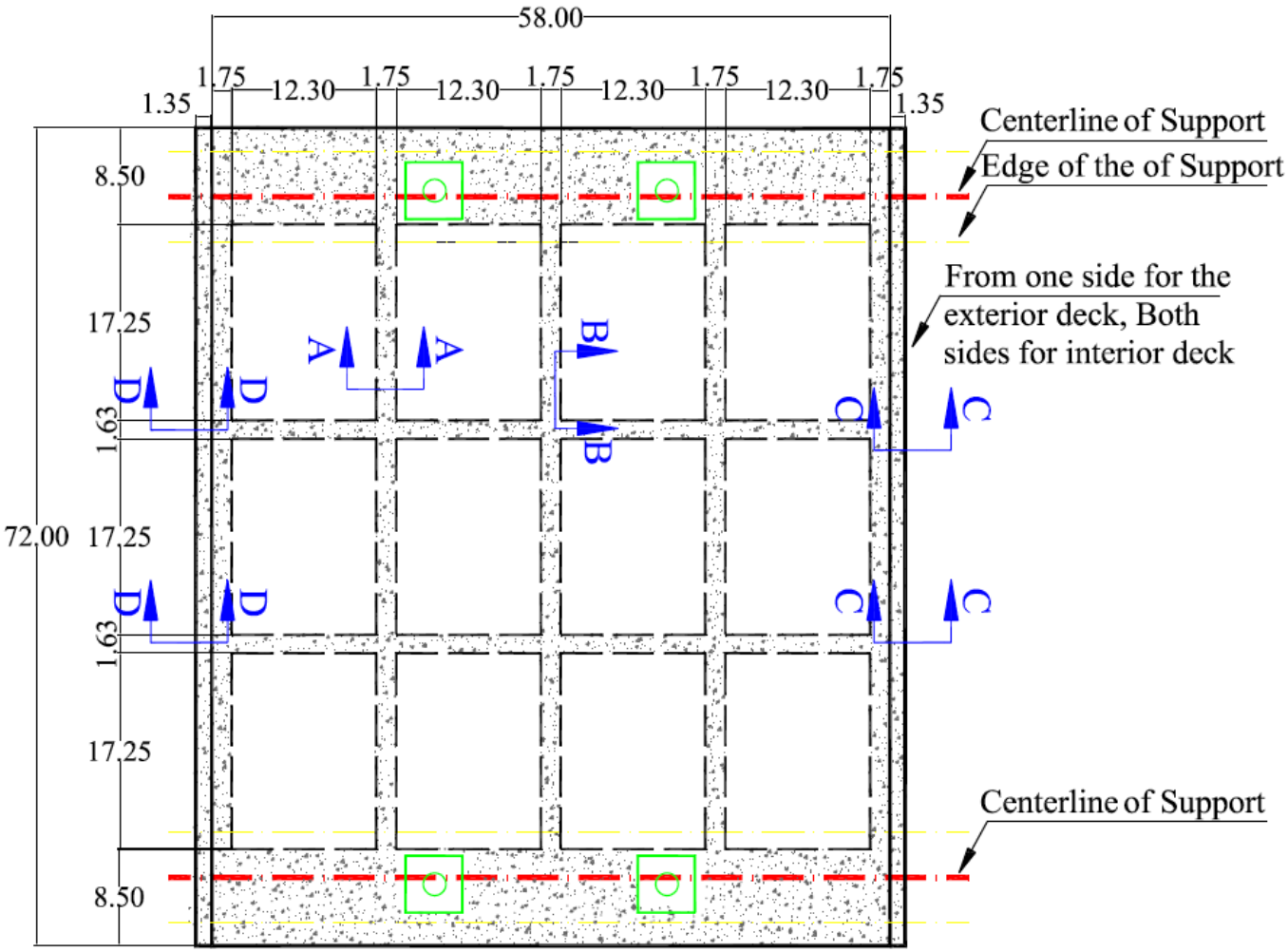

Figure 2.41 Panel 2 (UHPC-HSS)

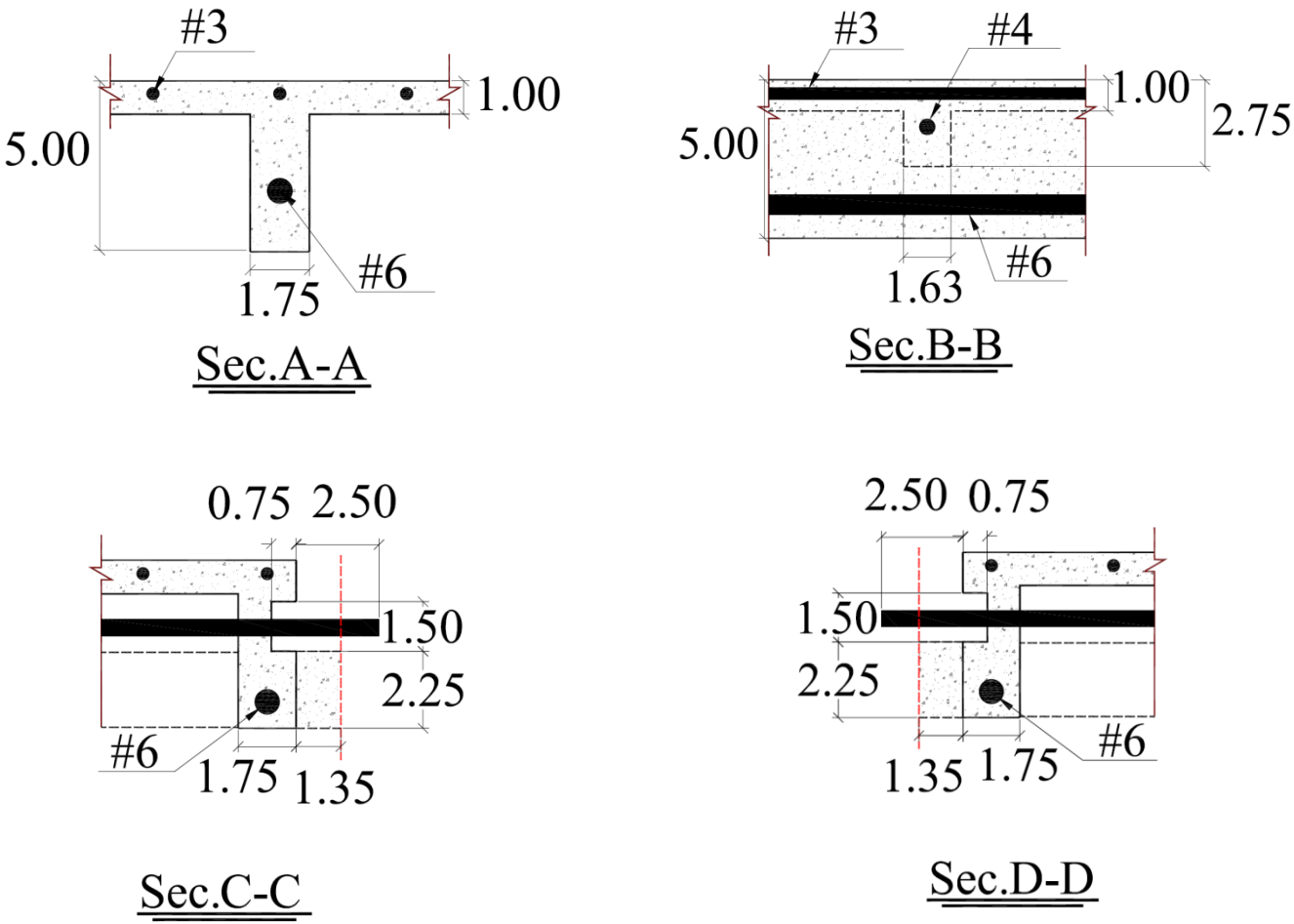

Figure 2.42 Detail of Panel 2 (UHPC-HSS)

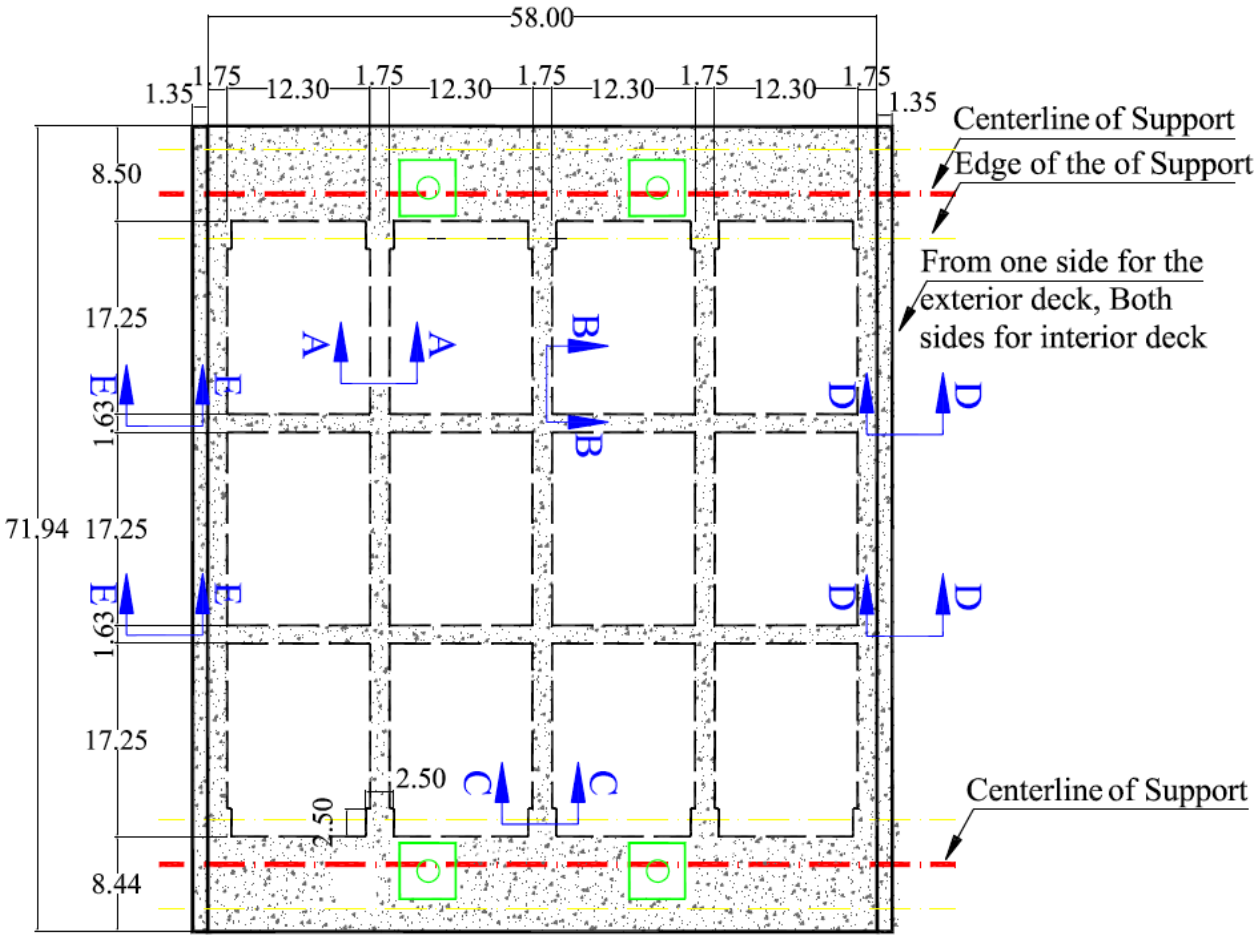

Figure 2.43 Panel 3 (UHPC-CFRP)

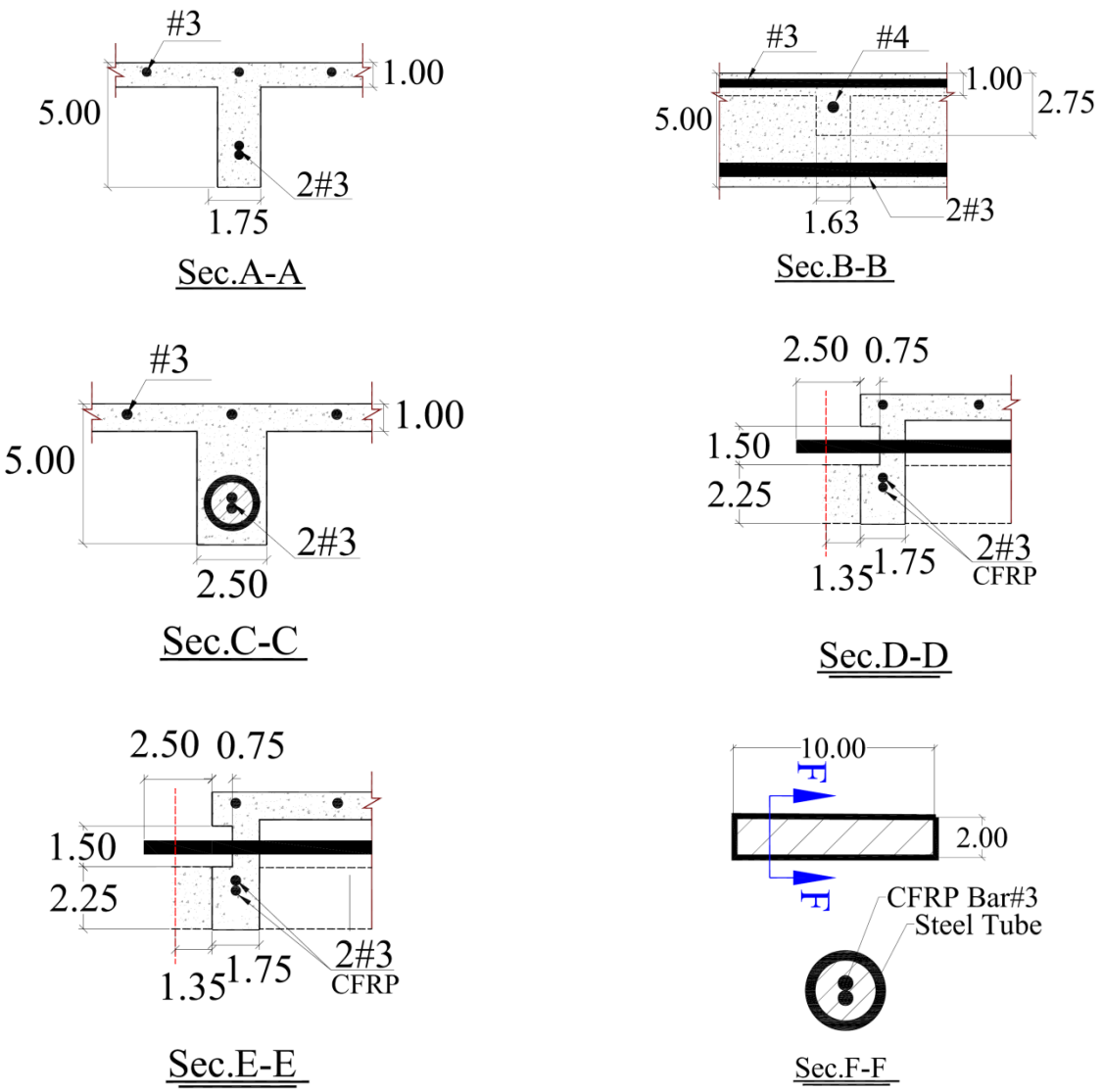

Figure 2.44 Detail of Panel 3 (UHPC-CFRP)

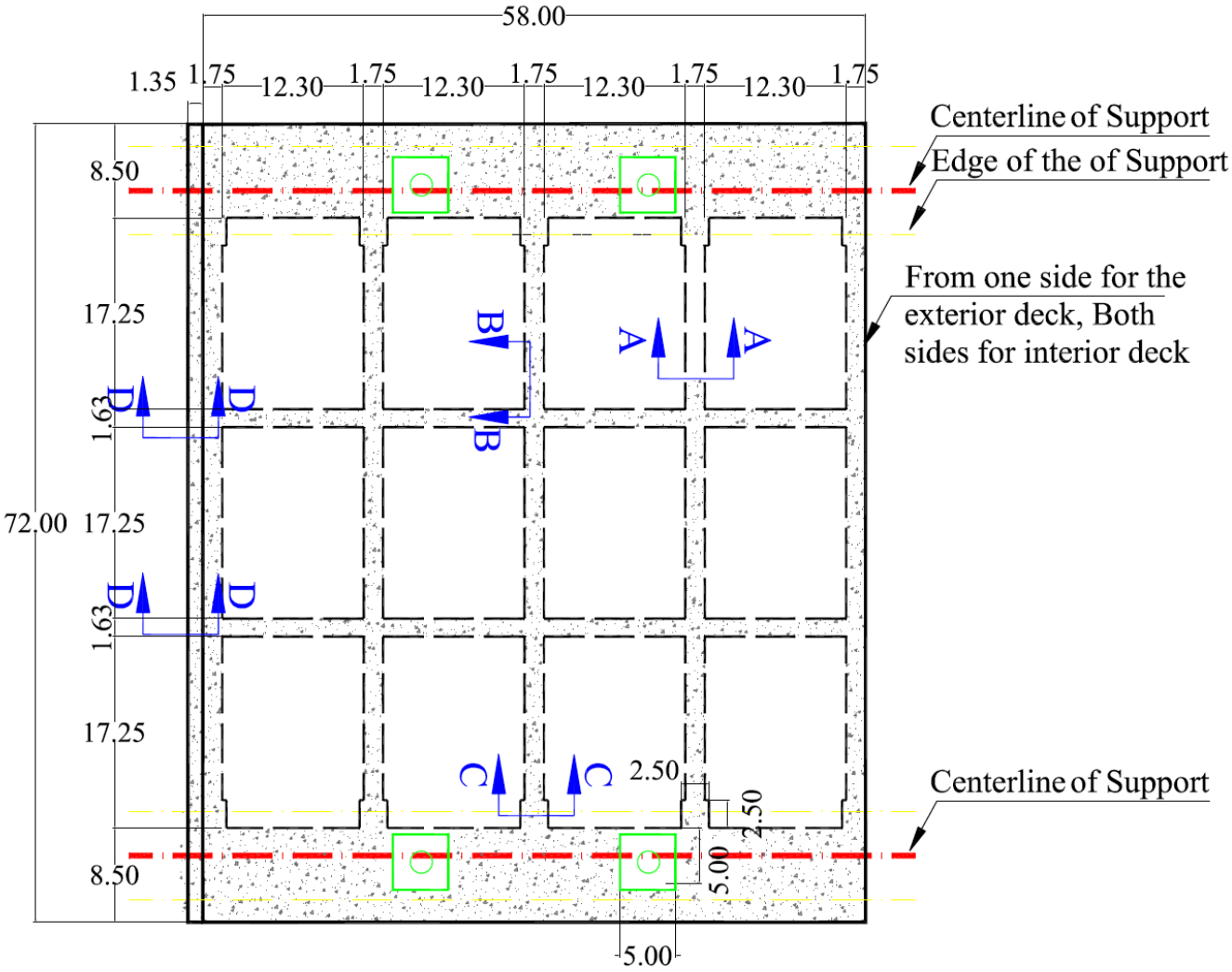

Figure 2.45 Panel 4 (UHPC-CFRP)

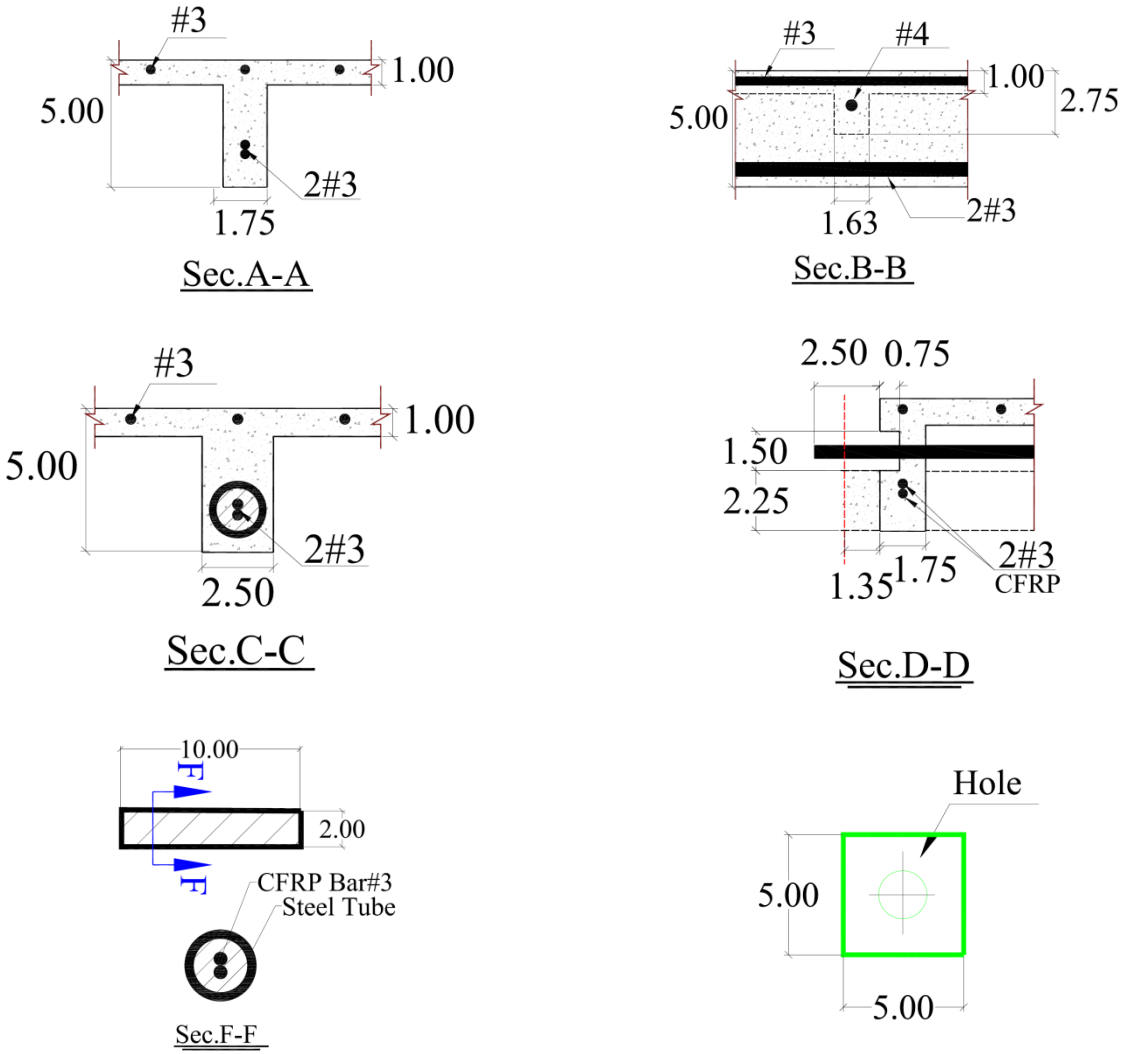

Figure 2.46 Detail of Panel 4 (UHPC-CFRP)

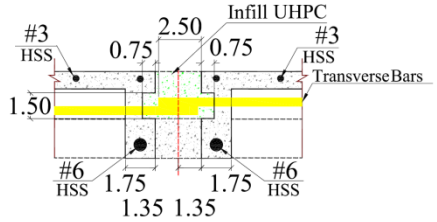

Detail A

UHPC-HSS to UHPC-HSS Connection

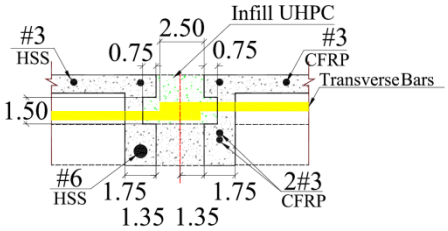

Detail B

UHPC-HSS to UHPC-CFRP Connection

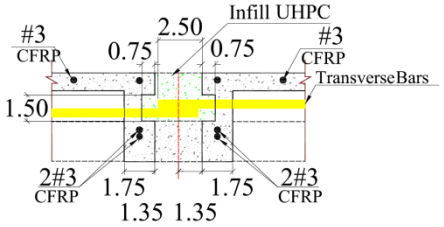

Detail C

UHPC-CFRP to UHPC-CFRP Connection

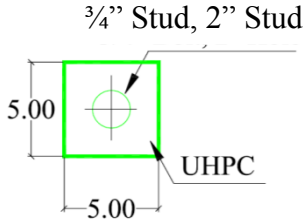

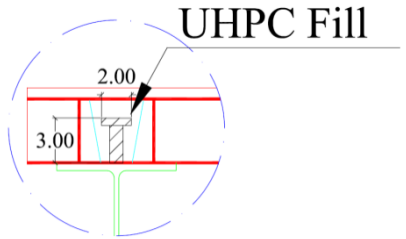

Figure 2.47 Detail of Connections

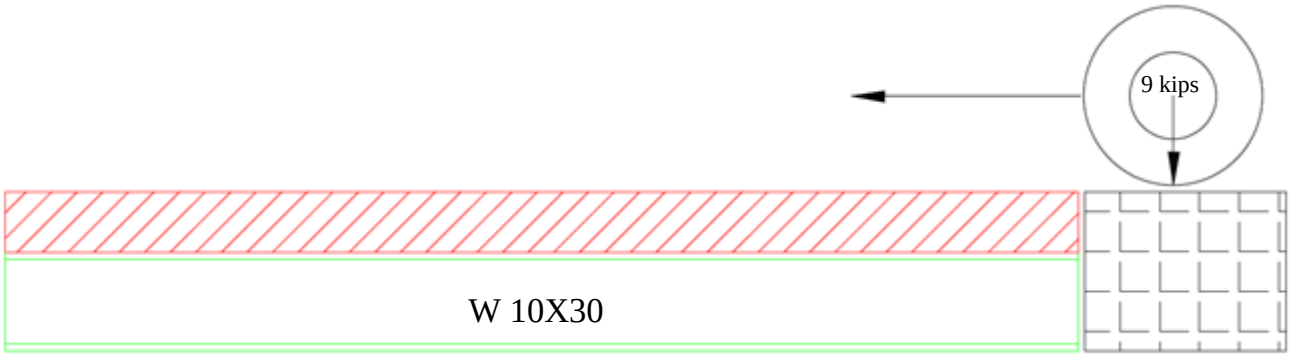

Figure 2.48 Loading Plan

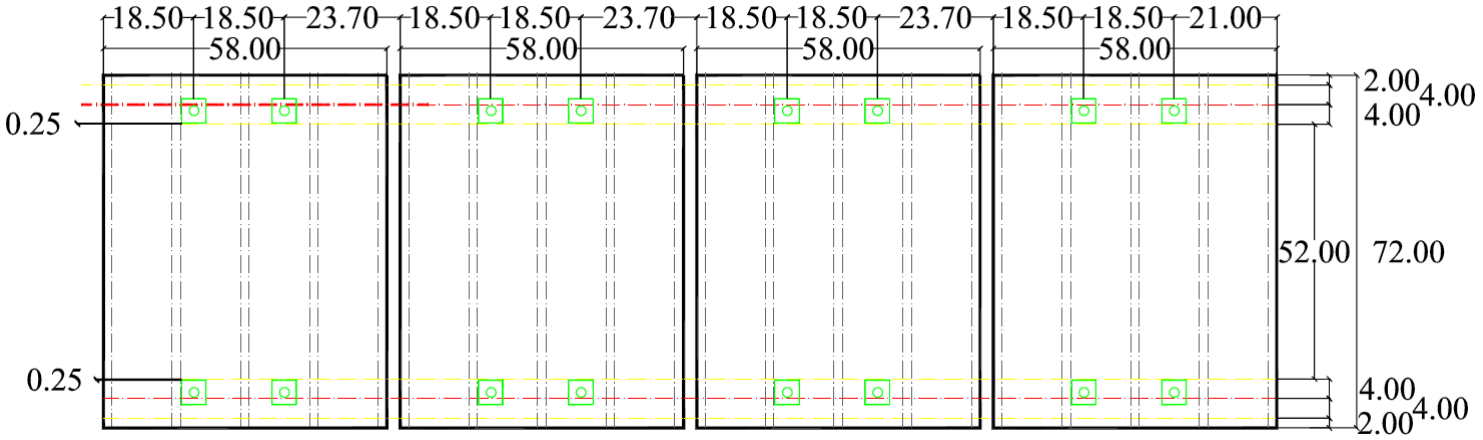

Figure 2.49 Location of Blockouts

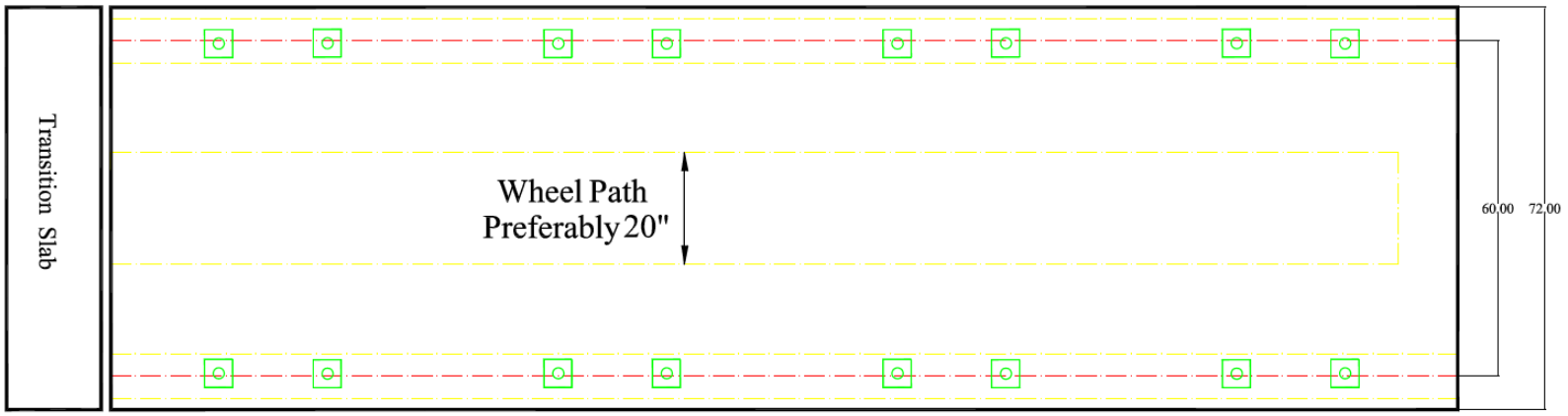

Figure 2.50 Wheel Path Dimensions

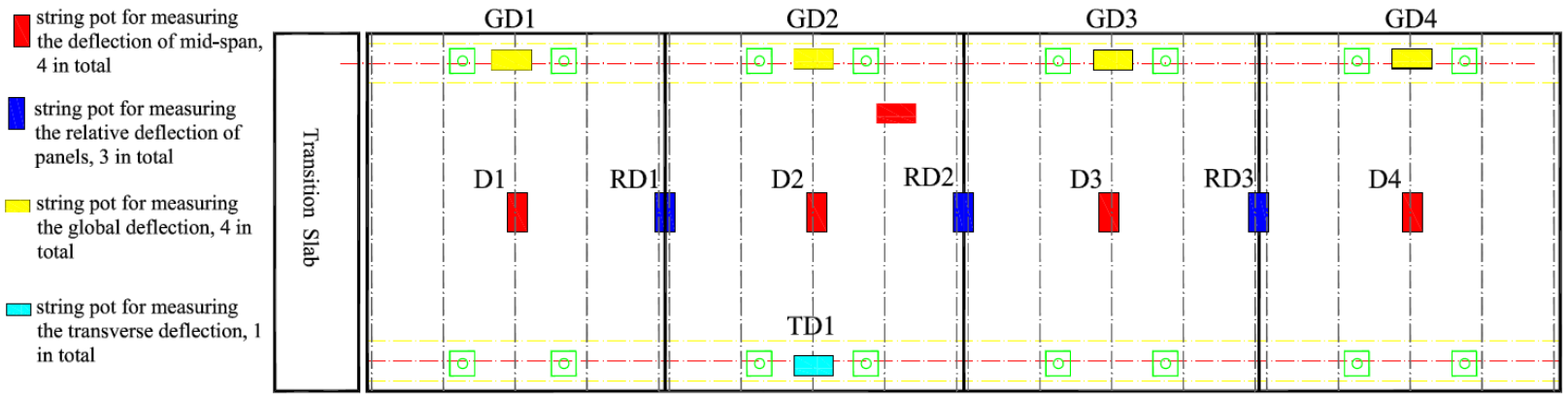

Figure 2.51 Instrumentation Plan (String Pots)

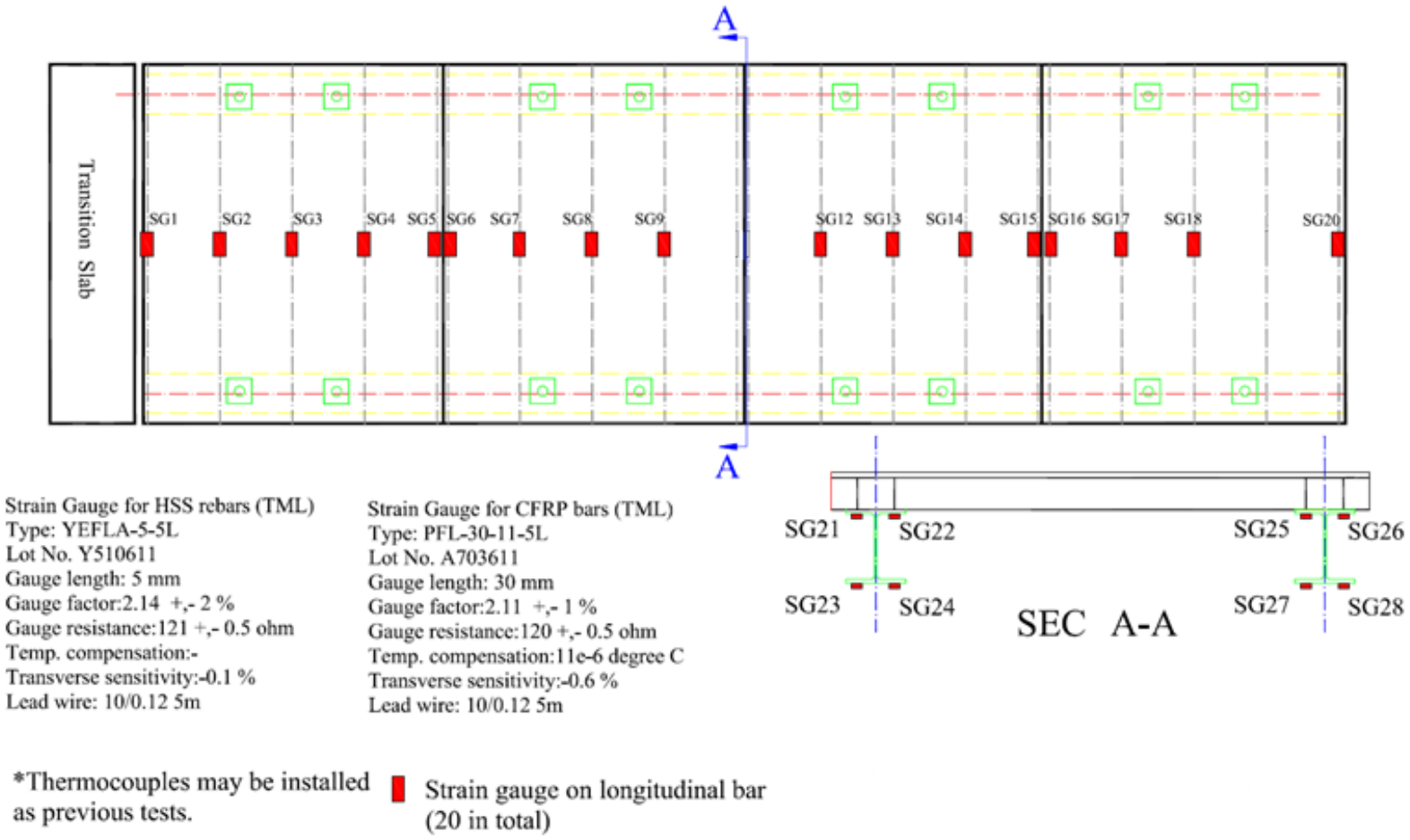

Figure 2.52 Instrumentation Plan (Strain Gauge)

2.5.4.1 Test Results and Discussion

In this chapter the test results for UHPC-HSS panels are presented. The results for panels with CFRP reinforcement are shown in chapter 3.

Figure 2.53 shows the strain responses of HSS bars vs. number of truck passages. According to the test results, the maximum strain recorded was 0.00039 which was significantly smaller than the yield strain of HSS bar, as 0.004.

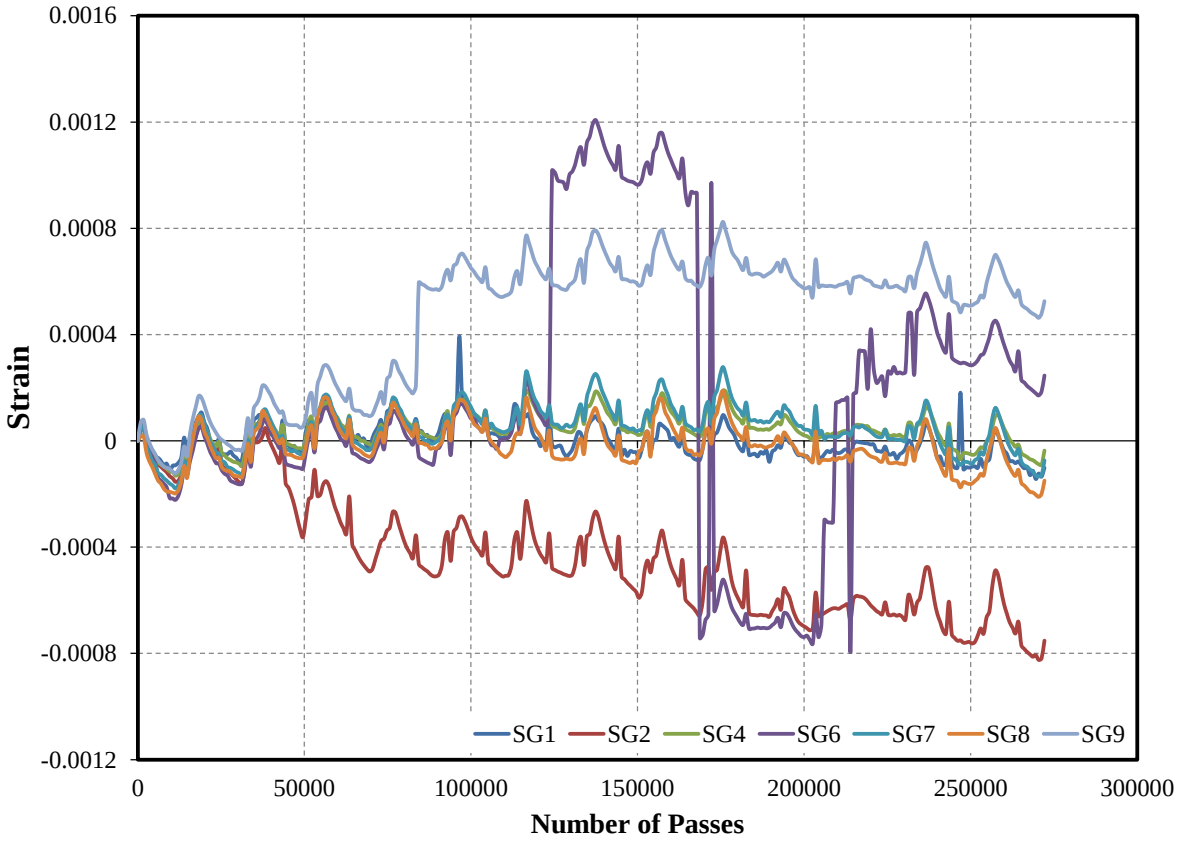

Figure 2.53 Strain Responses of HSS Bars vs. the Number of Truck Passages

Figures 2.54 and 2.55 represent the defection at the middle of each panels vs. the number of truck passages. The maximum deflection recorded for UHPC-HSS panels was 0.066 in. Comparing to the prior static test (3rd phase of testing on 5 ft. panels at FIU) results the deflections of the panels under APT was fairly lower. This phenomenon could be considered as a result of three reasons. First of all, there is an increase in the thickness of the slab from ¾ in. to 1 in. Secondly, the connections between the panels enhanced the overall performance of the bridge deck by benefiting the better load distribution as compared to a single panel deck. At last, the blockouts which used to connect the bridge deck to the stringers made the supports slightly fixed comparing to the pinned-pinned supports in the previous phases.

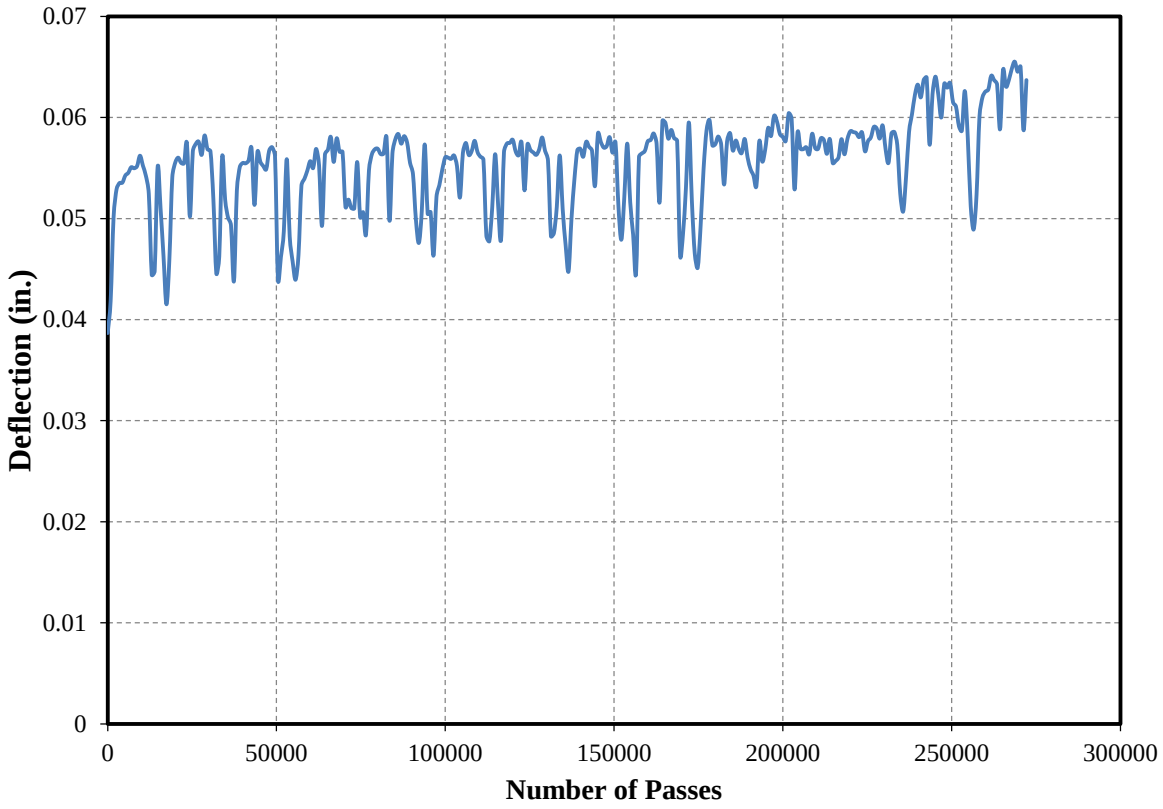

Figure 2.54 Deflection of Panel1 (D1) vs. the Number of Truck Passages

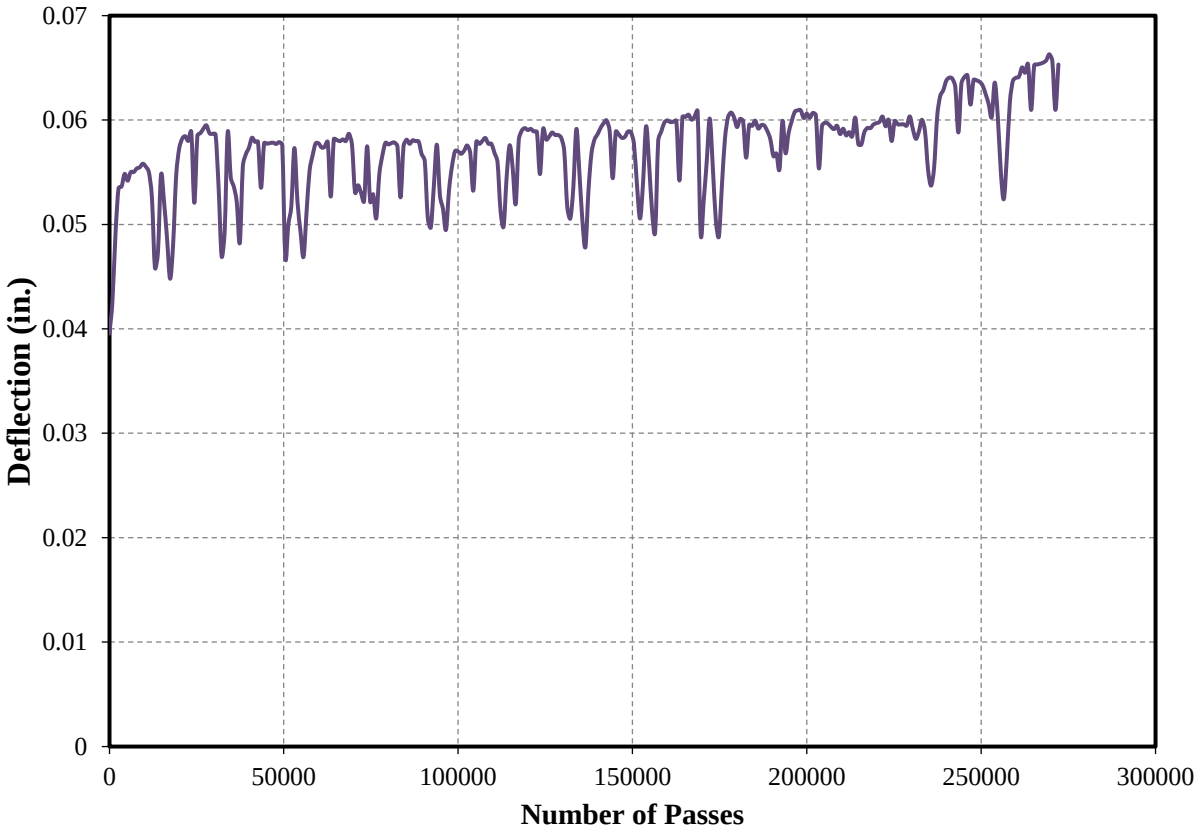

Figure 2.55 Deflection of Panel2 (D2) vs. the Number of Truck Passages

The joint deflection between panels 1 and 2 is illustrated in the Figure 2.56. According to the curve, the maximum joint deflection between the UHPC-HSS panels recorded as 0.06 in. which is slightly less than the maximum deflection at the mid-span of UHPC-HSS panels.

Figure 2.57 shows the deck after the test. As seen in the Figure 2.57(b), some minor cracks were observed. Also, Figure 2.57(c) presents the cracks formed on the top of the panel 2 (UHPC-HSS Panel) followed by a close up view of the cracks in Figure 2.57(d). The average crack width measured was 0.015-0.02 inch. Future testing of the deck panels is planned. However, given the strength and durability of UHPC the minor cracks observed do not seem to pose a concern.

Lastly, it is important to note that given the tight tolerances for the reinforcement cover, strict quality control and quality assurance is needed to address any potential fabrication and construction challenge.

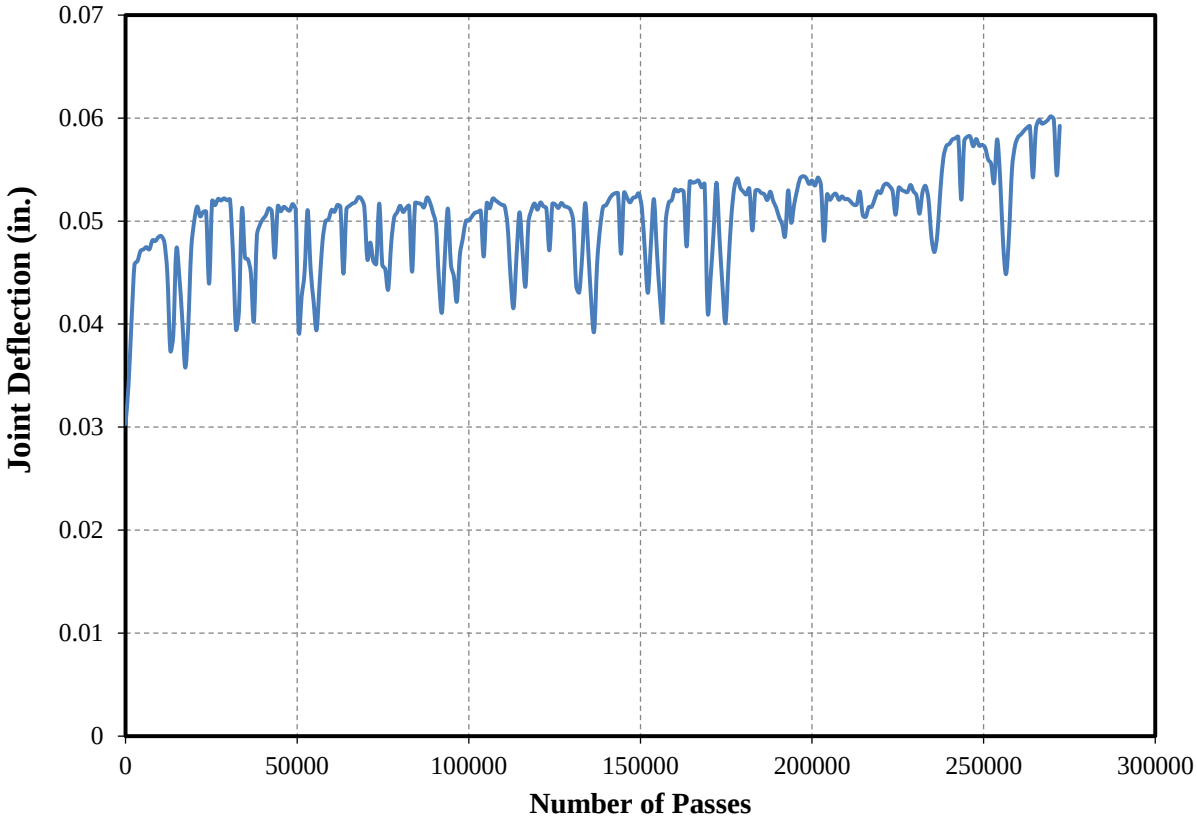

Figure 2.56 Joint Deflection between Panel 1 and Panel 2 vs. the Number of Truck Passages

(a)

(b)

(c)

(d)

Figure 2.57 Deck Status after the APT, (a) Deck Overview, (b) Cracks on the Connection Parts, (c) Cracks on the Top of Panel 2 (d) Close-up View of the Cracks on Panel 2

2.6. Conclusion

A comprehensive experimental study was carried out to develop an optimized lightweight bridge deck system primarily for movable bridges, while it is expected to have extended applications in other bridge deck replacement and widening projects. The objective of the research was to reduce the weight of a recently developed low-profile asymmetric waffle UHPC slab reinforced with HSS rebars. A weight limit of 21 psf was imposed on the bridge deck with a stringer spacing of 4 ft. In a two-step optimization process, both the size and the reinforcement of the deck were modified, reducing the weight by over 37%. Test results showed that the optimized section can suitably meet the load demand and ductility requirements, while staying within the weight limits for movable bridges for 4-ft spacing of the stringers.

The main conclusions of this study are as follows:

1. The proposed deck system fails in a clearly ductile manner, despite its apparent shear failure and in the absence of consistent yielding in steel reinforcement.
2. The proposed deck system is not susceptible to punching shear of its thin slab, due to the arrangement of the primary and secondary ribs, which promotes one-way shear of the primary ribs instead.
3. The load distribution for the center rib in the optimized deck is about 33%, very similar to that observed for the original deeper deck.
4. Minor cracking was observed on panel 2 under HVS; however the overall performance of the panels showed that the strain and displacement values were lower than the criterion.

Chapter-3

A Novel UHPC-CFRP Waffle Deck Panel System for Accelerated Bridge Construction

3.1. Introduction

Fiber reinforced polymer (FRP) is another advanced material with high strength-to-weight ratio and excellent corrosion resistance. An FRP deck weighs 80% less than a comparable reinforced concrete deck (Mu et al., 2006). Chen and El-Hacha (2011) proposed a hybrid UHPC-FRP beam, made up of a pultruded glass FRP hollow box section with a cast-in-place UHPC layer on top and a carbon FRP sheet bonded along its soffit. Saleem (2011) conducted experiments on a hollow core UHPC deck made with pultruded carbon FRP tubes. Both systems showed potential for combining the excellent properties of FRP and UHPC. Frostlechner (2012) studied flexural behavior of a thin-walled UHPC-GFRP hollow rectangular section, and subsequently made a strong case for combining UHPC with FRP shapes or FRP reinforcement to fully utilize the benefits of the two advanced materials.

The present study expands the work of Aaleti et al. (2011) and Heimann (2013) on UHPC waffle deck with mild steel reinforcement and the work of Saleem et al. (2011) on low-profile UHPC waffle deck with HSS reinforcement, by (a) significantly reducing the depth and weight of the panels, and (b) replacing the steel reinforcement with carbon FRP (CFRP) bars. It is believed that not only the ultra-high strength of UHPC is best matched with the high strength of CFRP reinforcement for an efficient system, but more importantly, the ductile behavior of UHPC can help mask the linear elastic response of CFRP reinforcement and result in an overall ductile system. This is the first time that UHPC and CFRP reinforcement are combined in an ultra-lightweight super shallow waffle deck for bridge applications. The issues of consideration from the design and constructability perspectives include strength and stiffness, bond and development length for the reinforcement, punching shear and panel action. A series of experiments are conducted to help address these issues for the development of this new type of bridge deck.

3.2. Experimental Work

As depicted through a three-dimensional perspective in Figure 1, the proposed waffle deck consists of a very thin slab with primary ribs perpendicular to the direction of traffic, and shallower and less frequent secondary ribs in the direction of traffic. In order to study the behavior of the deck, two groups of specimens were investigated; single-rib and multi-rib specimens. The experiments also aimed at finding the optimal depth of the panels. Given the size of the specimens, it was important to assess the bond and development length of CFRP bars with UHPC, and if needed, provide appropriate anchorage device.

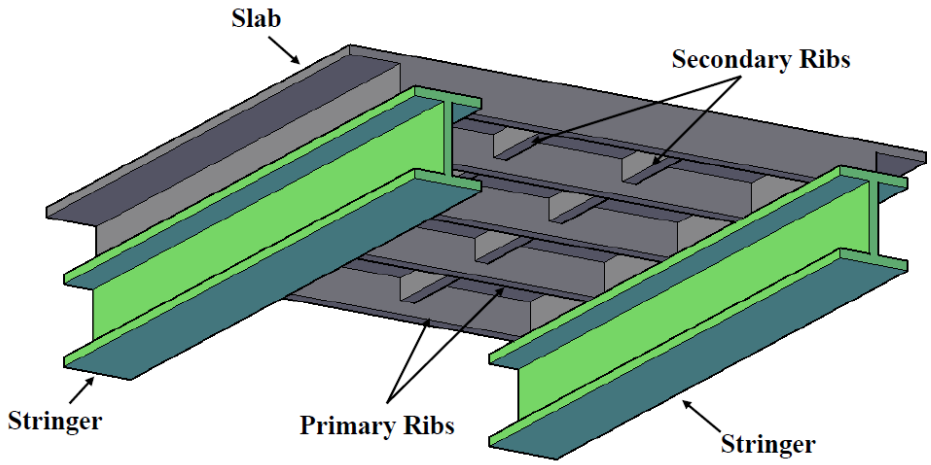

Figure 3.1 Schematic of the Proposed UHPC Waffle Deck System

3.2.1. Test Matrix and Specimen Preparation

Table 3.1 shows the test matrix for this study with two groups of specimens made and tested in two consecutive phases. The specimen names include number of ribs (T), number of spans (S), specimen depth and sample number (if more than one). Group 1 consisted of four single-rib specimens tested in a simple-span configuration, with two identical samples for each of the two depths of 4 and 5 inch (see Figure 3.2). Group 2 included three specimens, all with the same depth of 4 inch, but in three different configurations; single-rib simple-span, single-rib two-span, and multi-rib simple-span (see Figure 3.3). The multi-rib specimen featured 2¾ inch deep transverse ribs to help with load distribution among primary ribs. For comparison, the table also shows three groups of UHPC waffle deck specimens with HSS reinforcement tested in previous studies (Saleem et al., 2011).

Table 3.1 Test Matrix

Group	Specimen Name& Graph Label	Test Phase	Overall Depth (in.)	Rib Spacing (in.)	Slab Thickness (in.)	Unit Weight (psf)	28-Day UHPC Compressive Strength (ksi)	Flexural Reinforcement	
								Slab	Primary Rib
UHPC-CFRP									
CFRP-1	1T1S-4#1	1	4	15	¾	18.80	24	No. 3	No. 4
	1T1S-4#2	1					24		
	1T1S-5#1	1	5			21.30	24		
	1T1S-5#2	1					24		
CFRP-2	1T1S-4#3	2	4	15	¾	18.80	27		
	4T1S-4	2					27		
	1T2S-4	2					26		
UHPC-HSS									
HSS-0[1]	1T1S-5#1	0	5	12	1¼	32.37	18	No. 4	No. 7
	1T1S-5#2	0					27		
	4T1S-5	0					26		
	1T2S-5	0					22		
HSS-1	1T1S-4½#1	1	4½	15	¾	21.72	24	No. 3	No. 5
	1T1S-4½#2	1					24		
HSS-2	1T1S-4#3	2	4	15	¾	20.26	27		
	4T1S-4	2					27		
	1T2S-4	2					25		

[1] Taken from Saleem et al. (2011).

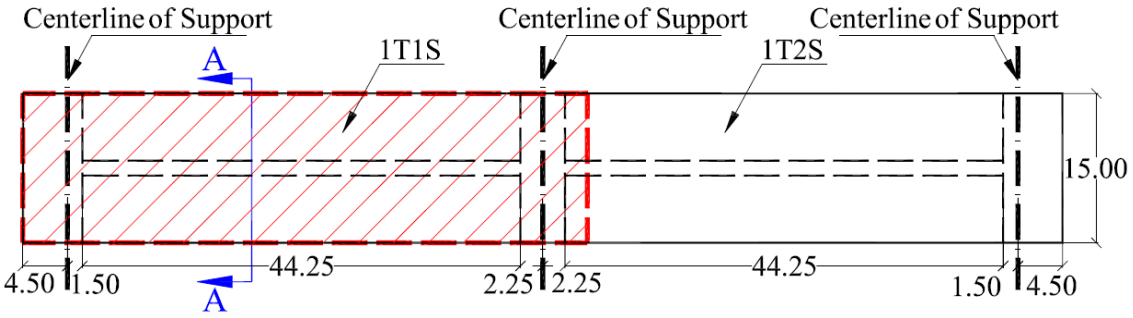

(a)

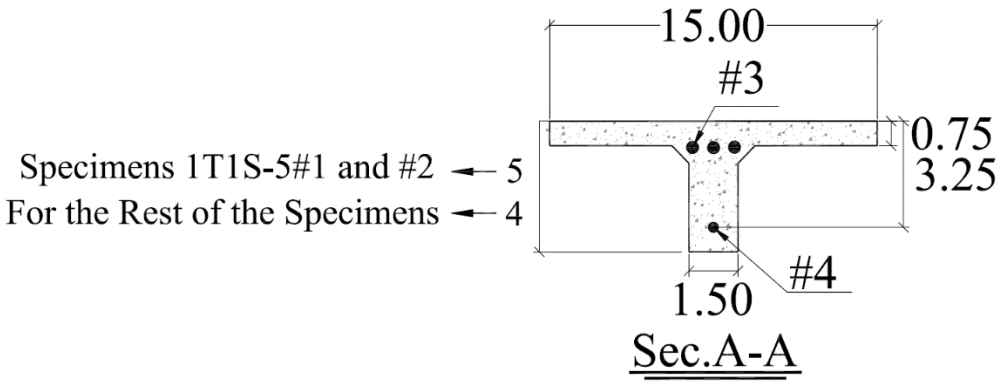

*****All measurements are in inch.

(b)

Figure 3.2 Schematics of Single-Rib Specimens in Simple-Span or Two-Span Configurations: (a) Plan View, and (b) Section

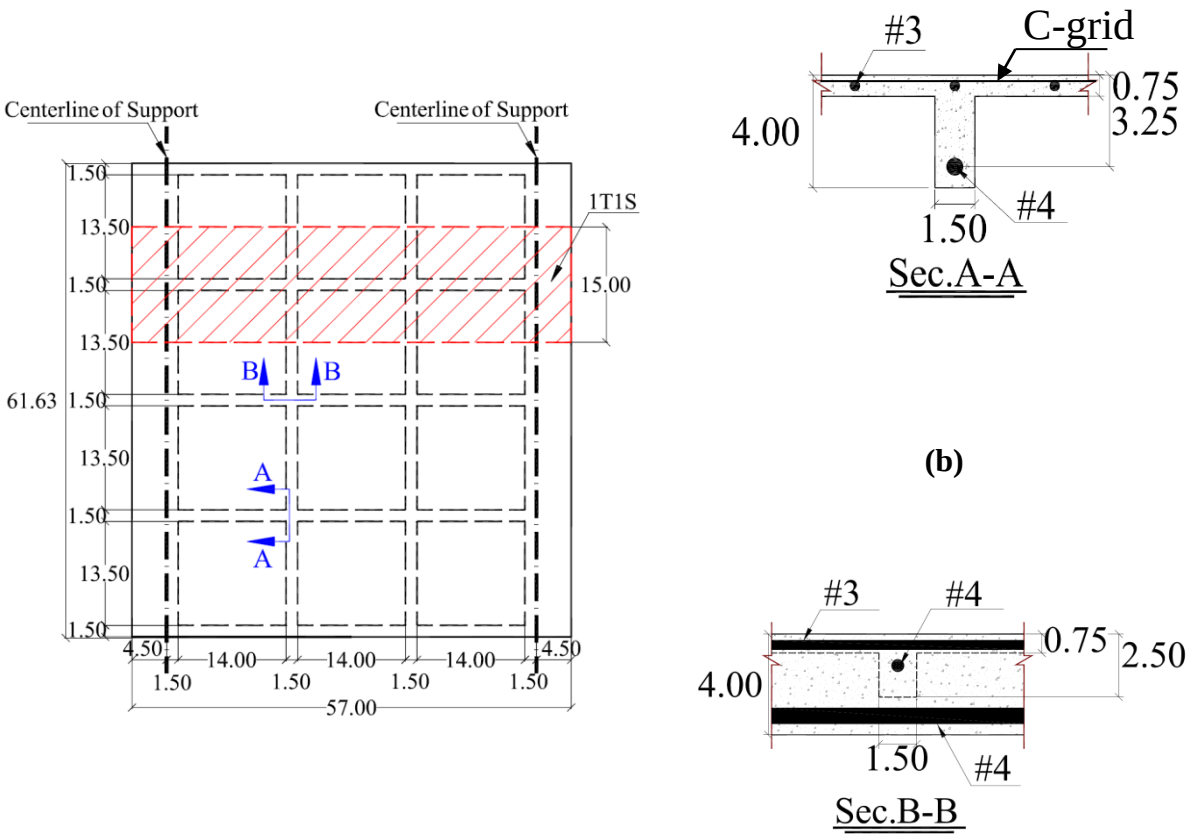

*All measurements are in inch.

Figure 3.3 Schematics of Multi-Rib Simple-Span Specimen: (a) Plan View, and (b) and (c) Sections

Six different batches of UHPC were mixed for casting the specimens in formwork made of Styrofoam and timber (see Figure 3.4). All specimens were air cured in the laboratory for a period of 28 days. Two companion 4 × 8 inch cylinders were used to measure the average 28-day compressive strength of each batch, as shown in Table 3.1.

(a)

(c)

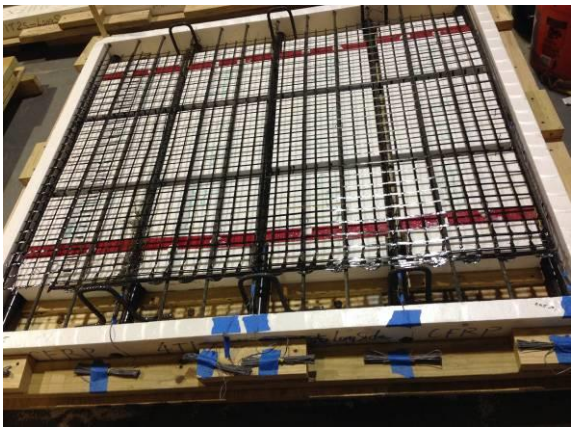

(b)

(d)

Figure 3.4 Specimen Preparation: (a) and (b) Formwork, and (c) and (d) Casting

A C-grid CFRP mesh made by Chomarat of Anderson, SC, was used in the thin slab to improve its load-carrying capacity (see Figure 4b). The mesh has an elastic modulus of 34083 ksi and an ultimate strain of 0.76%. ASLAN 200 CFRP bars made by Hughes Brothers of Seaward, NE, were used as primary reinforcement. A clear cover of ½ inch was maintained for all bars in the main ribs at the bottom. Table 3.2 lists the geometric and material properties of CFRP bars.

Table 3.2 Geometric and Material Properties of CFRP Bars

Nominal Diameter (in)	Cross-Sectional Area[1] (in.^{2})	Nominal Cross-Sectional Area[2] (in.^{2})	Tensile Strength (ksi)	Modulus of Elasticity (psi 10^6)	Ultimate Strain (%)
3	0.121	0.110	315	18	1.75
4	0.201	0.196	300	18	1.67

Note: As reported by the manufacturer.

[1] Cross-sectional area determined by immersion testing, as per ASTM D7205, Section 11.2.5.

[2] Cross-sectional area used in tensile strength calculations.

Figure 3.5 shows the anchorage for the main CFRP bars in the specimens of Group 1 as a series of wrapped unidirectional E-glass fiber fabric (SikaWrap Hex 100G), made by Sika Corp. of Lyndhurst, NJ. The GFRP wrap was impregnated using Sikadur 32 Hi-Mod epoxy resin by the same manufacturer, for a total thickness of ¾-inch. The end surface of the wrap was then ground to facilitate monitoring of the bar slippage. As seen in Figure 3.5b, the anchorage was found insufficient to prevent the slippage of CFRP bar. Therefore, for specimens of Group 2, a more elaborate anchorage system was adopted from Schesser et al. (2013), consisting of a grout-filled steel tube. The tube was sized according to ASTM (2011) with a 10-inch length, 1½-inch outside diameter and ¼-inch wall thickness. The tube was filled with Bustar, an expansive grout made by Demolition Technologies of Greenville, AL. A wooden frame was made to ensure proper alignment of CFRP bars during the grouting process (Figure 3.6a). A gauge length of ¾-inch was used for the bars, with at least ¼-inch of the bar exposed at each end (Figure 3.6b) to help measure slippage. The ancillary tests, as will be described later, showed no bar slippage for this anchorage system.

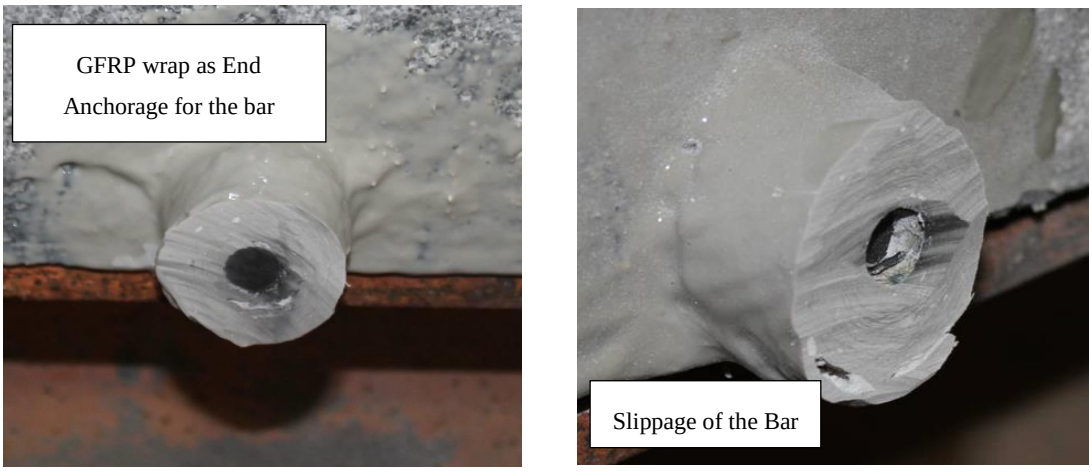

(a) **(b)**

Figure 3.5 Simple End Anchorage System for CFRP Bars in Phase 1: (a) Grinded End, and (b) Slippage of CFRP Bar

The preliminary design of specimens was conducted using a finite element model. The required live load demands, shown in Table 3.3, were calculated using the equivalent strip method and the deck slab design table (AASHTO LRFD 2013) for each group of specimens based on the specimen width, load factors, multiple presence factors, dynamic load allowance, and the loading configuration. It should be noted that a similar approach was used by Aaleti and Sritharan (2014) for the design of their UHPC waffle deck system.

(a)

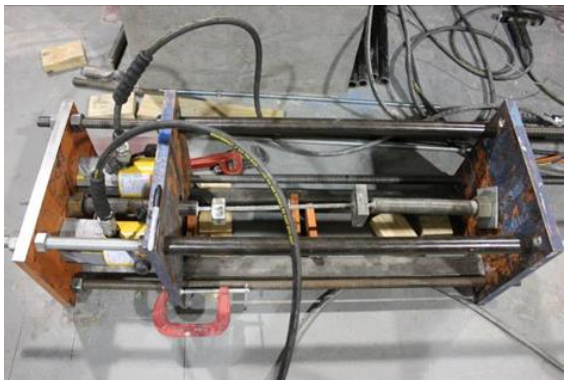

(c)

(b)

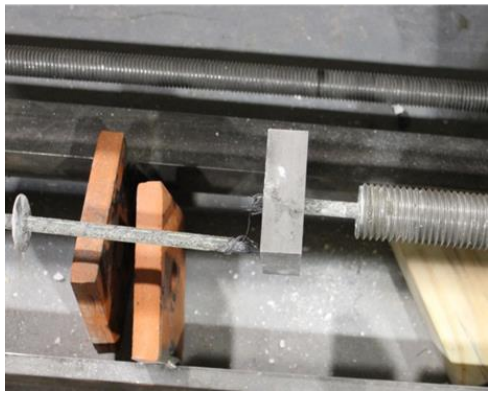

(d)

Figure 3.6 Anchorage System for CFRP Bars in Phase 2: (a) Casting of Expansive Grout, (b) Close-up View, (c) Ancillary Test Setup, and (d) Failure of CFRP Bar

3.2.2. Test Setup and Instrumentation

Figure 3.7a shows the test setup with one of the 1T1S specimens resting on two W24×76 stringers placed at 4 ft. on center on W12×16 floor beams with 3 ft. spacing. This arrangement was designed to simulate the typical superstructure of a movable bridge. The loading patch of an HS20 truck dual-tire wheel (AASHTO LRFD 2013) was simulated using a 10 × 20 inch steel plate over a neoprene pad. Except for the punching shear test, the loading patch was placed at the center of the span and aligned in the direction of traffic. The simple-span specimens were subjected to a single load at their mid-span (Figures 3.7a and 3.7c), while two equal loads were applied concurrently in the middle of both spans in two-span specimen (Figure 3.7b). At the conclusion of its flexure test, the multi-rib specimen was tested for punching shear in between the first and second ribs with the same loading patch (Figure 3.7d).

Several strain gauges were used to monitor responses of CFRP bars and UHPC at critical locations. String pots were also used to measure deflections of the specimen under each rib. Loading was applied using a 230 kips capacity hydraulic actuator, at an average rate of

0.03 in. /min. The data was recorded at a frequency of 1 Hz, and tests were stopped at around 30% load drop, unless preceded by a clear sign of failure.

Ancillary tests were conducted to assess the performance of the anchorage system in CFRP bars of Group 2. Figure 3.6c shows the self-reacting test frame with two 60 kips hydraulic jacks controlled by a single hydraulic pump. The frame was assembled with three 1 inch thick plates of 16 × 24 inch and four No.7 high-strength steel threaded rods.

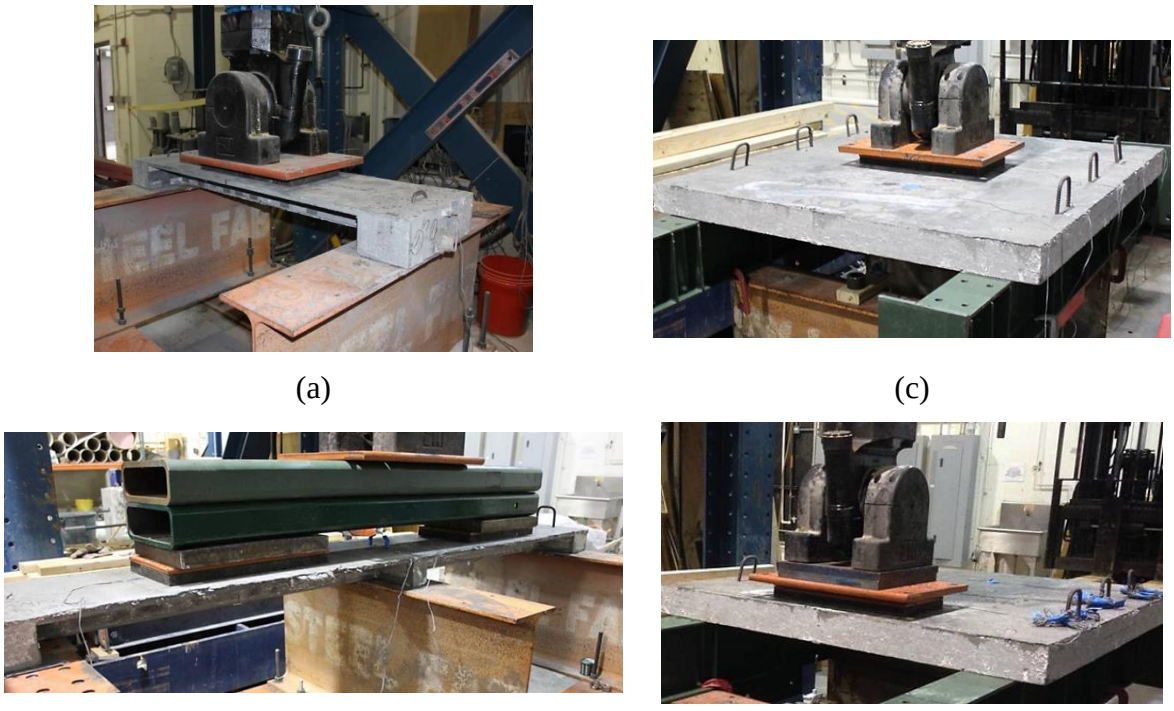

(a) (c)

(b) (d)

Figure 3.7 Setup for Flexure Tests of (a) Specimen 1T1S, (b) Specimen 1T2S, (c) Specimen 4T1S, and (d) Punching Shear Test of Specimen 4T1S

3.2.3. Test Results and Discussion

Table 3.3 shows a summary of test results for the two groups of specimens, as well as results from prior experiments on the UHPC waffle decks with HSS reinforcement (Saleem et al. 2011). The table shows the required live load demand for each group of specimens, along with capacity/demand ratio and capacity/demand per unit weight of the deck panel for each specimen. All specimens met their respective demand loads. In the following sections, test results are grouped together for discussion of each performance metric.

Table 3.3 Summary of Test Results

Group	Specimen Name& Graph Label	Overall Depth (in.)	Service Load Deflection (in.)	Ultimate Deflection (in.)	Ultimate Load (kip)	Demand Load (kip)	Capacity/ Demand	Capacity/ Demand per Unit Weight
UHPC-CFRP								
CFRP-1	1T1S-4#1	4	0.54	1.19	16.77	10.25	1.6	0.09
	1T1S-4#2		0.48	1.06	17.15		1.7	0.09
	1T1S-5#1	5	0.37	1.03	21.49		2.1	0.10
	1T1S-5#2		0.35	0.97	19.56		1.9	0.09
CFRP-2	1T1S-4#3	4	0.45	1.03	18.66		1.8	0.10
	4T1S-4		0.50	0.83	51.26	42.04	1.2	0.06
	1T2S-4		0.19	0.80	26.75	15.65	1.7	0.09
UHPC-HSS								
HSS-0[1]	1T1S-5#1	5	0.06	0.98	40.02	8.21	4.9	0.15
	1T1S-5#2		0.1	0.98	46.99		5.7	0.18
	4T1S-5		0.19	0.79	84.98	34.17	2.5	0.08
	1T2S-5		0.9	1.26	55.08	12.52	4.4	0.14
HSS-1	1T1S-4½#1	4½	0.1	0.83	27.65	10.25	2.7	0.12
	1T1S-4½#1		0.14	0.87	24.73		2.4	0.11
HSS-2	1T1S-4	4	0.15	0.91	22.71		2.2	0.11
	4T1S-4		0.18	0.87	51.48	42.04	1.2	0.06
	1T2S-4		0.07	0.87	44.96	15.65	2.9	0.14

[1] Taken from Saleem et al. (2011).

3.2.3.1 Anchorage of CFRP Bars

Ancillary tests showed the adequacy of the steel tube for the anchorage of CGRP bars, as evident by the rupture of the bar with no slippage (Figure 3.6d). On the other hand, the simple GFRP wraps in specimens of Group 1 did not provide adequate anchorage, leading to premature slippage of the CFRP bars (Figure 3.5b), and affecting the overall deflection (Figure 3.8a) and failure mode of deck specimens. The bar slippage was observed in specimens of Group 1 at about half the ultimate load or 80% of the demand load. Based on data from Table 3.3, the average service-level deflection of Specimens 1T1S-4 in Group 1 was about 15% higher than the similar specimen in Group 2. Also, specimens of Group 1 showed a pronounced shear anchorage failure (Figure 3.8b), as compared to the shear-flexure cracks in similar specimen in Group 2 (Figure 3.8c). The tubular anchorage system effectively increased the stiffness and capacity of the deck, and decreased the corresponding deflection. This behavior was quite similar to that observed for UHPC waffle deck specimens in previous studies with HSS reinforcement that were effectively anchored using 180^{o} hooks (Saleem et al., 2011).

(a)

(b)

(c)

Figure 3.8 Flexure Test and Failure Mode of Specimens 1T1S, (a) Deflected Shape of Specimen 1T1S, (b) Close of View of Beam Shear Crack, and (c) Shear Crack at the Edge of the Loading Pad

3.2.3.2 Flexural Behavior

Figure 3.9 shows the load-deflection responses of the two groups of single-rib simple-span specimens (1T1S) with different depths. For comparison, one response curve is shown for a similar 4-inch deep specimen with HSS reinforcement. The difference in the latter part of the responses for the two identical 5-inch deep specimens may be attributed to the slippage of the bars occurring at two different load levels of 21.60 and 19.11 kips, respectively, and rather prematurely due to the ineffective wrapping of CFRP bars in Group 1. Although all specimens clearly exceeded the required demand load, both the stiffness and capacity of the specimen with HSS reinforcement are higher than those with CFRP. On the other hand, Table 3 shows that UHPC decks with CFRP reinforcement provide a more optimal design solution, given their lower capacity/demand ratio and capacity/demand per unit weight of the deck. Table 3.3 also shows measured deflections for each specimen at the levels of service and ultimate loads. The ratio of these two deflection levels indirectly suggests a reasonable ductility for each deck specimen. Figure 3.10 shows load-strain responses of 1T1S specimens, based on strain gauges attached at the mid-span to the CFRP bar in the primary rib. The figure shows a maximum strain of 0.8%, which is less than half of the rupture strain of CFRP bars. As such, ductile behavior of the specimens is attributed mainly to the dowel action of CFRP bars and the fiber pull-out mechanism in UHPC.

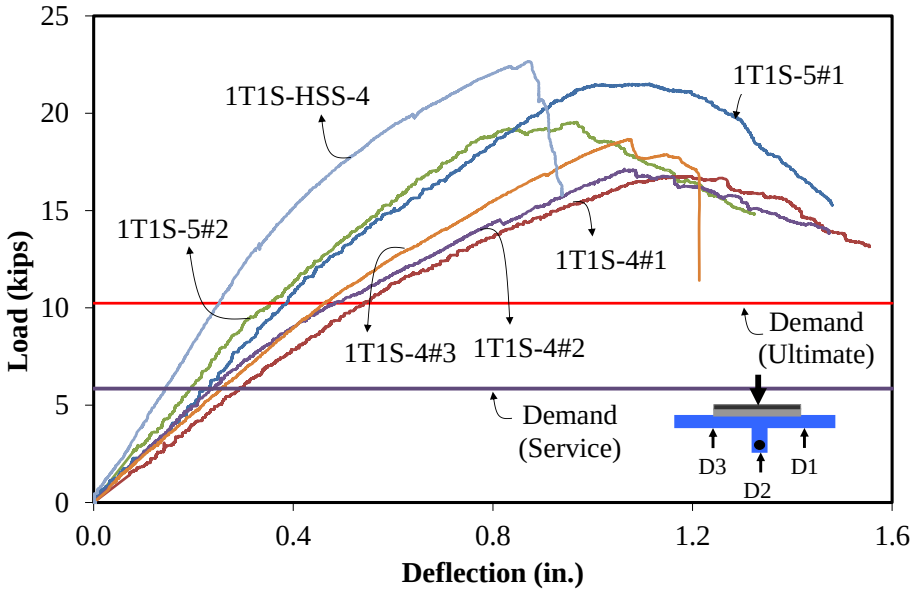

Figure 3.9 Load-Deflection Responses of Specimens 1T1S

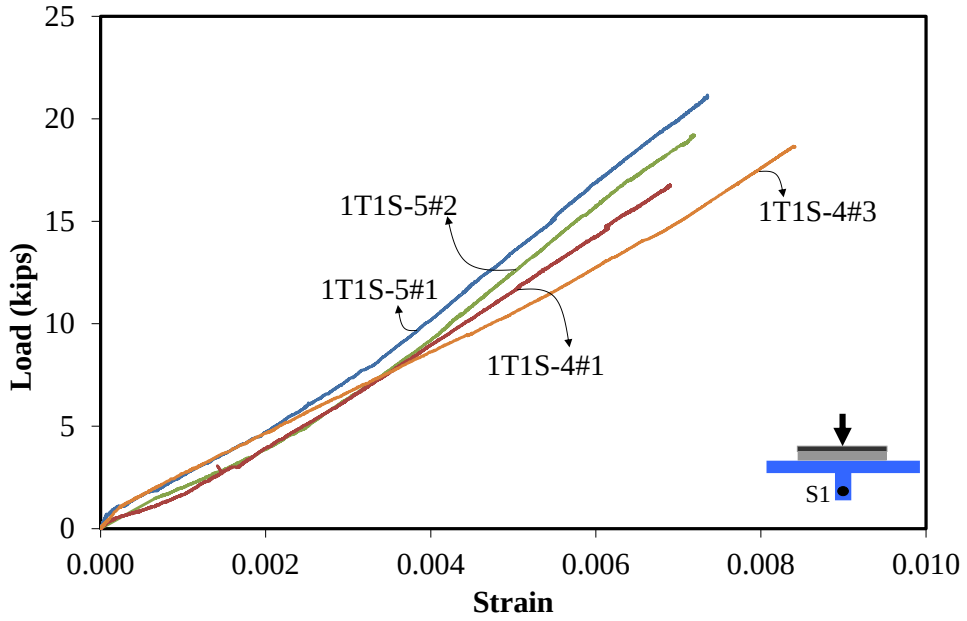

Figure 3.10 Load-Strain Responses of CFRP Bars in Specimens 1T1S

Additional strain gauges were attached to the top surface of the UHPC slab and to the web of the section in order to capture the strain in the UHPC. Test results are shown in Appendix A.

3.2.3.3 Panel Action

Figure 3.11 shows the top and bottom views of the multi-rib simple-span Specimen 4T1S after its flexural test, shown in Figure 3.7c. The failure mode was similar to that observed for single-rib specimens. The cracks appeared in the main ribs under the loading patch, and grew in length and width until failure. Figure 3.12 shows the load-deflection responses under each rib for the same specimen. The failure load at 51.26 kips was about 20% higher than the ultimate demand of 41.81 kips. The ductility and plastic deformation, on the other hand, were considerably larger than that observed for the single-rib specimens. The reason for higher load capacity may be attributed to the presence of additional ribs and their participation in carrying the load through panel action.

For comparison, Figure 3.12 also shows the response curves under each rib for a similar 4 inch deep multi-rib specimen with HSS reinforcement. It is clear both from the figure and from Table 3.3 that the capacity of the multi-rib specimen is the same with either type of HSS or CFRP reinforcement, while the panel with the CFRP bars showed to be more flexible. Load distribution among the ribs may be calculated based on mid-span deflections of each rib or mid-span strains in CFRP bar in each rib. Using either approach, the load distribution among the ribs is found as 33% for the center rib and 22% and 11% for the next two ribs. These factors are quite similar to those for UHPC-HSS specimens, as reported by Saleem et al. (2011).

Figure 3.13 shows load-strain responses of the multi-rib specimen, based on strain gauges attached at the mid-span to the CFRP bar in each rib. The figure shows a maximum strain of

0.6% in the center rib, higher than that observed in single-rib specimens, but still about half of the rupture strain of CFRP bars. Again, the apparent ductile behavior of the specimen may be attributed to the dowel action of CFRP bars and the fiber pull-out mechanism in UHPC. It is clear from both deflection and strain responses in Figures 3.12 and 3.13 that side ribs lose their effectiveness beyond service loads.

(a) (b)

Figure 3.11 Failure Modes in Specimen 4T1S: (a) Top View, and (b) Bottom View

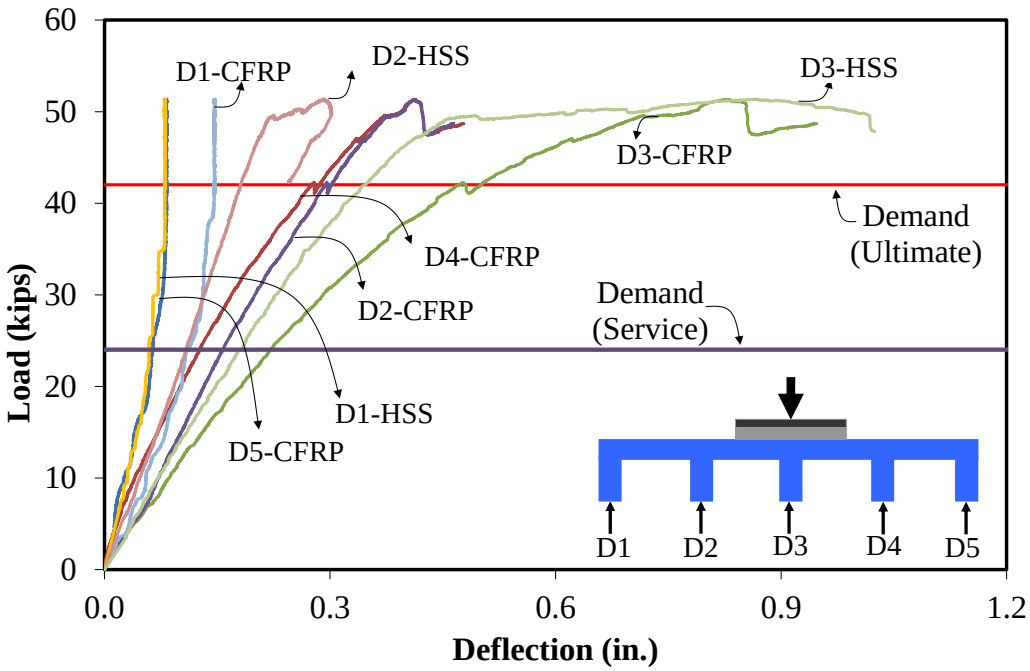

Figure 3.12 Load-Deflection Responses under Each Rib of Specimen 4T1S

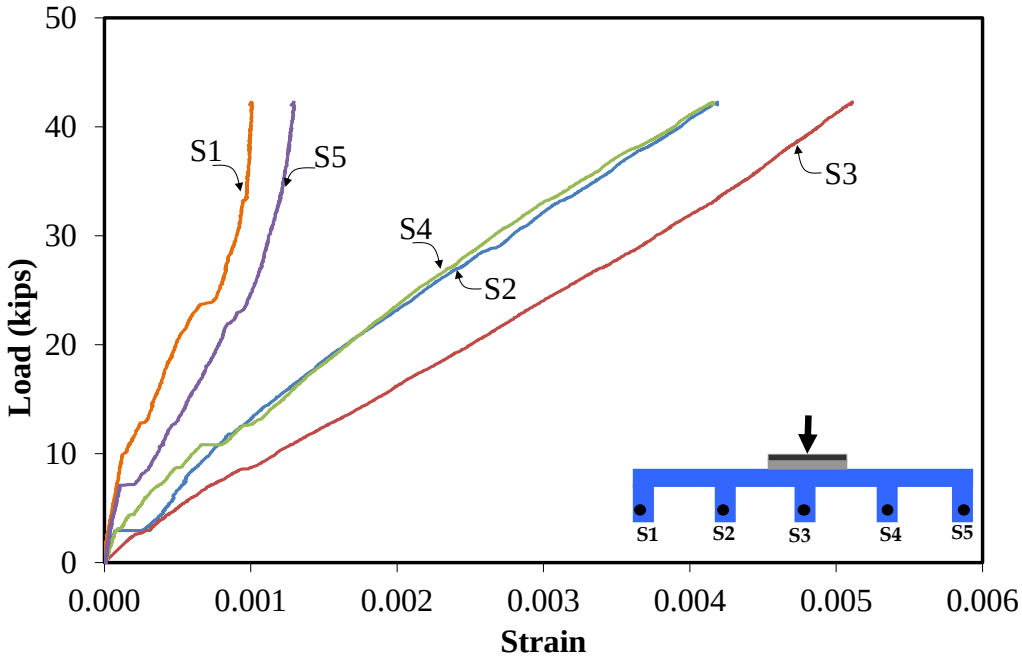

Figure 3.13 Load-Strain Responses of CFRP Bars in Each Rib of Specimen 4T1S

3.2.3.4 Punching Shear

Figure 3.14 shows the punching test and failure mode for Specimen 4T1S at the conclusion of its flexure test, where only the center rib was damaged. The failure was marked by major shear cracks forming in the two ribs adjacent to the loading patch, with no sign of punching. The load-deflection responses under each rib are shown in Figure 3.15, with the maximum deflection occurring right under the loading patch in between the two loaded ribs. It should be noted that the capacity of the specimen under the asymmetric punching was 32.15 kip, which is only 60% of its capacity under symmetric flexural loading (51.25 kip), primarily because of lack of contribution from adjacent ribs that were either damaged or away from the loading patch. Figure 3.15 also shows the response curves of a similar 4-inch-deep multi-rib specimen with HSS reinforcement, with clearly higher stiffness and capacity, as compared to UHPC-CFRP deck.

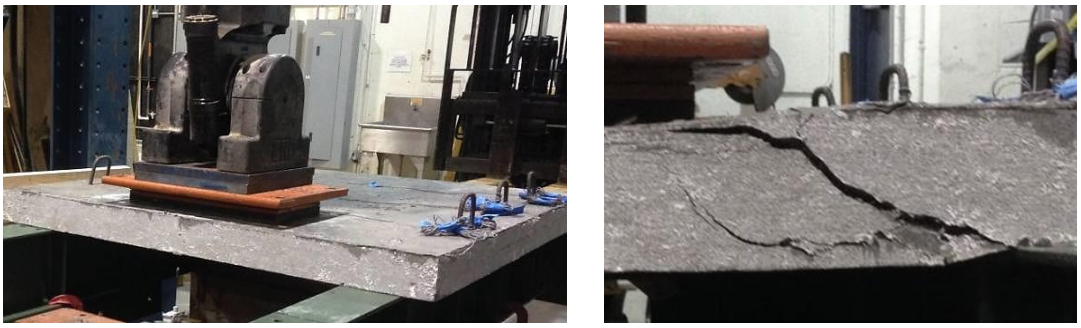

Figure 3.14 Punching Shear Test and Failure Mode in Specimens 4T1S

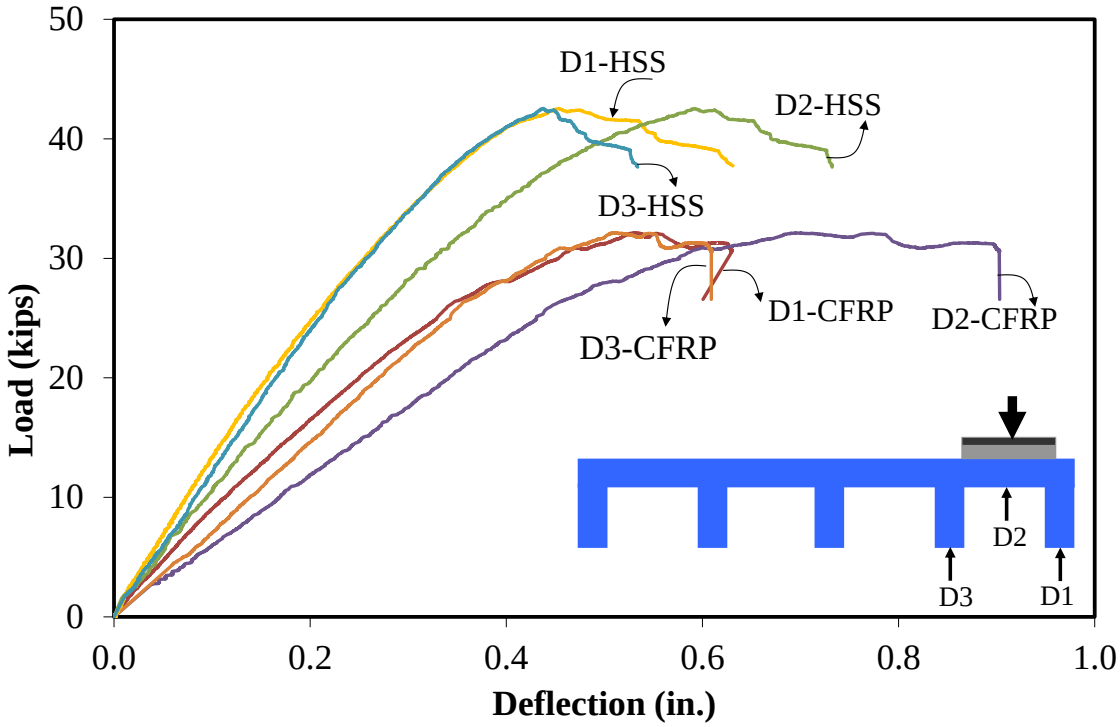

Figure 3.15 Load-Deflection Responses of Specimen 4T1S in Punching Shear

3.2.3.5 Continuity Effect

The behavior of the deck system in negative moment region was investigated by testing a single-rib two-span specimen, as shown in Figure 3.16. Shear in the main ribs near the support was seemingly the predominant mode of failure, similar to that observed in simple-span specimens. The shear cracks initiated in the web in one span and moved towards the top slab. Figure 3.17 shows the load-deflection responses of the specimen along with those of a similar specimen with HSS reinforcement. At 26.75 kips, the capacity of the specimen with CFRP reinforcement was 70% higher than the required demand of 15.65 kips, although only 60% of the capacity of similar specimen with HSS reinforcement (i.e., 44.96 kips). Both types of reinforcement resulted in a ductile response for the deck. It is also noteworthy that the capacity of Specimen 1T2S was 26.75 kips or 43% higher than that of Specimen 1T1S at 18.66 kips, which may be attributed to the continuity effect. Figure 3.18 shows the load-strain responses of the CFRP bar at the middle of both spans. The maximum strain is about 1/3 of the rupture strain of the CFRP bar.

Table 3.3 lists the deflection of Specimen 1T2S at the level of service load as 0.19 inch, which corresponds to L/254, where L = center to center spacing of stringers, which was 4 ft. Considering a modification factor of 0.74 comparing the deflections of two-span and five-span decks under two wheel loads, the modified deflection becomes L/343, which is about twice the deflection limit of L/800 (AASHTO LRFD 2013). It should be noted that continuity effect remains constant beyond five spans. It is also noteworthy that UHPC deck with HSS reinforcement has a modified deflection of L/914.

(a) (b)

Figure 3.16 Failure Mode of Specimen 1T2S: (a) Deflected Shape, and (b) Shear Crack

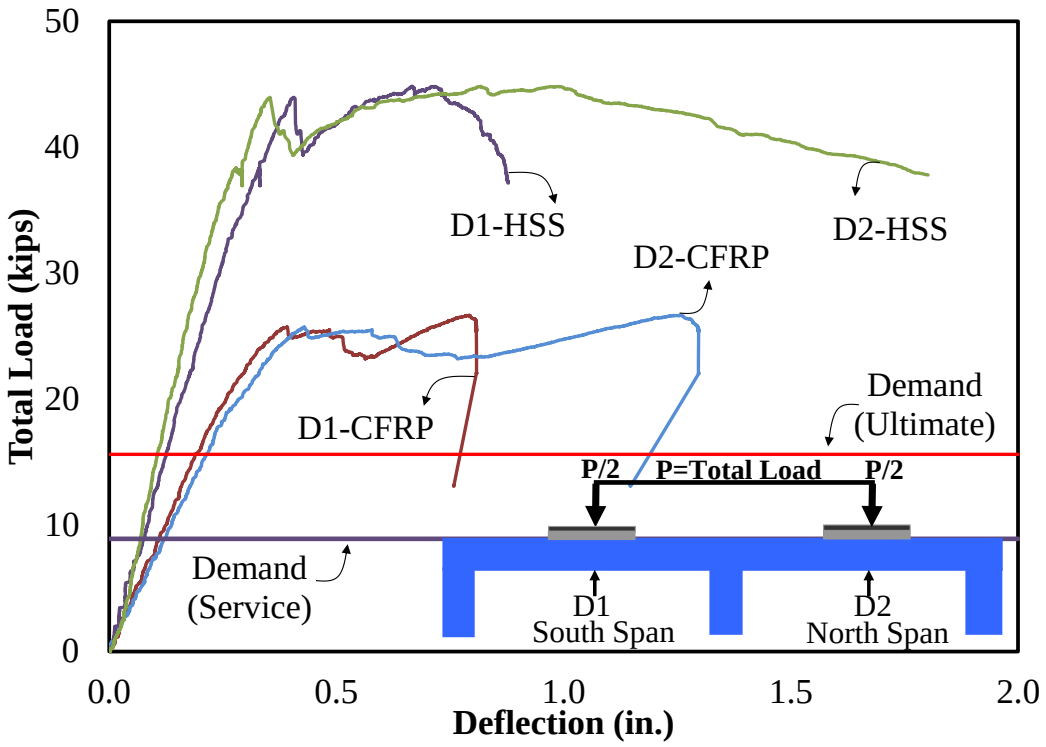

Figure 3.17 Load-Deflection Responses of Specimens 1T2S

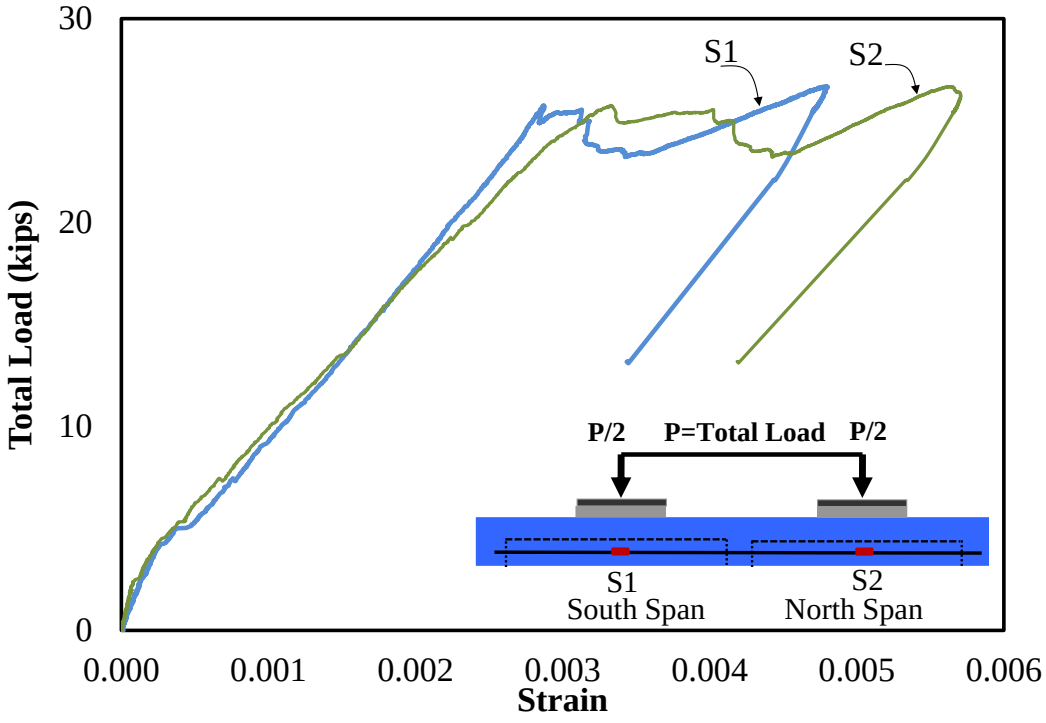

Figure 3.18 Load-Strain Responses of CFRP Bar in Specimen 1T2S

3.3. Finite Element Modeling

3.3.1. General Modeling

Similar to Section 2.3, all UHPC-CFRP specimens were modeled in MSC.Marc finite element software. The geometry and material input is the same as explained in Section 2.3.1. The material properties for CFRP bars are shown in Table 3.4, including cohesive energy (Gc), critical opening displacement (vc), and maximum opening displacement (vm), beyond which traction is reduced to zero. The interface parameters were calibrated to model the weak and strong interface configurations using the 1T1S-5 tests where slip of the CFRP bars was observed.

Table 3.4 Interface Element Parameters

Section	**Strong Interface**			**Weak Interface**		
	G_c	V_c	V_m	G_c	V_c	V_m
CFRP	35	0.15	0.35	0.9	0.05	0.1

3.3.2. Modeling and Results for 1T1S Section

The mesh and the geometry of 1T1S-CFRP is the same as Section 2.3.2. The interface at the support was assumed to be very strong to simulate the end anchorage for the CFRP. The stress distribution, comparison of load-displacement curve, and the comparison of load-strain response are shown in Figures 3.19 and 3.20. It can be noticed that the finite element results showed a good agreement with the test results in the linear portion of the curve while the model overestimates the ultimate load capacity for the CFRP option around 4 kips. This overestimation is due to the interface model parameters utilized in the analysis. Unlike the calibration cases available in the HSS specimens, in the experimental tests utilized for CFRP interface calibration, slip occurred due to insufficient anchorage at the end of specimen. Therefore, the weak and strong interface parameters could not be calibrated independently. The resulting weak interface strength and cohesive energy are too high, leading to over prediction of finite element strength, and the interface stiffness is too low, leading to an under prediction of finite element stiffness.

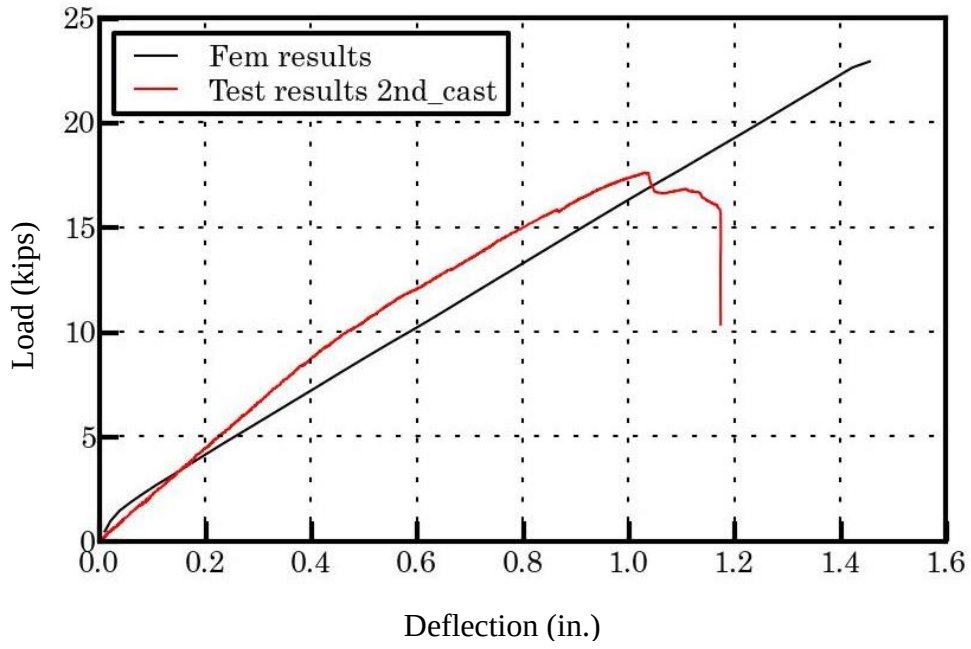

Figure 3.19 Load-Deflection Responses for Specimen 1T1S

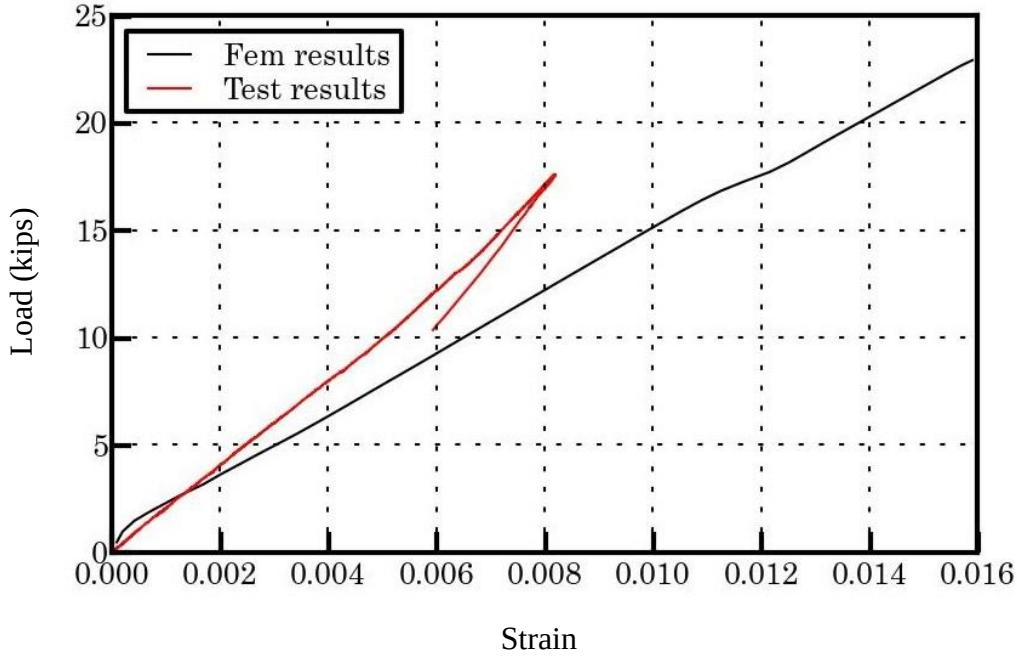

Figure 3.20 Load-Strain Responses for Bars at Mid-Span

3.3.3. Modeling and Results for 1T2S Section

The finite element model for 1T2S specimens is the same as described in Section 2.3.3. The load displacement curve, and load strain response are shown in Figure 3.21 and 3.22, respectively. From these figures, it can be seen that the model captured the initial stiffness for the deck but also overestimates the load capacity for both options.

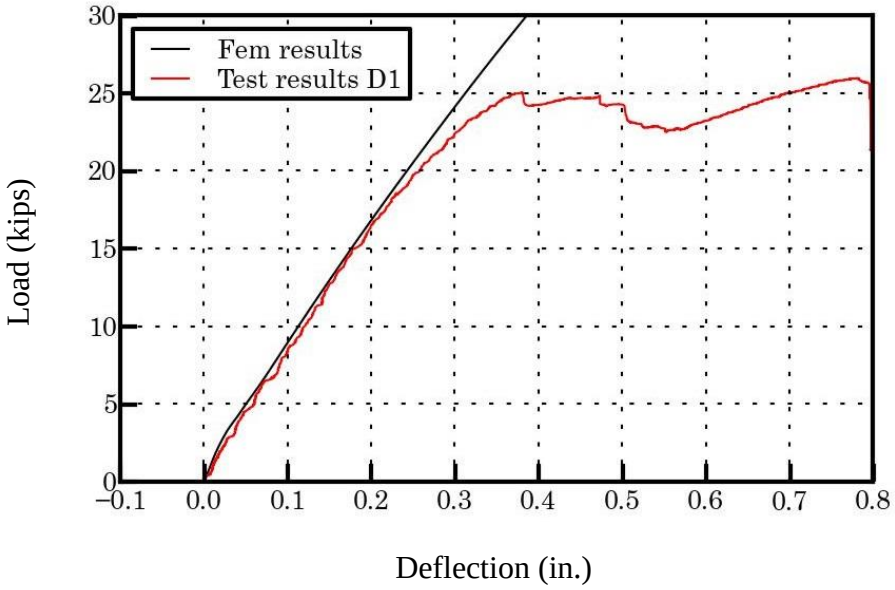

Figure 3.21 Load-Deflection Responses for Specimen 1T2S

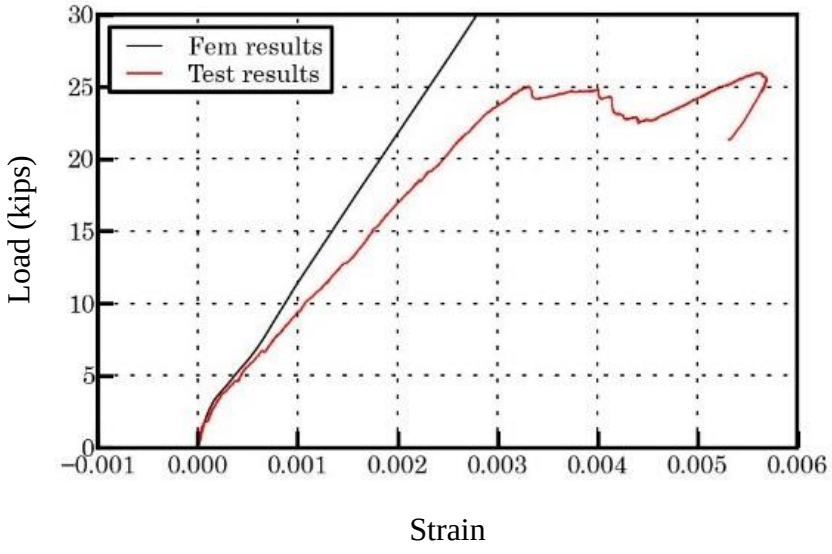

Figure 3.22 Load-Strain Responses for Bars at the Middle of First Span

3.3.4. Modeling and Results for 4T1S Section

The finite element model for 4T1S deck with the boundaries is similar to Section 2.3.4. The load deflection responses and load-strain response are shown in Figures 3.24 and 3.25.

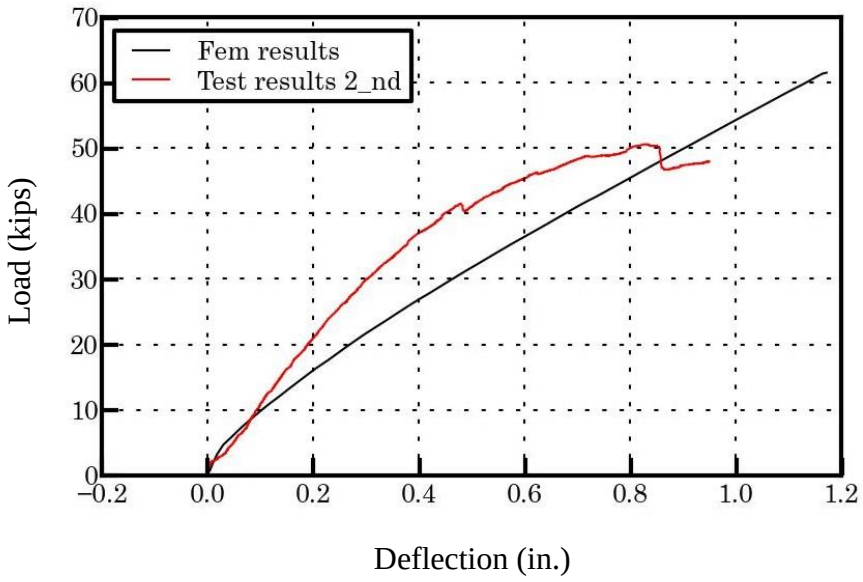

Figure 3.23 Load-Displacement Responses for Specimen 4T1S

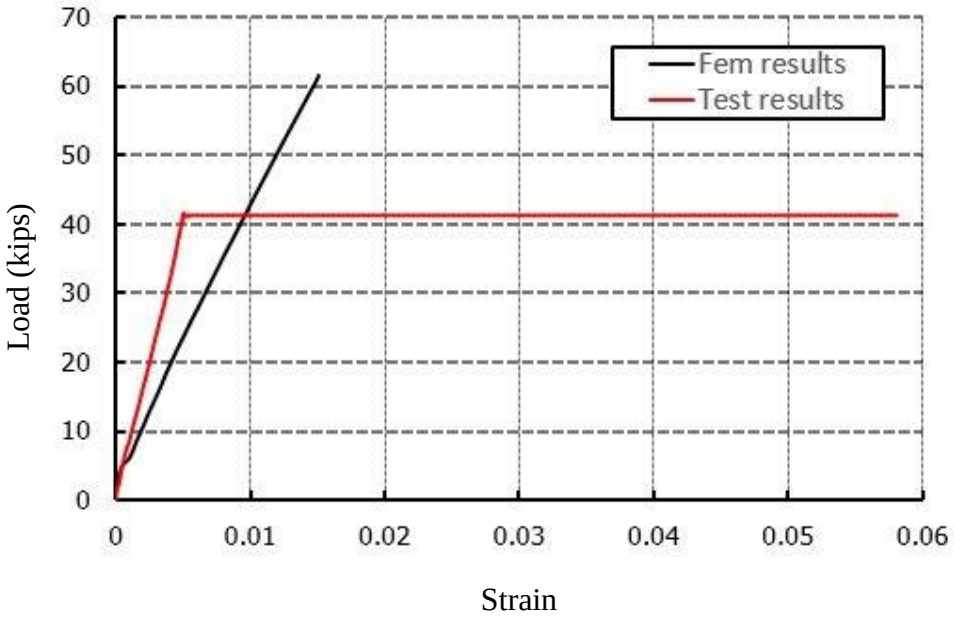

Figure 3.24 Load-Strain Responses for Mid-Span Bars for Specimens 4T1S

It appears that while there is generally a good agreement within the linear behavior between the experimental and analytical results, there are also some differences. The finite element modeling results showed that both 1T1S and 4T1S initial stiffness are more flexible than the experimental results whereas the stiffness is very close to experimental results for 1T2S. As mentioned for the 1T1S case, the weak interface parameters were calibrated based on the available 1T1S results with partial anchorage. This led to an artificially high cohesive energy and strength for the CFRP interface. Additional calibration studies need to be performed on pull-out tests and flexural tests to more accurately determine the properties of the weak and strong interfaces in the future.

3.4. Accelerated Pavement Testing

Test results of UHPC-CFRP panels under HVS based on the information shown in section 2.4 are presented in the following sections.

3.4.1. Test Results and Discussion

The test matrix for all group of specimens with CFRP reinforcement in different types of configurations is summarized in Table 3.5. Table 3.6 shows a summary of test results for the experiments on the UHPC waffle decks with CFRP reinforcement. The table shows the required live load demand for each group of specimens, along with capacity/demand ratio and capacity/demand per unit weight of the deck panel for each specimen.

Table 3.5 Test Matrix

Group	Specimen Name	Test Phase	Overall Depth (in.)	Rib Spacing (in.)	Slab Thickness (in.)	Unit Weight (psf)	28-Day UHPC Compressive Strength (ksi)	Flexural Reinforcement	
								Slab	Primary Rib
UHPC-CFRP									
CFRP-3	1T1S-5	3	5	15	¾	24.22	24	No. 3	No. 6
	4T1S-5	3	5	15	¾		25	No. 3	No. 6
	1T2S-5	3	5	15	¾		24	No. 3	No. 6
UHPC-CFRP									
CFRP-1	1T1S-4#1	1	4	15	¾	18.80	24	No. 3	No. 4
	1T1S-4#2	1					24		
	1T1S-5#1	1	5			21.30	24		
	1T1S-5#2	1					24		
CFRP-2	1T1S-4#3	2	4	15	¾	18.80	27		
	4T1S-4	2					27		
	1T2S-4	2					26		

Table 3.6 Summary of Test Results

Group	Specimen Name	Graph Labels	Overall Depth (in.)	Service Load Deflection (in.)	Ultimate Deflection (in.)	Ultimate Load (kip)	Demand Load (kip)	Capacity/ Demand	Capacity/ Demand per Unit Weight
UHPC-CFRP									
CFRP-3	1T1S-5	CFRP-5#3	5	0.23	1.76	21.80	8.14	2.68	0.11
	4T1S-5	CFRP-5#3		0.64	2.71	48.48	52.13	0.93	0.04
	1T2S-5	CFRP-5#3		0.12	1.24	38.45	17.45	2.20	0.09
UHPC-CFRP									
CFRP-1	1T1S-4#1	CFRP-4#1	4	0.54	1.19	16.77	10.25	1.6	0.09
	1T1S-4#2	CFRP-4#2		0.48	1.06	17.15		1.7	0.09
	1T1S-5#1	CFRP-5#1	5	0.37	1.03	21.49		2.1	0.10
	1T1S-5#2	CFRP-5#2		0.35	0.97	19.56		1.9	0.09
CFRP-2	1T1S-4	CFRP-4#3	4	0.45	1.03	18.66		1.8	0.10
	4T1S-4	CFRP-4#3		0.50	0.83	51.26	42.04	1.2	0.06
	1T2S-4	CFRP-4#3		0.19	0.80	26.75	15.65	1.7	0.09

3.4.1.1 Flexural Behavior

Similar to Sections 2.5.3.1 and 3.2.3.2, the flexural behavior of Specimens 1T1S was assessed. Figure 3.25 shows the test setup, failure mode, and load-deflection responses of single-rib simple-span specimen UHPC-CFRP. Similar to previous experiments, failure was initiated by minor web shear cracks near supports. Minor flexural cracks were also present near mid-span without having any impact on the overall failure. Shear cracks gradually widened as testing progressed, eventually leading to a load drop and failure of the deck panel.

Figure 3.26 shows the load-deflection responses of the single-rib simple-span specimen compared to all previous specimens of the current research projects. The load capacity is normalized to the corresponding ultimate demand load for each specimen according to the data presented in Table 3.6. As seen in the figure, in all of the specimens, the capacity exceeded the ultimate demand load.

(a) (b)

Figure 3.25 Flexure Test and Failure Mode of Specimens 1T1S-CFRP, (a) Deflected Shape of Specimen 1T1S, and (b) Beam Shear Crack

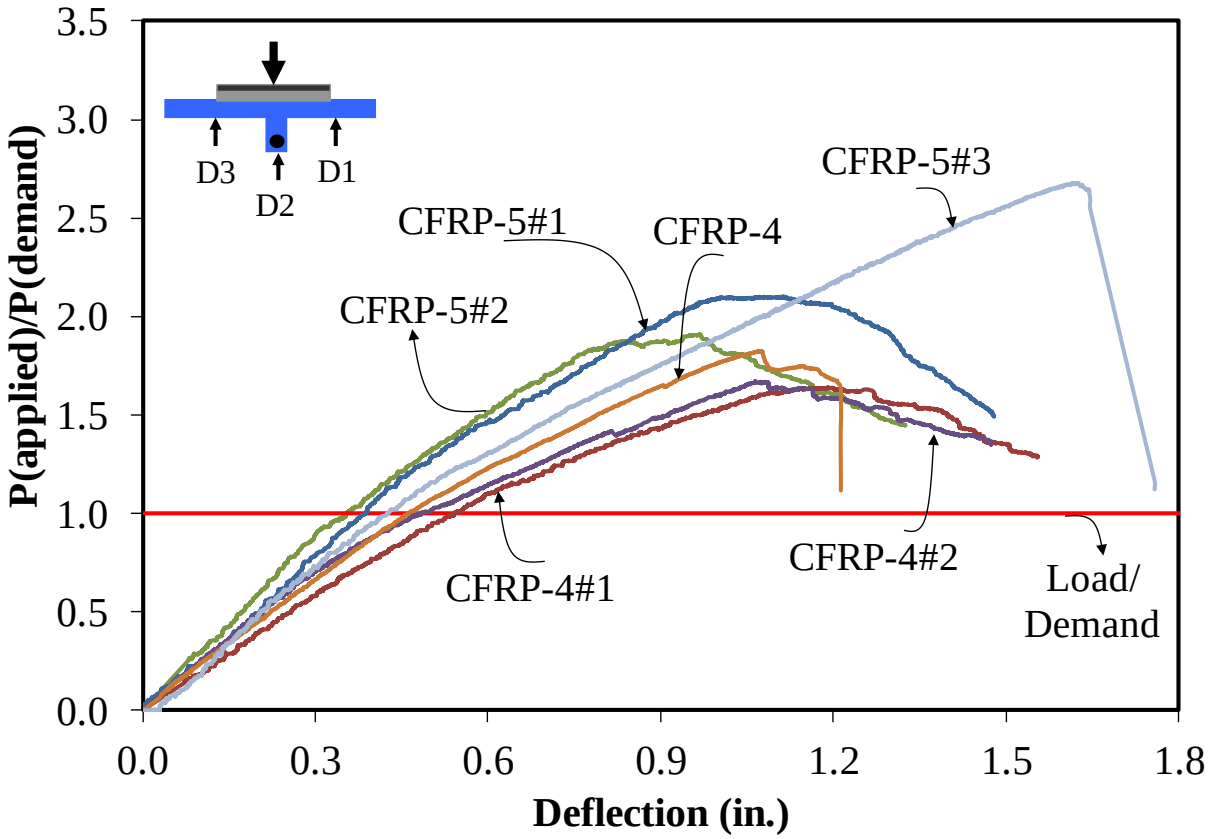

Figure 3.26 Load-Deflection Responses of All Specimens 1T1S

Figure 3.27 shows the load-strain responses for all specimens with CFRP reinforcement. As expected, there is similarity between the results of this phase and those of previous phases.

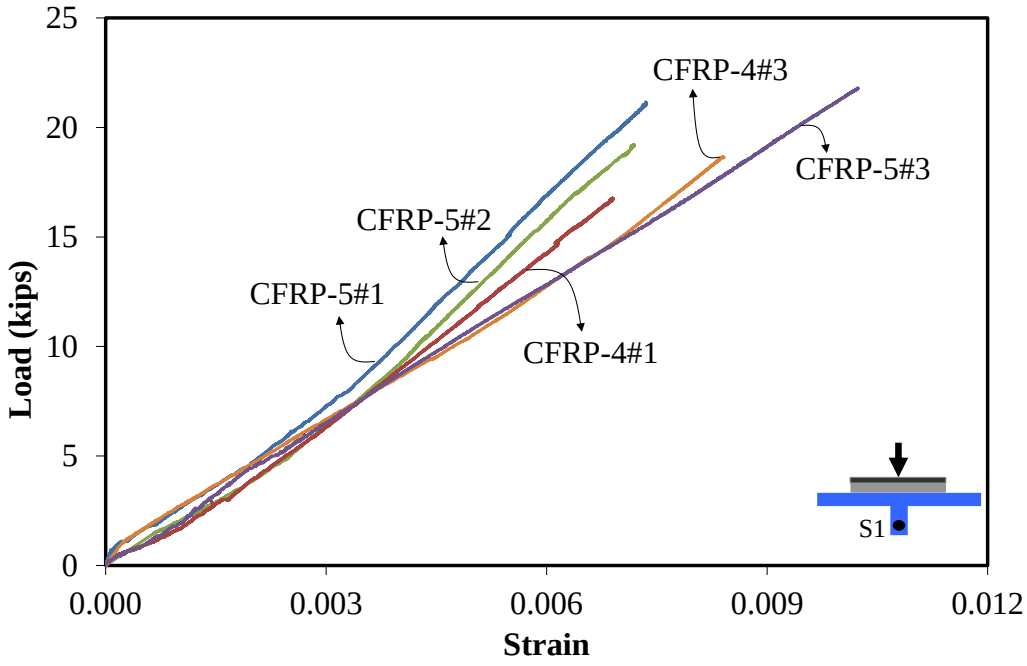

Figure 3.27 Strain Responses of CFRP Bars in Specimens 1T1S

Additional strain gauges were attached to the top surface of the UHPC deck and to the web in order to capture the strain in the UHPC. The results are shown in Appendix B.

3.4.1.2 Panel Action

Performance of Specimens 4T1S was evaluated similar to Sections 2.5.3.2 and 3.2.3.3. Figure 3.28 illustrates the top and bottom views of the multi-rib simple-span Specimen 4T1S after its flexural test for Specimen 4T1S-CFRP. The failure mode was similar to that observed for single-rib specimens of this phase and the previous multi-ribs simple-span specimens.

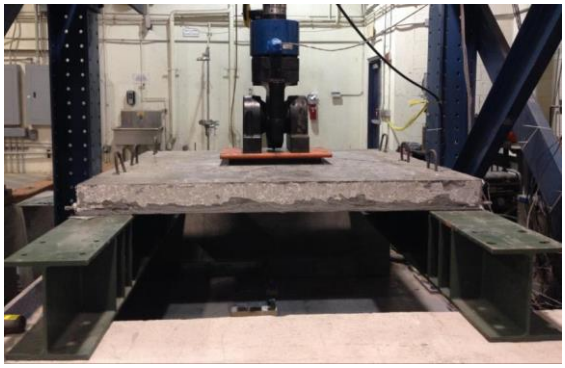

(a)

(b)

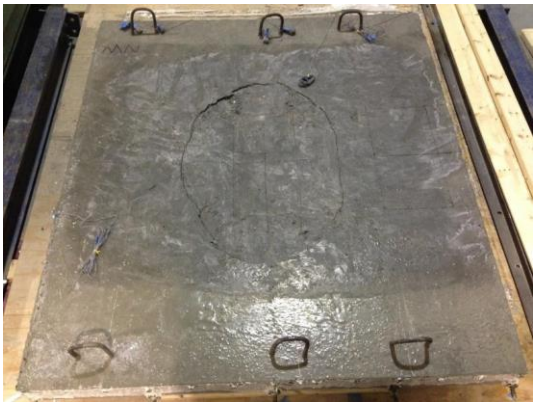

(c)

Figure 3.28 Flexure Test and Failure Mode of Specimens 4T1S-CFRP, (a) Test Setup, (b) Beam Shear Crack, and (c) Cracks on the Top of the Slab

For comparison, Figure 3.29 shows the response curves under each rib for current Specimen 4T1S-5#3 along with the previous CFRP specimen (4T1S-4) in a normalized load capacity basis. Generally, the panel with CFRP bars is more flexible, as expected. Also, the 5 inch deep panel with CFRP bars did not meet the ultimate demand load criteria. Only the load-deflection response of the middle rib (D3) is shown in the figure for all specimens.

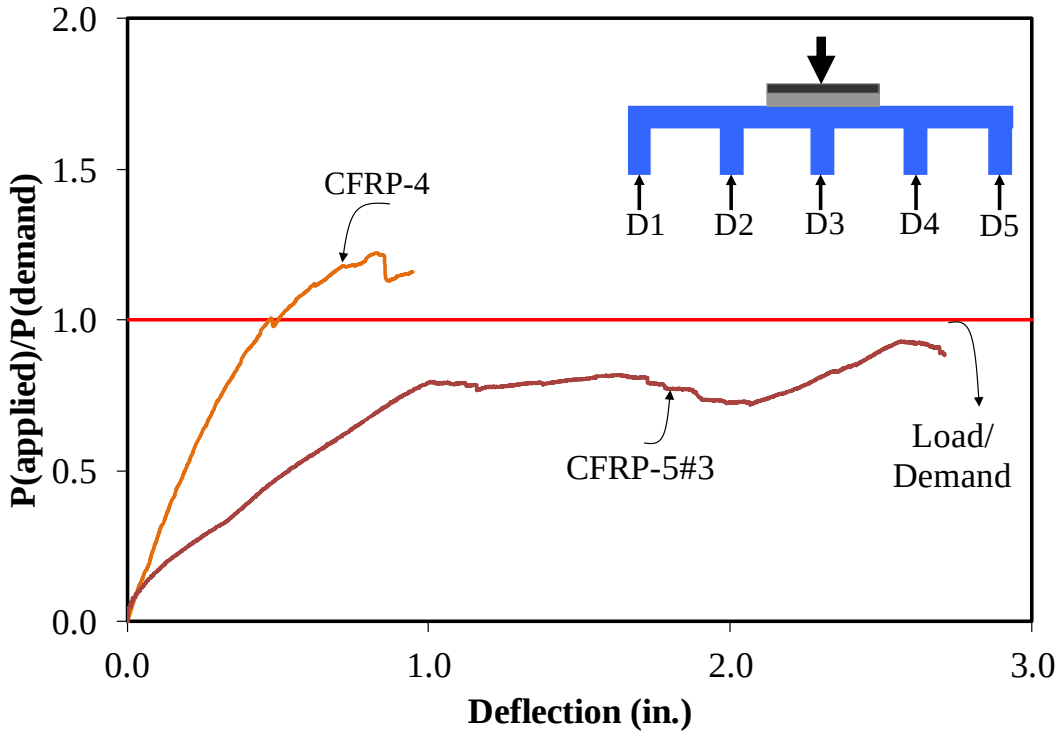

Figure 3.29 Load-Deflection Responses of All Specimens 4T1S

Figure 3.30 shows load-strain responses for all Specimens 4T1S with CFRP reinforcement based on strain gauges attached at the mid-span to the rebar in the primary rib. The results are considerably similar to previous phases.

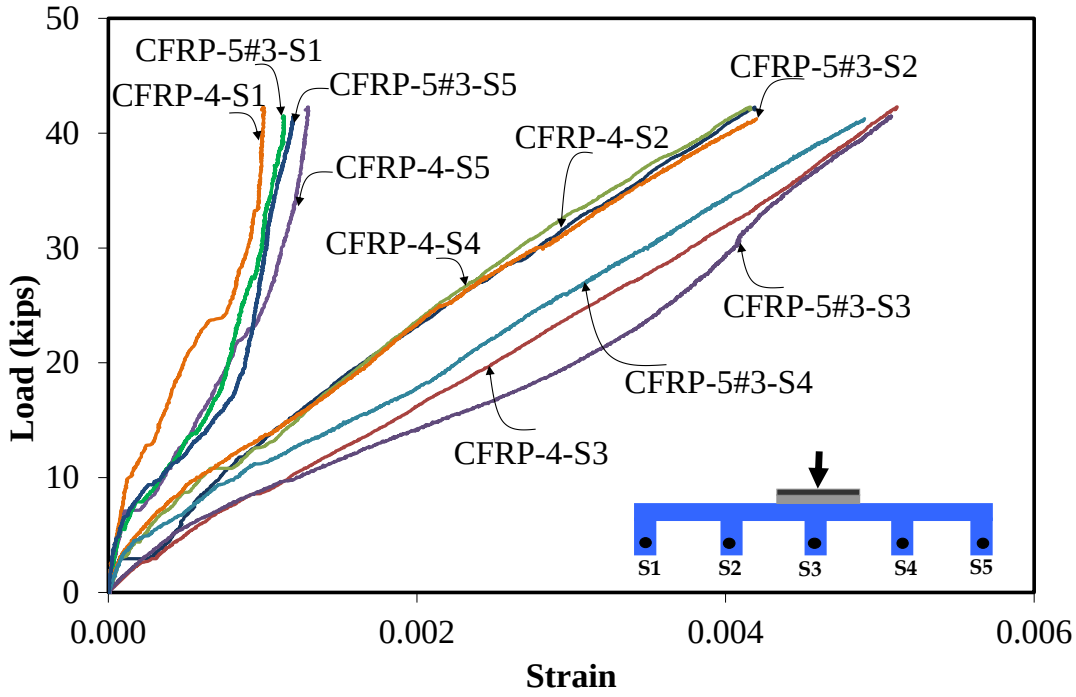

Figure 3.30 Load-Strain Responses of All Specimens 4T1S-CFRP

3.4.1.3 Punching Shear Behavior

Similar to Sections 2.5.3.3 and 3.2.3.4 the punching shear behavior of the Specimens 4T1S was assessed on the same specimens 4T1S after flexural tests. Figure 3.31 shows the punching shear test carried out on exterior panel of Specimen 4T1S-CFRP. The load-deflection response of the punching shear test is presented in Figure 4.32. The slab has experienced severe cracks under flexural tests. Therefore, string pot 2 which was recording the deflection on the slab showed higher value as compared to the other two string pots which were recording the deflections at the primary ribs.

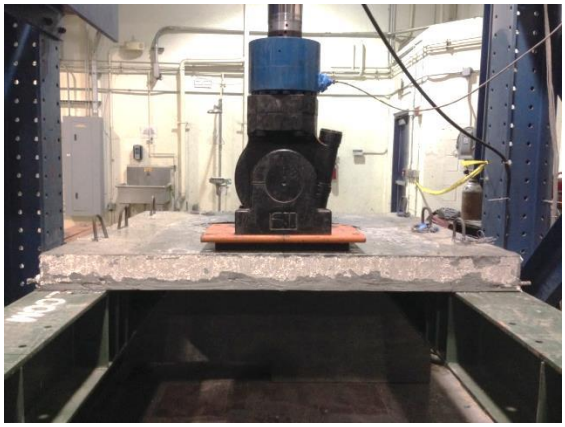

(a)

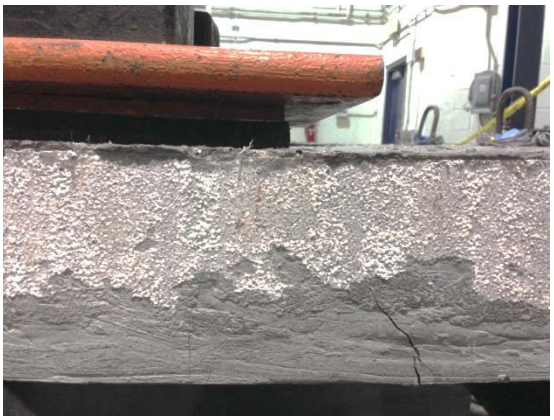

(b)

(c)

Figure 3.31 Punching Shear Test of Specimen 4T1S: (a) Test Setup, (b) Beam Shear Crack, and (c) Cracks on the Top of the Slab

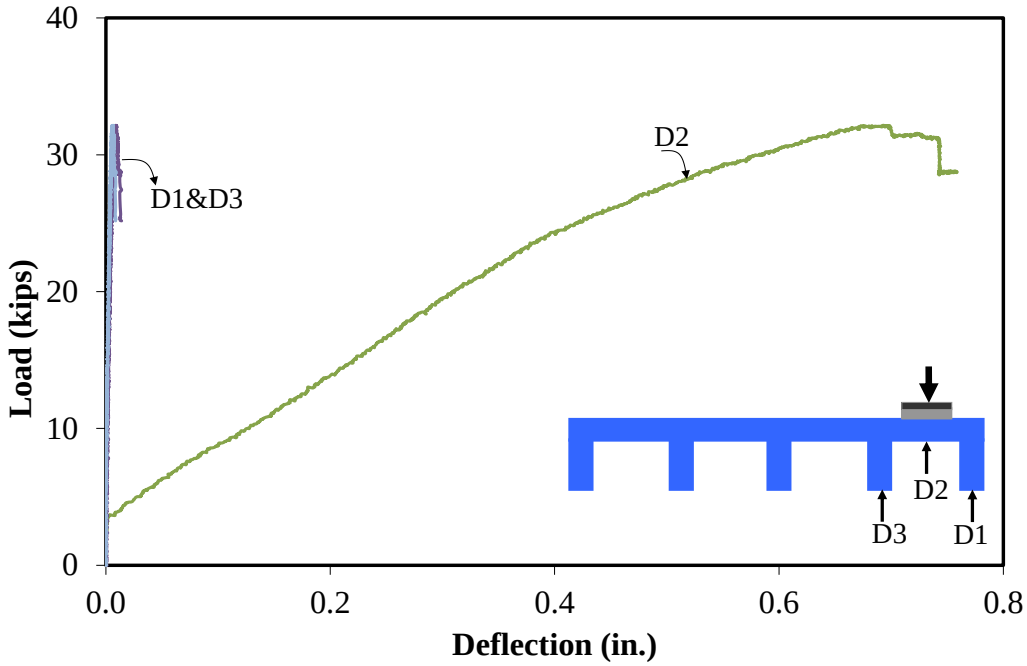

Figure 3.32 Load-Deflection Responses of Specimen 4T1S-CFRP

3.4.1.4 Continuity Effects

The effects of continuity and negative moments were investigated using the single-rib two-span Specimen 1T2S. Figure 3.33 shows the test setup, deflected shape and the failure mode, for Specimen 1T2S-CFRP. Similar cracking pattern as was observed in UHPC-HSS specimen was followed in UHPC-CFRP specimen. (See Figure 3.33.d).

(a)

(b)

(c)

(d)

Figure 3.33 Flexure Tests of Specimen 1T2S-CFRP: (a) Test Setup, (b) Deflected Shape, (c) Failure Mode (Beam Shear Crack), and (d) Flexural Crack on the Interior Support

Figure 3.34 compares the mid-spans response curves for Specimens 1T2S with all previous specimens. The responses are normalized based on load capacity. All specimens meet the ultimate demand load capacity.

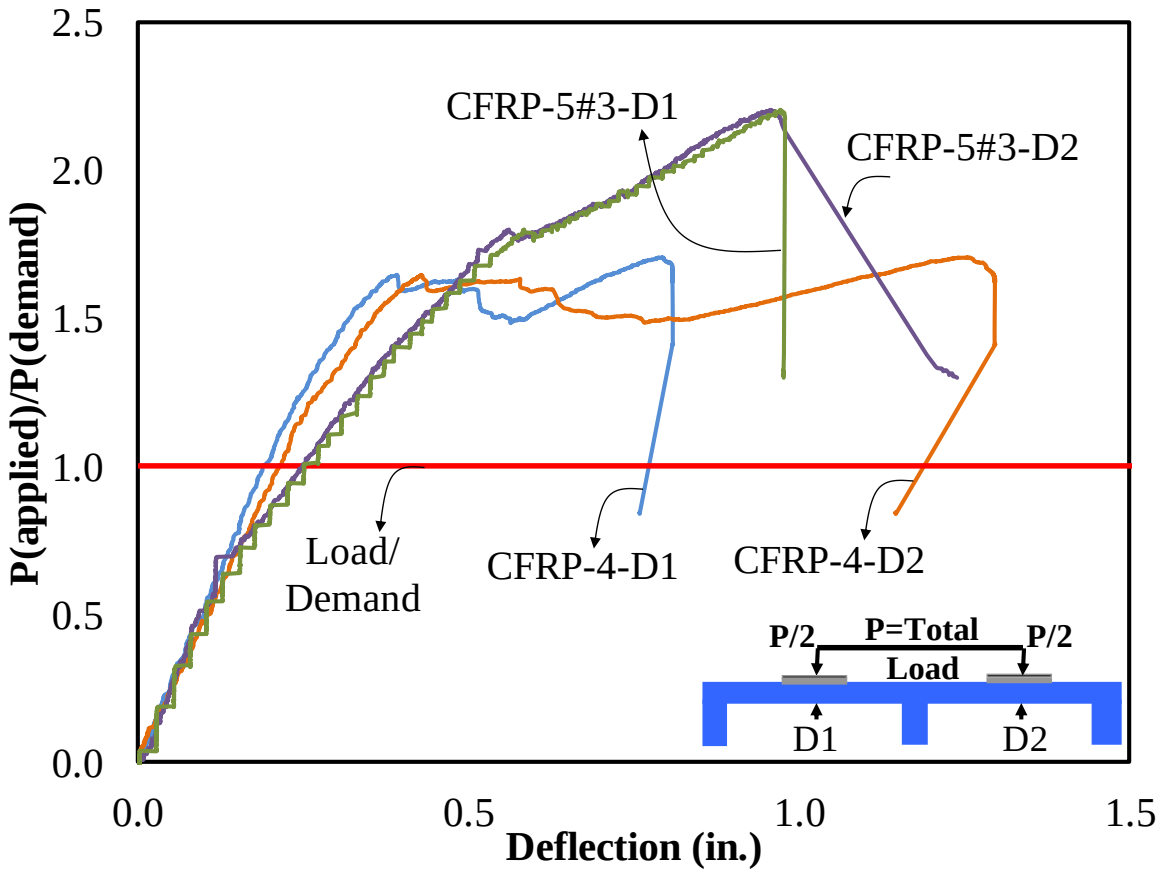

Figure 3.34 Load-Strain Responses of All Specimens 1T2S

Figure 3.35 shows load-strain responses for all based on strain gauges attached at the mid-span to the rebar in the middle of the primary ribs.

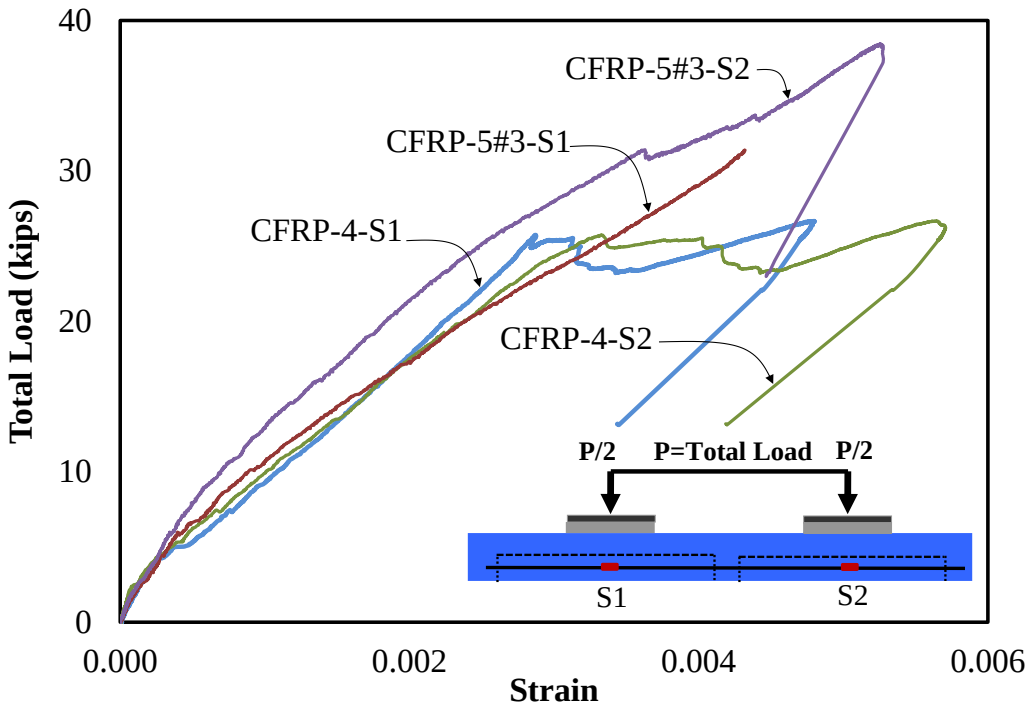

Figure 3.35 Load-Strain Responses of All Specimens 1T2S-CFRP

3.4.2. Accelerated Pavement Testing under Heavy Vehicle System

According to Figures 3.31 (b) and 3.31 (c) the punching shear cracks occurred on the slab. Also, according to Figure 3.29, Specimen 4T1S-CFRP did not meet the ultimate demand load criteria. Therefore, for the final slabs which will be tested under HVS, the thickness of the slab and the amount of reinforcement were both increased.

Since the test setup, the panels' layout, the loading pattern and the instrumentation was fully described in Section 2.5.4, only the test results corresponding to UHPC-CFRP panels are presented in this part. The loading rate and data collection frequencies are the same as defined in section 2.4.

3.4.2.1 Test Results and Discussion

The strain responses of CFRP bars vs. number of truck passages are illustrated in Figure 3.36. Figures 3.37 and 3.38 represent the defection at the middle of panels 3 and 4 vs. the number of truck passages. The maximum deflection recorded for UHPC-CFRP panels was 0.095. Comparing to the prior static test (3rd phase of testing on 5 ft. panels at FIU) results the deflections of the panels under APT was fairly lower.

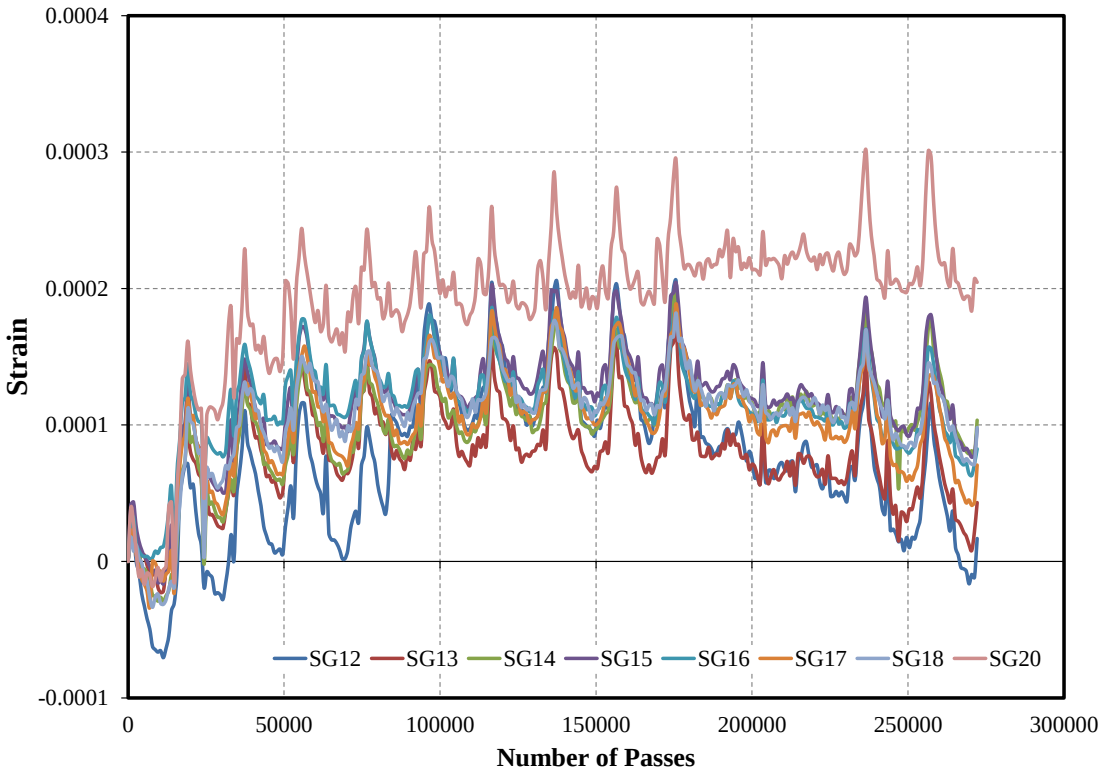

Figure 3.36 Strain Responses of CFRP Bars vs. the Number of Truck Passages

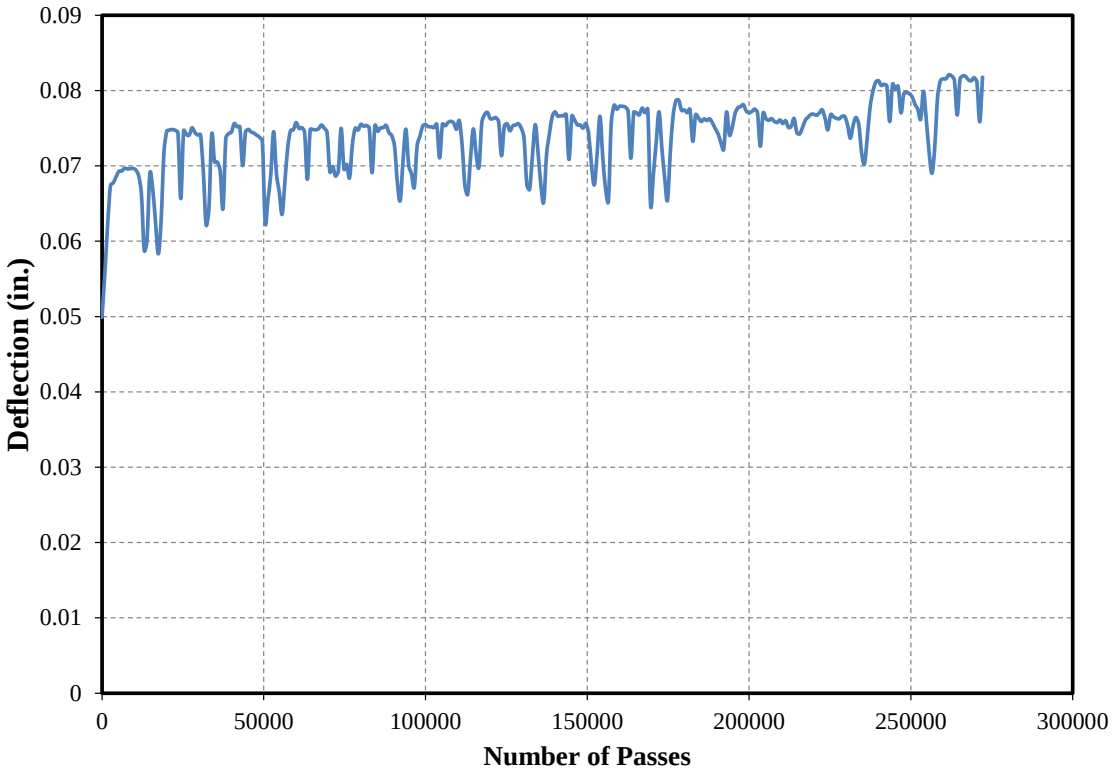

Figure 3.37 Deflection of Panel3 (D3) vs. the Number of Truck Passages

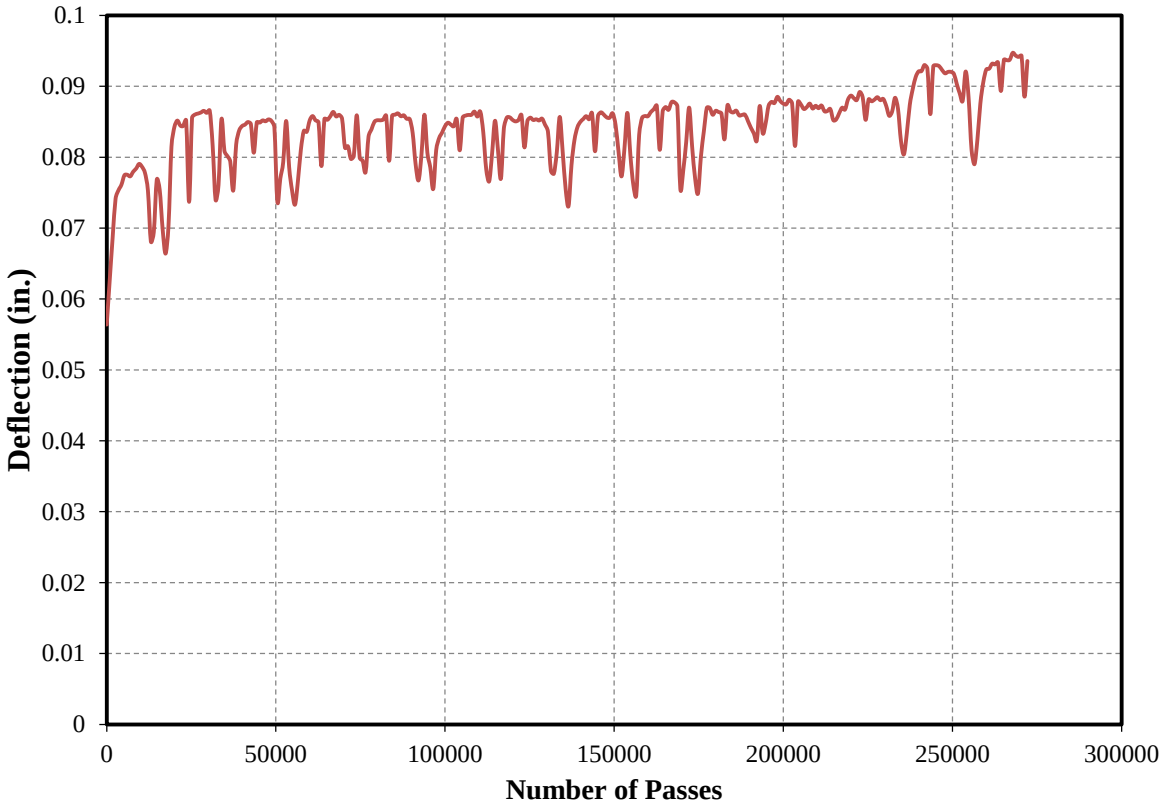

Figure 3.38 Deflection of Panel4 (D4) vs. the Number of Truck Passages

Joint deflections between the panels were recorded to assess the performance of the connections. The result of joint deflections between the UHPC-HSS panel and the UHPC-CFRP panel (RD2) is presented in Figure 3.39 and the joint deflection between the UHPC-CFRP panels (RD3) is shown in Figure 3.40. The maximum joint deflection was recorded as 0.071 in. which is 1/845 of the total length of the deck.

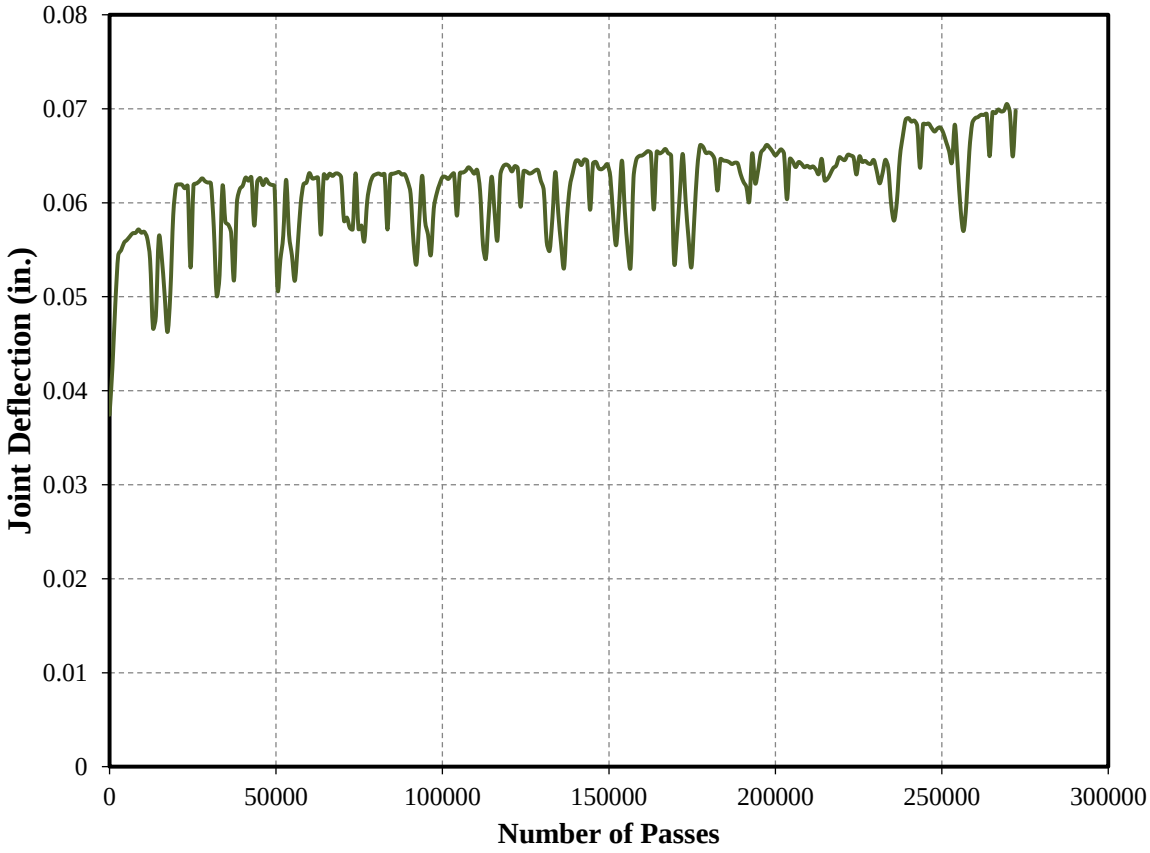

Figure 3.39 Joint Deflection of UHPC-HSS and UHPC-CFRP Panels vs. the Number of Truck Passages

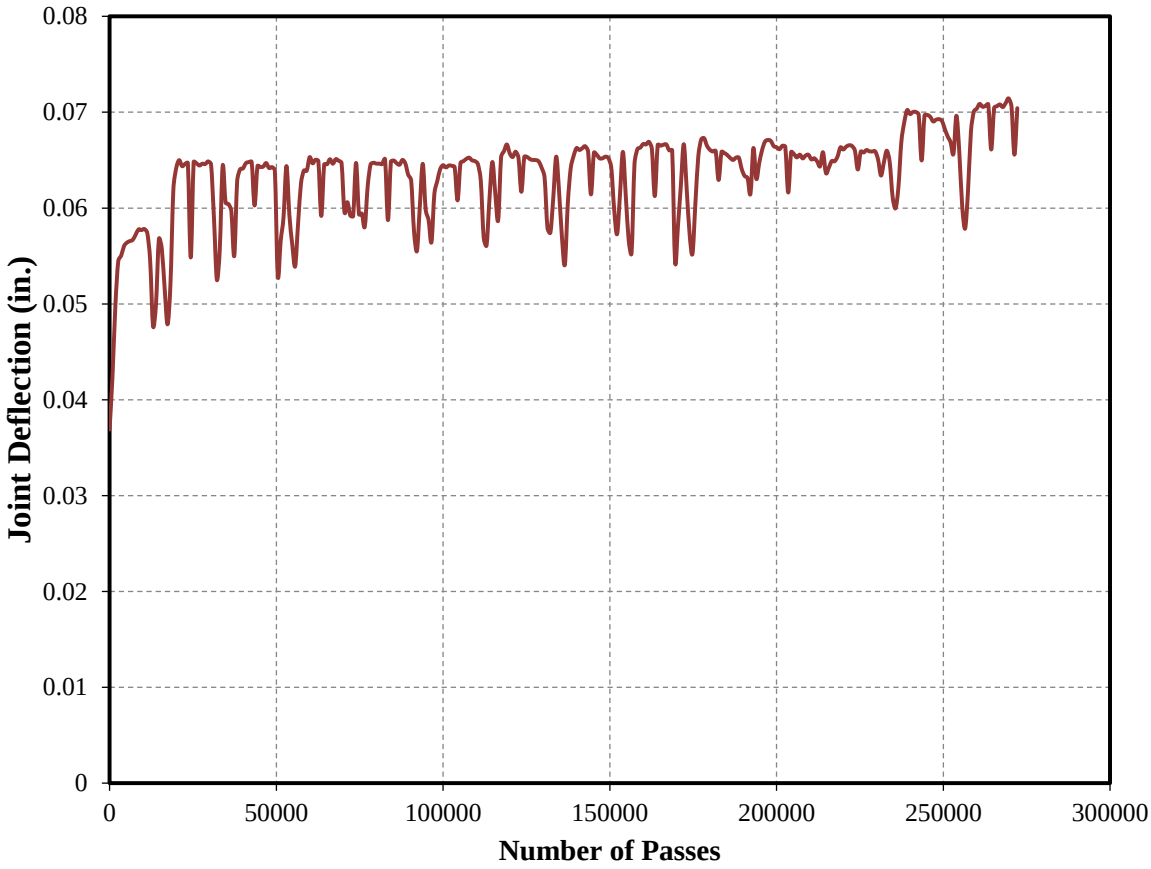

Figure 3.40 Joint Deflection of UHPC-CFRP Panels vs. the Number of Truck Passages

3.5. Conclusion

An innovative deck system is proposed for accelerated bridge construction, using ultra high performance concrete (UHPC) in the form of an ultra-lightweight super-shallow waffle slab reinforced with carbon fiber reinforced polymer (CFRP) bars. The novel combination of the two advanced materials leads to a deck panel with only 4 inch overall depth and only 18.80 psf self-weight, while still meeting the load demands for a 4 ft. typical stringer spacing. The serviceability requirements were not satisfied. In this study, seven specimens with two different overall depths, with single or multiple ribs, and in simple or two-span configuration were tested in two consecutive phases. The following conclusions can be drawn from this study:

- The experiments confirmed the potential of the proposed deck system, and its comparable performance to a similar deck using high-strength steel reinforcement. Further research is needed to address serviceability requirements.
- It is expected that the proposed deck is not susceptible to punching shear of its thin slab, due to the arrangement of the primary and secondary ribs, which promotes one-way shear of the primary ribs instead.
- The proposed deck system fails in a ductile manner, despite its apparent shear failure and in the absence of yielding of the reinforcement. The ductility stems from dowel action of CFRP bars and the fiber pull-out of UHPC.
- Load distribution among the ribs, whether calculated based on deflections or strains, are quite similar to those for UHPC-HSS specimens. The load distribution for the center rib is 33%, with the next two adjacent ribs at 22% and 11%, respectively.

Future research on ultra-lightweight super-shallow bridge decks may concentrate on composite action with stringers, long-term durability, along with further refinements to meet the serviceability requirements.

Chapter-4

Lightweight UHPC-FRP Hybrid System

4.1. Introduction

Fiber reinforced polymer (FRP) composite materials have been studied for several decades and have shown great potential as alternative construction materials, especially in the field of repair and rehabilitation of existing bridges and, to some extent, in new bridge construction. FRP composites applications in the bridge industry have been accelerated in recent decades because of their superior properties such as high strength, long-term durability, fatigue resistance, and good corrosion resistance. Moreover, FRPs are a good choice for mass production of structural shapes because of their light weight, which allows rapid installation of FRP modular decks on bridges. The prefabricated FRP bridge deck weighs approximately 80% less than a concrete deck. The lightweight FRP deck could be especially beneficial for movable bridges (i.e., in which spans have to be lifted for the passage of vessels). In addition, a light structure is always convenient to transport and install, which enables shorter construction periods and lower construction costs.

A new lightweight UHPC-FRP composite system has been fabricated at the University of Central Florida structural lab using vacuum-assisted resin transfer molding (VARTM) infusion and tested to examine its applicability in the new bridge construction field. This composite deck can work also as an integral wearing surface, so no additional layer is needed during the replacement or the construction. The UHPC-FRP hybrid system tends to be a very good alternative due to its extremely light weight. The self-weight of the new UHPC-FRP composite has been found to be in the range of 12-14 psf compared to the 20-25 psf for the 1T1S deck. It is known that UHPC has very high compression strength, while FRP has very high tension strength. Theoretically, therefore, a deck system with UHPC cast as the upper layer for compression resistance, CFRP distributed on the bottom layer for tension resistance, and GFRP as shear reinforcement, as shown in Figure 4.1, is optimal. In this chapter, the fabrication, testing, and the results of this new hybrid system will be presented.

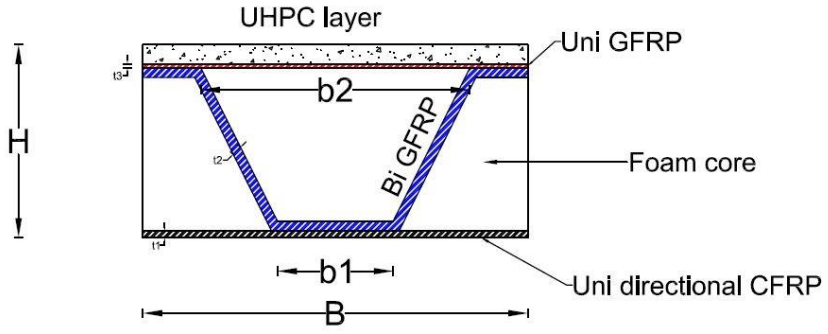

Figure 4.1 Details of the New Hybrid Deck

4.2. Literature Review

Previously, different FRP deck systems and their connections have been studied to characterize the static and dynamic performance. Connections of FRP decks were studied by Keller and Gürtler (2005), Righman et al. (2004), and Davalos et al. (2010). Material constituents and mechanical properties were investigated by Davalos et al. (2001) and Alagusundaramoorthy et al. (2006). Deflection and deformation, ultimate capacity, and failure modes were studied by Wu et al. (2003), Kumar et al. (2004), and Davalos and Chen (2005). Creep and fatigue in FRP decks were investigated by Scott et al. (1995), Cole et al. (2006), Alnahhal et al. (2006), and Wu et al. (2004).

Five different decks panels that were made of FRP webbed cores was fabricated and evaluated by Robinson and Kosmatka (2008) and compared with an existing aluminum deck that previously tested as one option of the composite army bridge. Each deck has different core configuration and was composed of either glass/carbon web, and 3/8 in. carbon face sheet. Three of the five cores were fabricated using machine process while the other two were fabricated using hand wrapping. Their goal was to develop a system which its one bending shear strength is greater than 740 psi and the compressive strength exceed 1340 psi. Therefore, only a three point bending and compression tests were performed. Also, the buckling load of the web is also studied by using beam on elastic foundation theory. They found that four of their cores met and exceed the shear and compressive requirements. Their results showed that there is a got a good agreement between the experimental and finite element model. Also, they found that using FRP webbed cores can increase the mechanical properties with up to 35% weight saving comparing to existing aluminum deck.

Williams et al. (2003) studied the performance and behavior of filament-wound GFRP bridge deck. Different decks were constructed using different number of triangular filament wound glass tubes and a GFRP plates were bonded to the bottom and top of the tubes to form one modular unit. They fabricated their deck in two generations. In the first generation, there decks were tested and based on the results they modified the design and fabrication in the second generation to enhance the deck performance. The performance of the deck was examined based

on the capacity, strain, deflection at service load, and the mode of failure. The failure mode in the first generation was the delamination and buckling of the top plate. Different mode of failure has been observed in the second generation such as top plate and tube buckling, slippage of the tube, and bottom plate delamination. Also, an analytical model within the elastic range was presented to predict the behavior of the GFRP decks. They showed that the GFRP deck is able to support an HS30 design truck load and the deflection met a preset limit of L/360.

Chakrabortty et al. (2011) studied the performance of outside filament-wound hybrid FRP-concrete beams. Their beam was made of concrete block, GFRP pultruded hollow section, and CFRP laminate all wrapped together using filament winding. Three different types of concrete were studied in their experiment: normal concrete, high strength concrete and steel fiber high strength concrete. The CFRP laminate was used in the bottom to provide the required stiffness for the section. The use of the filament-wound laminate has two advantages. First, to provide some confinement to the beam. Second, to enhance the shear strength of the pultruded section. It was mentioned that the wrapping eliminated the risk of the premature failure that resulting from the debonding between the concrete block and the pultruded profile. Also, it enhances the stiffness and load capacity of the beam.

Alagusundaramoorthy et al. (2006) tested and evaluated four commercial FRP decks that were available commercially and compared them with the test results of reinforced concrete deck panels. The force deformation response of 16 FRP composite deck and four conventional reinforced concrete decks were evaluated under effect of AASHTO MS22.5 wheel load until failure. The results of all tested panels were compared with shear, flexural, and deflection criteria for Ohio department of transportation specifications. Also, flexural and shear rigidities were calculated for the deck depending on the experimental results in order to use it in the modelling of the First Salem bridge in Ohio. All deck panels met and satisfied the Ohio performance criteria and the factor of safety against failure ranged from 3 to 8.

Over 40 FRP bridge decks have been installed on existing or new bridges in the US during the past decades. These bridges mainly are located in California, Florida, Delaware, Iowa, Kansas, Idaho, Illinois, Maryland, Missouri, New York, Ohio, Oregon, Pennsylvania, Virginia, North Carolina, South Carolina, West Virginia, and Wisconsin. Several commercial FRP deck systems are available in US. Some of them are adhesively bonded pultrusions manufactured such as DuraSpan deck from Martin Marietta Composites, Superdeck from Creative Pultrusions, Teckdeck from fiber reinforced system, EZspan deck and ZellComp deck. Also, there are sandwich constructed deck which they are fabricated using either hand/automated lay-up or VARTM process such as Kansas Structural Composites deck, Hardcore composite, TYCOR deck from 3TEX, and Structural Composite deck which still under investigation. Due to proprietary design and manufacturing methods of FRP decks, their design guidelines and specifications are often performance-based.

4.3. UHPC-FRP Composite Deck

4.3.1. Material Properties

The carbon fiber cloth used in this project is FG-CF121250U, 12oz - 12k unidirectional from iILSTREET Composites and it is fully compatible with polyester resin, epoxy resin, and vinyl ester resin. The unidirectional GFRP that was placed under the UHPC plate is JBMTG-13-U-50 from JAMESTOWN Distributors, while the bidirectional GFRP that was used for the web shear reinforcement is 18 oz. E-Glass Fiberglass Cloth from US composites. A chopped mat was used with the bi-directional glass fiber in the web to build the thickness and enhance resin transfer. Chopped mat is a randomly oriented long fiberglass strands that are linked together with a styrene-soluble binder that works like glue connecting the fibers. This mat allows the resin to flow easily through the glass fiber and provide more stiffness to the attached laminates. The laminate mechanical properties are summarized in Table 4.1.

Table 4.1 Material Properties from Coupon Tests

FRP Type	Modulus (ksi)	Poisson's Ratio
Carbon	7500	0.2
Bidirectional glass	2000	0.25
Unidirectional glass	4500	0.18

The matrix used in this research was #1110 Vinyl Ester resin from Fibre Glast Development Corporation. It has desirable properties like affordable cost, good corrosion resistance, good tensile strength, fast curing time, and low viscosity of 275 cps, which makes it an ideal choice for resin infusion applications. According to the manufacturer, this resin has a pot life of 15-30 min, tensile strength of 12,000 psi and modulus of elasticity of 5.4×10^5psi based on the ASTM D638 tests.

4.3.2. Specimen Preparation and Test Setup

The composite, or hybrid, system is infused with low viscosity resin using VARTM infusion system to get a high quality system with better adhesion and fiber volume content than would be achieved using typical wet layup. The method is typically suitable for manufacturing of carbon and glass fiber composites and it is commonly used by professional manufacturers for the production of any fiber body panels such as boats and motor manufacturers. In the method, dry fabric is placed in the mold, and then applied in a special configuration the bagging materials (such as peel ply, infusion mesh and bagging film) before being subjected to vacuum pressure

using a composites vacuum pump. Once the specimen is prepared then it will be fully sealed so the air can be evacuated from the bag, resin is drawn through the part and is then fully cured under vacuum.

Two sets of decks were constructed with different geometry. Six UHPC plates were cast for the hybrid system in the first set with total length of 48 in. Five of these UHPC plates had a thickness of 0.5 in, whereas the sixth plate was 0.75 in. During the casting, several holes with dimensions of 0.25 in. × 0.25 in. × 0.25 in. were made in the plates to enhance the bond and the shear transfer between the UHPC and fibers. Also, after casting, several longitudinal and transverse canals were drilled in the plates in order to allow the resin to flow and improve the bond between the UHPC plate and top GFRP layers. The construction stages of the hybrid deck are shown in Figure 4.2. One layer of chopped mat only was used with one specimen that has UHPC plate thickness equal to 0.5 in. to see if this mat enhanced the resin transfer and the performance of the system. According to the findings of this stage, a decision was made to use multiple layers of chopped mat in the second set of decks. In the second set of the decks, three plates were cast in the second stage with 34 in. total length and 0.5 in. thickness.

The first set was infused as one system including the UHPC plate while in the second set the infusion process was done in two stages. The first stage included preparing and infusing the foam core with web FRP reinforcement to ensure that the resin would be transferred and impregnate all the FRPs along the total length. Then after two days, the product of the first stage was bagged and infused with the UHPC, top GFRP and bottom CFRP to get the final deck.

The first set of hybrid specimens had a 48 in. (4-ft) overall length and 43.5 in. center-to-center spacing between the supporting steel girder as shown in Figure 4.3. All specimens were loaded at the middle of the span, where the load on an AASHTO prescribed foot-print of 20 in. × 10 in. for an HS20 truck tire wheel using neoprene pad with a steel plate on top and with longer side parallel to the length of the specimen as shown in Figure 4.4. The instrumentation plan and loading arrangement are shown in Figure 4.6. Four strain gauges were attached to the bottom surface (CFRP layer in the tension side). One strain gauge was attached to the top UHPC plate (compression side). In addition to the strain gauges, two string pots were used at the center of each specimen to record the maximum deflection. After preparing the setup, the decks were tested using a loading rate of 0.03 in/min.

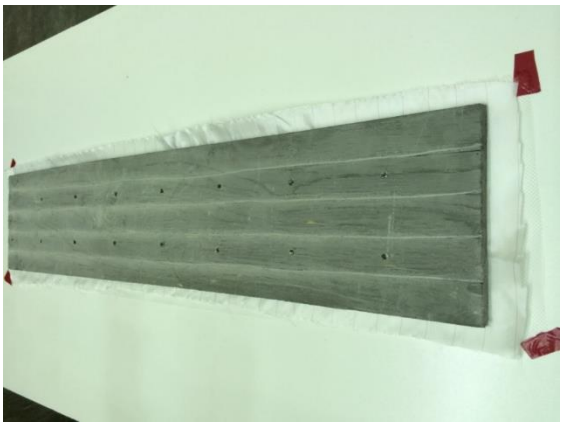

(a) Laying the peel ply, infusion mesh, and UHPC plate

(b) Putting the side mold and laying the top glass fiber sheets

(c) Installing foam and laying shear fiber

(d) Laying carbon fiber sheets

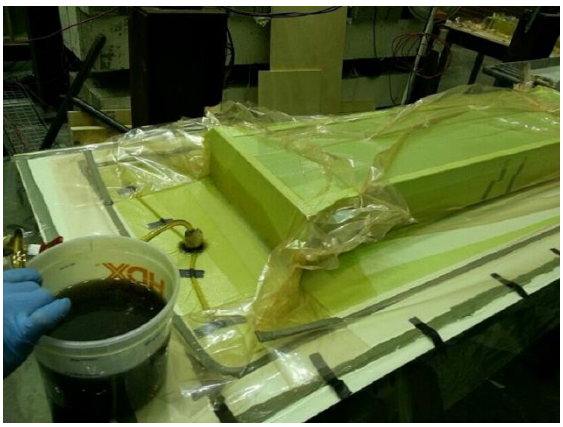

(f) Final deck after demolding

(e) VARTM Process

Figure 4.2 Construction Stages of Hybrid System

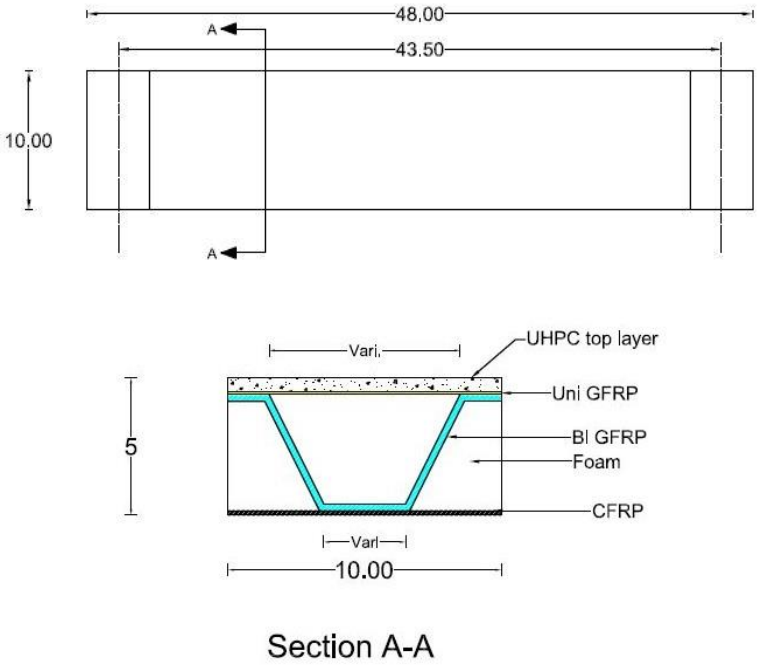

Figure 4.3 Detail of First Set of Decks

The second set of the specimens had a 34 in. total length with 30 in. center-to-center spacing between the two supports as shown in Figure 4.4. These specimens were tested using four point load configuration. All specimens were tested using Universal Testing Machine (UTM) with a loading rate equal to 0.03 in/min. The test setup of the hybrid sections (UHPC-FRP) are shown in Figure 4.7. Three strain gauges were attached to the bottom CFRP and one strain gauge was attached to the top UHPC plate. Linear variable differential transformer (LVDT) was used to record the displacement at the mid-span. Also, LVDT are placed at the two supports to calculate the relative displacement. The instrumentation plan of this system is shown in Figure 4.8.

The first specimen in the first set experienced premature bearing failure resulted in the rotation of the actuator. The reason for this failure may be that some eccentricity at low load level existed with concentrated load reaction from support. So, the web at end wall failed due to compression. The bearing capacity was increased for the remaining specimens of the first set of deck by excavating the foam within the first 4.5 in. of each end of the specimens (which are placed on the supports) and filling the voids with grout, as shown in Figure 4.9.

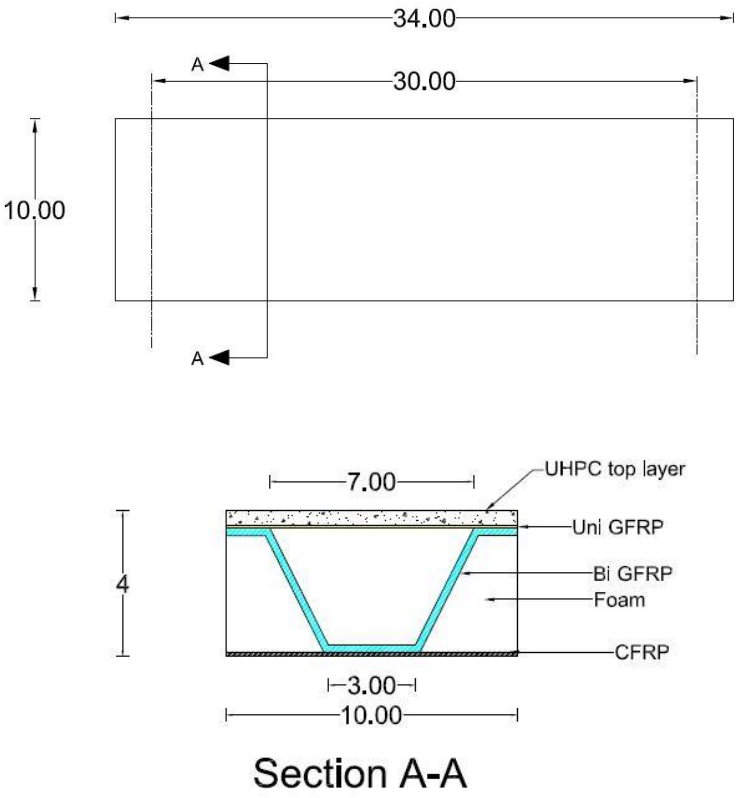

Figure 4.4 Details of Second set of decks

Figure 4.5 Test Setup for the First Set

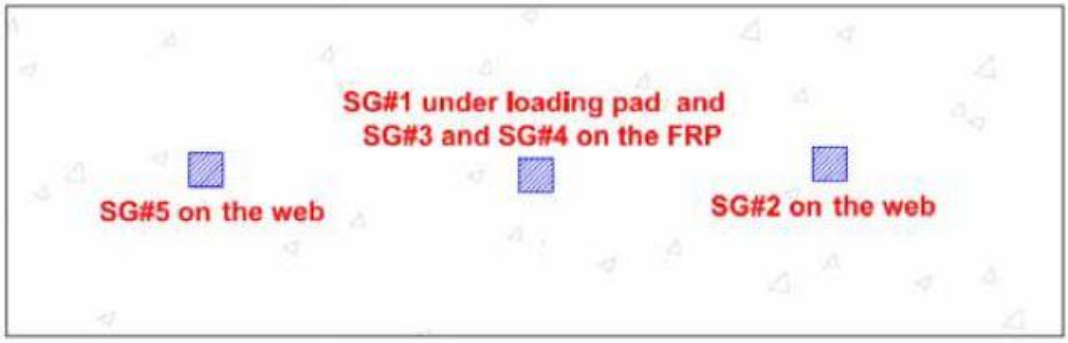

Figure 4.6 Instrumentation Plan for the First Set

Figure 4.7 Test Setup for the Second Set

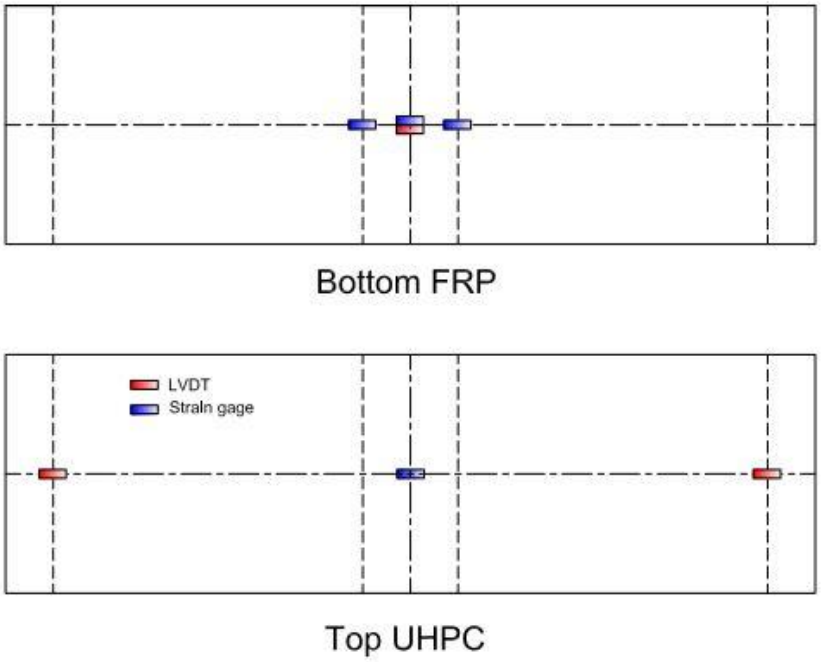

Figure 4.8 Instrumentation Plan for the Second Set

Figure 4.9 End of the Specimen after Grouting

4.4. Experimental Results

4.4.1. First Set of Specimens

Figure 4.10 shows the load-deflection responses for all specimens at the mid-span. From observing the result of these tests, it can be seen that chopped mat in the diagonal GFRP web had a significant effect on the behavior of the system. It was shown that the ultimate load for specimen #6 is 14.37 kips, while the ultimate load for the other specimen that had the same UHPC plate thickness ranged between 6.05 and 8.7 kips. The deflection at the peak load for specimen #6 is 0.48 in., while it was more for the other specimens at their peak loads.

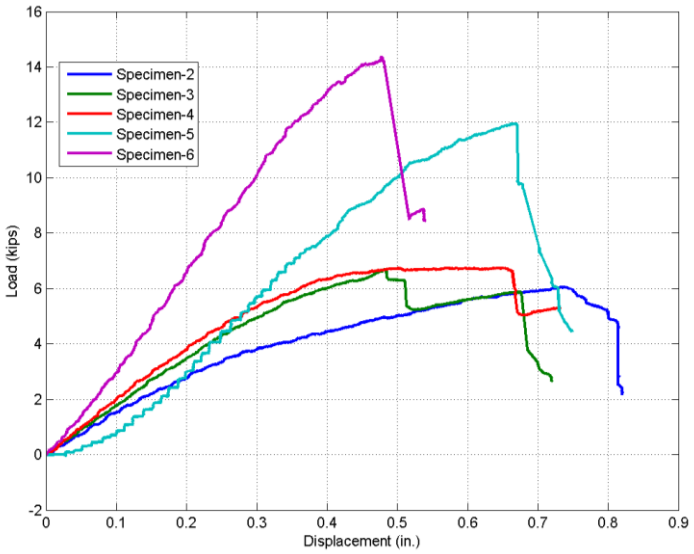

Figure 4.10 Load-Deflection Responses for the First Set

Another reason for this difference in the results is due to resin transfer inside the deck. After the test, all the specimens were cut to investigate the quality of the infusion. As shown in Figure 4.11, all the fibers in the web area (shear reinforcement) were completely dry, and resin only transferred through short distance from the edge. The exception was for specimen no. 6, where the resin transferred all the way to end due to the advantage of the chopped mat. This issue prevented load transfer from the UHPC plate to the other parts. The mode of failure as shown in Figure 4.12 was local failure due to the crushing of UHPC at the end of the loading pad or at the end of the grouting due to high shear force. Also, Figure 4.13 shows that the interface between the UHPC and top FRP was sufficient to ensure the composite action between the two materials, but the debonding failure happened between the FRP and side foam core as shown in Figure 4.14.

Figure 4.11 The FRP Cloth after Testing

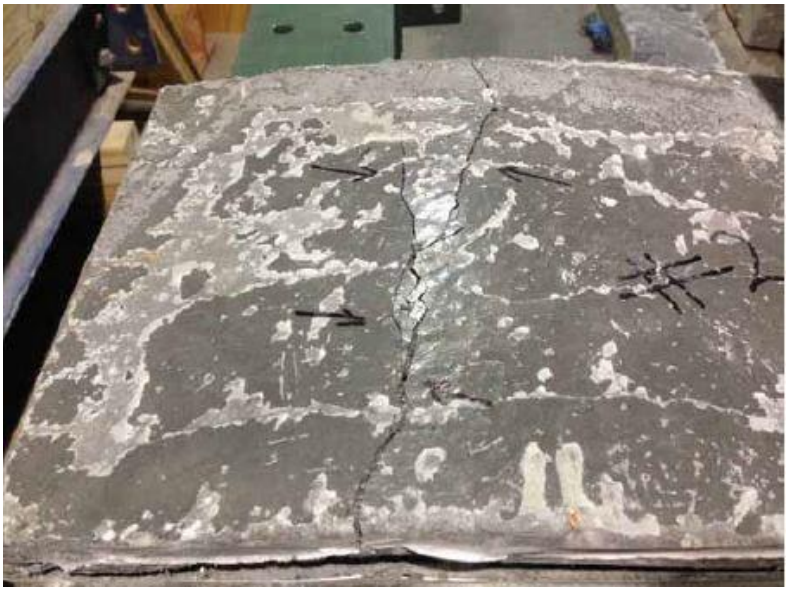

Figure 4.12 Failure Mode near the End of the Grouted Region

Figure 4.13 Bond between UHPC and Top FRP

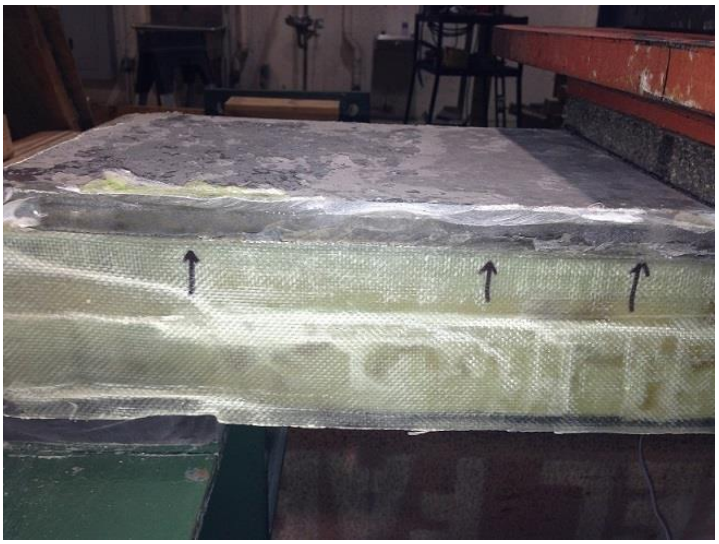

Figure 4.14 The Failure Mode near the End of the Grouted Region

Figure 4.15 and Figure 4.16 show the load-strain curve for all the specimens at UHPC plate (at the top of the specimen) and at the CFRP layer (at the bottom of the specimen). From the strain results, it can be noted that the strain at UHPC plate at the mid-span is much lower than the crushing strain of the concrete (ε_{cr} =0.0032), and the strain in bottom FRP layer is lower than the yielding strain of the carbon laminate, so the failure will be most likely interface failure or the buckling of the web.

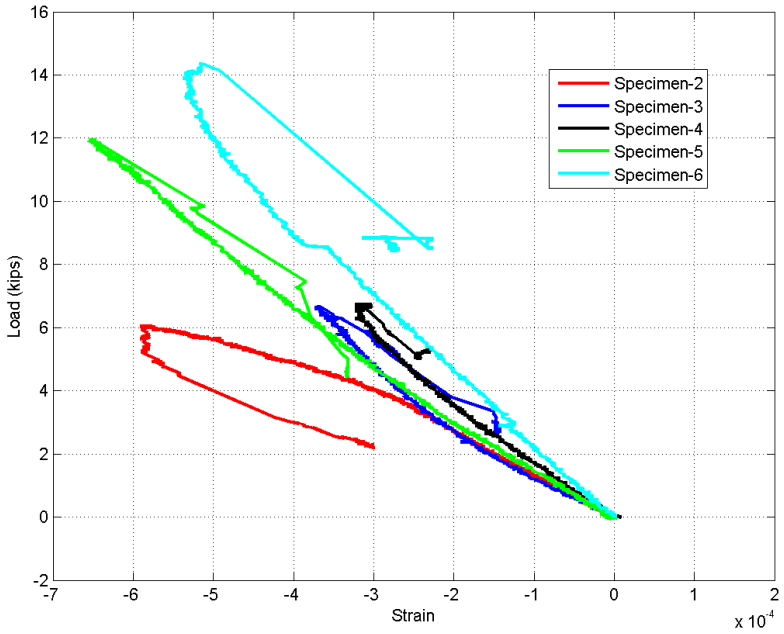

Figure 4.15 Strain at Top UHPC Plate for the First Set

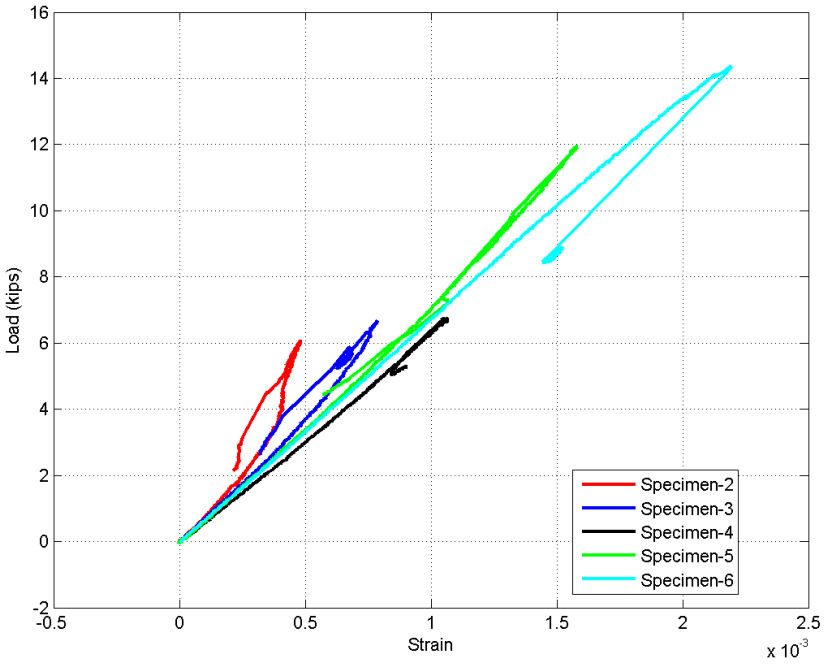

Figure 4.16 Strain at Bottom FRP for the First Set

4.4.2. Second Set of Specimens

The load-deflection curves for the second set of the lightweight system are shown in Figure 4.17. From this figure, it can be seen that both specimen no. 7 and no. 9 had a sudden drop in the load due to the initiation of the debonding at the supports. After this drop, the load began to increase again with the propagating the debonding prior to the final failure when the UHPC top plate was fully delaminated. Specimen no. 8 showed a linear behavior throughout the loading history. The maximum load was achieved with specimen no. 8 and it was around 15 kips with a 0.27 in. corresponding displacement. Also, it was observed that in this specimen the delamination occurred at the support and then propagated along the length of the specimen.

The load versus strain curves for the second set of deck at the top UHPC plate and bottom CFRP layer are shown in Figure 4.18 and Figure 4.19, respectively. From these figures, the strain results of this sets decks below the crushing strain of the UHPC and the value governing the material strength of the CFRP. The maximum compressive strains in the UHPC plate 0.0022, which is equal to about 70% of the crushing strain of the concrete (ε_{cr} = 0:0032). The tensile strains at the maximum at bottom CFRP layer for the three of deck were 0.0026, 0.0022, and 0.00255 respectively, which are more less than the ultimate strain of CFRP material (ε_u = 0.01).

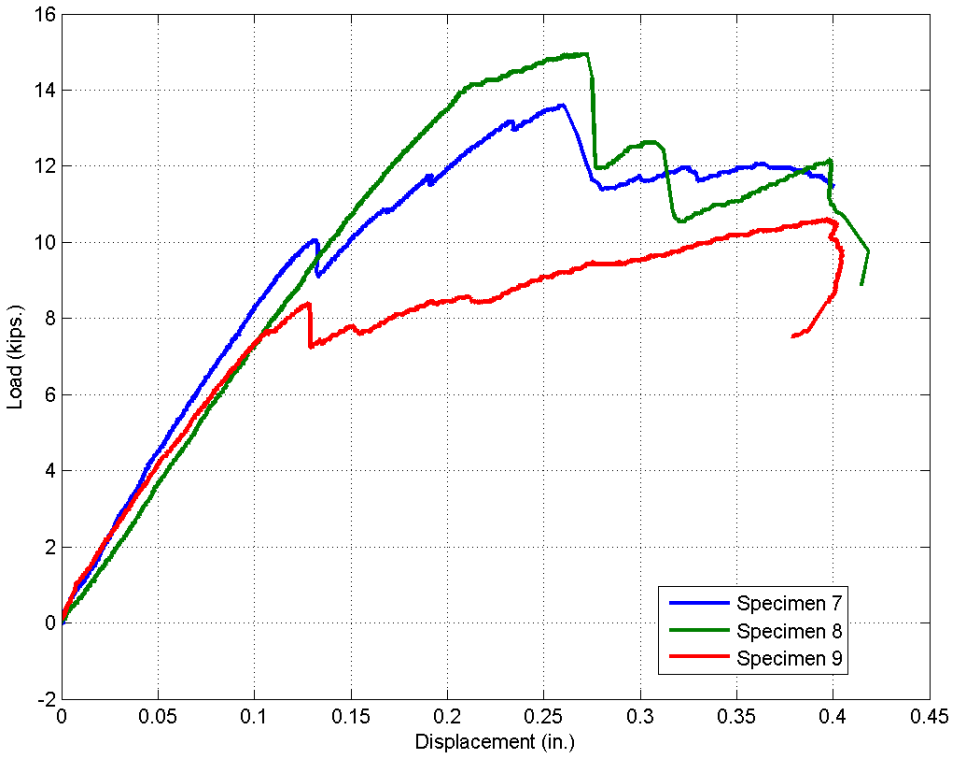

Figure 4.17 Load-Deflection Responses for the Second Set

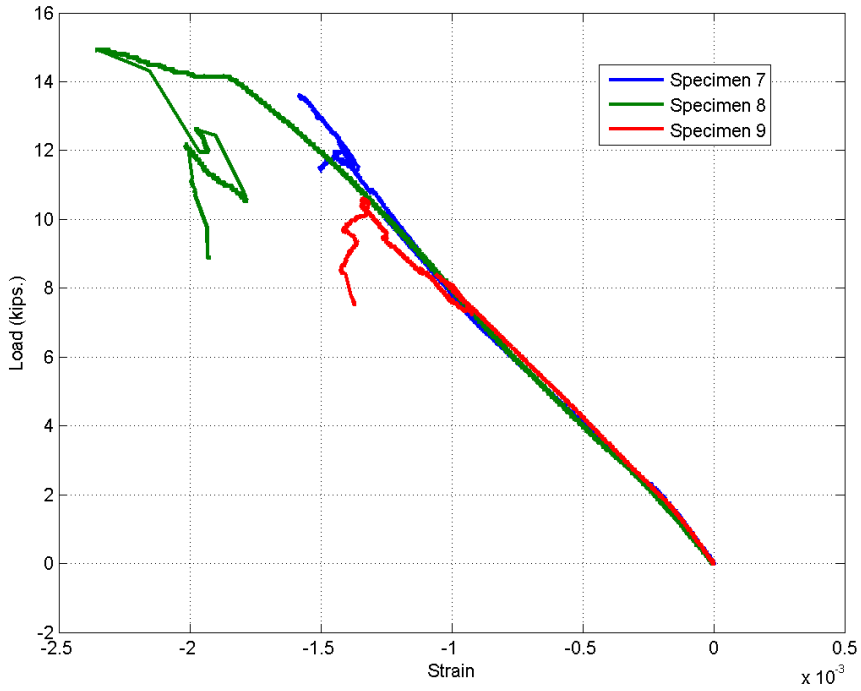

Figure 4.18 Strain at Top UHPC Plate for the Second Set

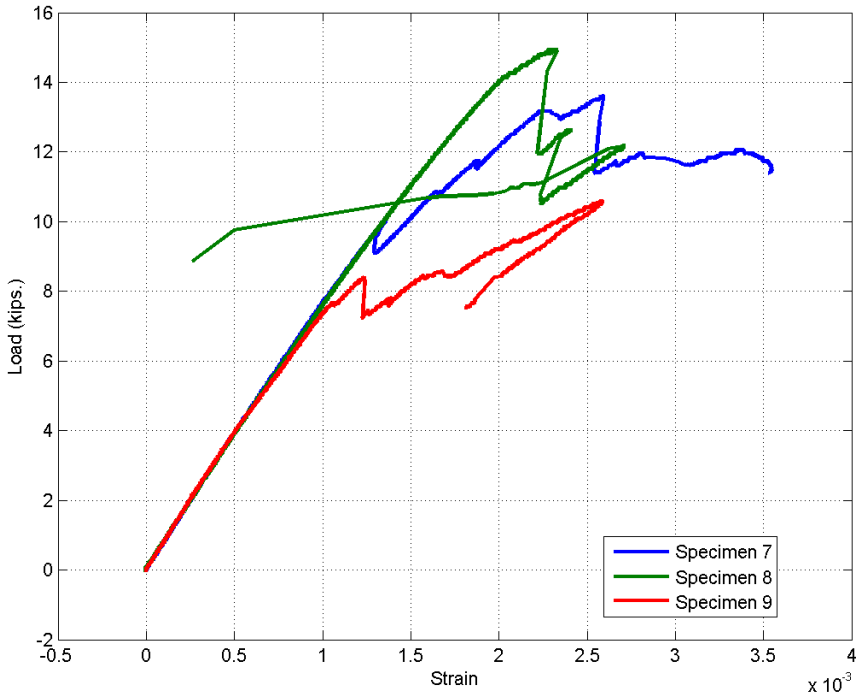

Figure 4.19 Strain at Bottom FRP for the Second Set

4.5. Comparison of Results

In order to compare the outcomes of the two sets of specimens, the results are normalized and plotted together as shown in Figure 4.20 and Figure 4.21, respectively. The specimens 2 to 6 represent the results of the first set of the hybrid specimens while the specimens 7, 8 and 9 represents the second set of the hybrid specimens. In Figure 4.20, the moment at the mid-span of the deck are scaled to the nominal moment of each deck from equilibrium analysis and plotted versus the scaled displacement, where the mid-span displacement was divided by the half length of the deck. Figure 4.21 represents the scaled load versus the scaled displacement for all hybrid specimens as well as the load for the 1T1S deck. Each load for each specimen was scaled to the demand load for each deck. As known, the demand load for the 1T1S is 16 kips, and since the hybrid specimen width (10 in.) is less than the width of the 1T1S (15 in.), the demand load for the hybrid deck was reduced by the ratio of the hybrid width/1T1S width.

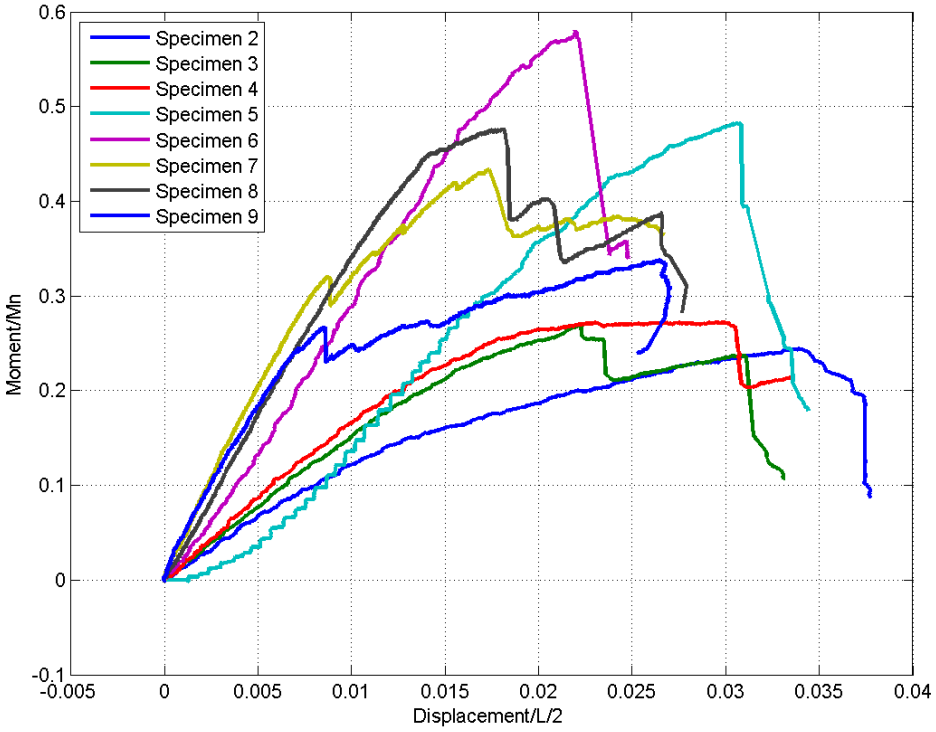

Figure 4.20 Scaled Moment-Scaled Displacement for the First and Second Set

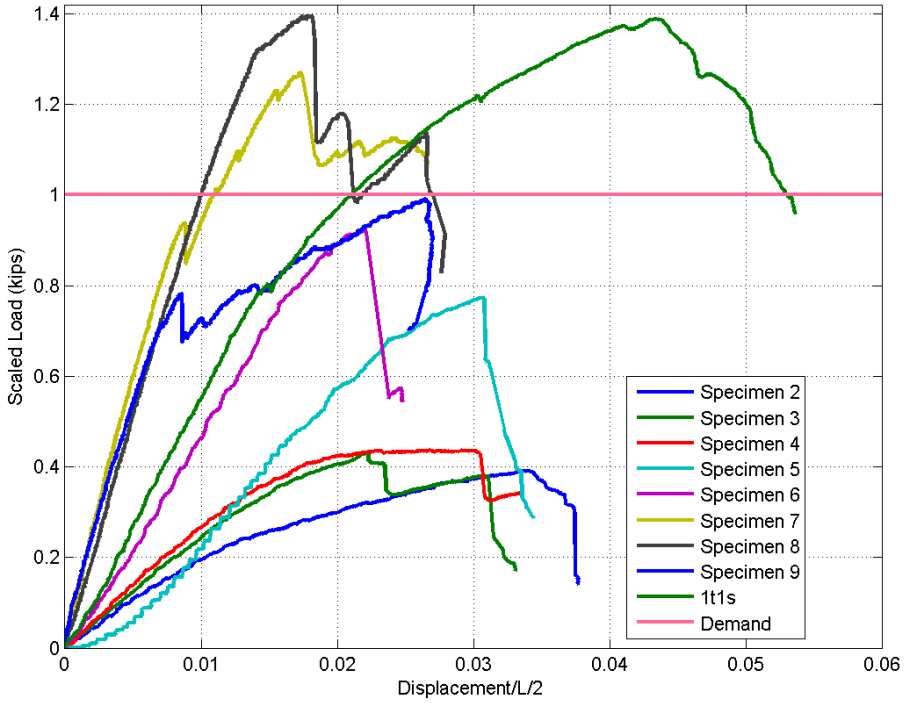

Figure 4.21 Scaled Load-Scaled Deflection for the First and Second Set

4.6. Conclusions

Test results showed that the strain at maximum load in both the UHPC and the bottom CFRP layer didn't reach the crushing strain and FRP ultimate strain respectively. So the failure mode in most cases was most likely at the interface or through buckling of the web. To enhance the bond between the UHPC and top fibers, the number of holes needs to be increased over that used previously and more longitudinal and transverse canals should be drilled to provide better bond. Moreover, different types of connections need to be considered to improve the bond between the UHPC and FRP like; mechanical connection, FRP connectors, resin beads, and more grooves and holes in UHPC.

Chapter-5

Accelerated Pavement Testing on FRP Bridge Deck System

5.1. Introduction

One of the previous decks evaluated was a composite FRP deck panel. Performance of the FRP bridge deck under static and fatigue loading testing have been evaluated in a previous phase of this research (Mirmiran et al., 2012). The deck is a composite section made of foam, GFRP layers, and polymer concrete. GFRP layers are used as shear reinforcement as well as flexural reinforcement and they are laid up in both longitudinal and transverse directions (See Figure 5.1)

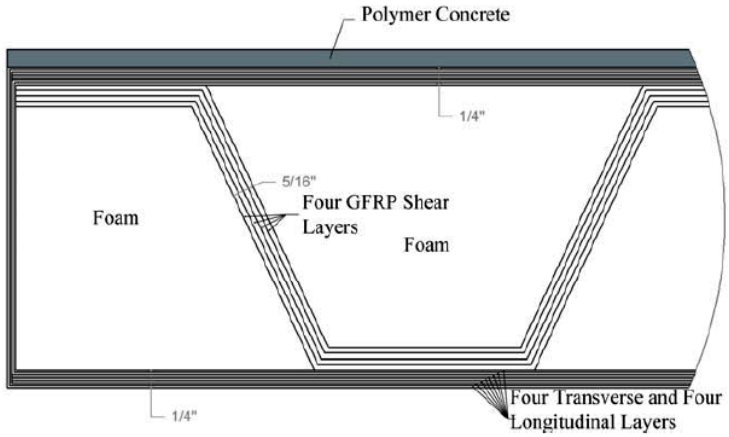

Figure 5.1 Components of the FRP Bridge Deck
(made by Structural Composite Inc.)

According to the results from previous phases (Mirmiran et al., 2012) , the FRP bridge deck met the AASHTO LRFD loading requirements under static and fatigue test and was able to withstand two million cycle of AASHTO-specified fatigue loading without any sign of damage or failure. The deflections exceeded the AASHTO criteria for deflection (i.e., L/800). In order to better understand the behavior of the deck under real traffic, the FRP composite deck was tested at the Accelerated Pavement Testing (APT) facility in Gainesville under Heavy Vehicle Simulator (HVS). The experimental work along with the results and discussion is presented.

5.2. Experimental Work

Figure 5.2 shows the 3D view of the test setup. Test setup and testing procedure were the same as 4.2.2. As seen in the figure four slabs are connected together to form a 20 ft. continuous bridge deck sitting on support beams (W10×39). Center to center of the support beams are 5 ft. and the total width of the slabs are 6 ft.

The heavy vehicle simulator applied a 15kip rolling wheel load to the specimens (See Figure 5.3 and 5.4a). Detail B presents the connections between the decks and the support beams (Figures 5.4b and 5.4c). The loading path is shown in Figure 5.5a along with the details of deck connections to the support beam in Figure 5.5b. Two types of connections including "butted epoxy joints" and "chevron epoxy joints" were used to connect the decks to each other. More details about the connections are illustrated in Figures 5.5c and 5.5d.

Figures 5.6 and 5.7 present the instrumentation plan on the slab including strain gauges and string pots. Moreover, eight strain gauges were used to measure the strain on the support beams. They were placed under the top and bottom flanges of the support beams at mid-span.

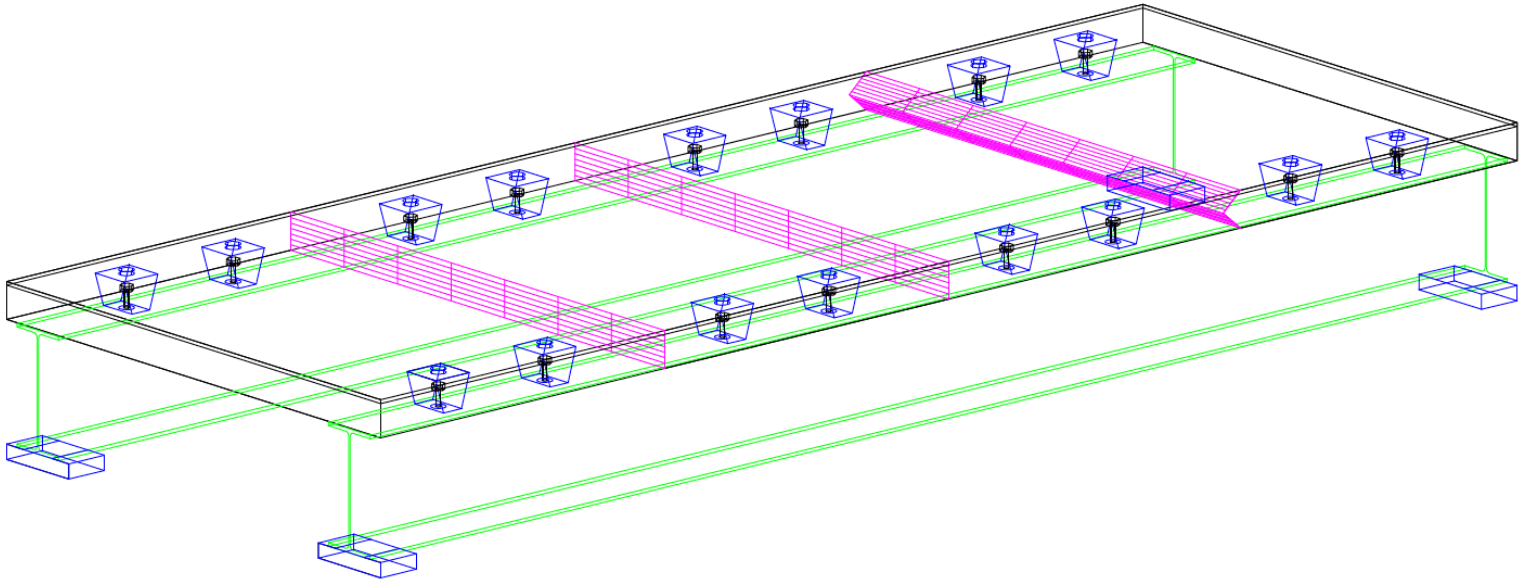

Figure 5.2 3D View of the Test Setup

Figure 5.3 HVS Machine

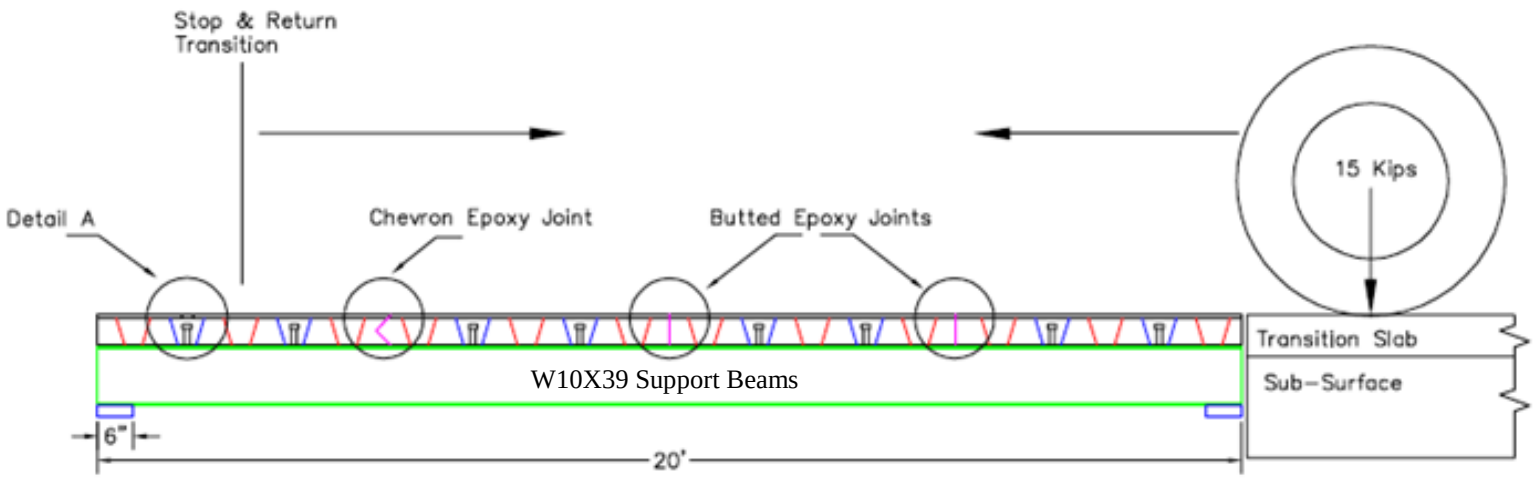

(a)

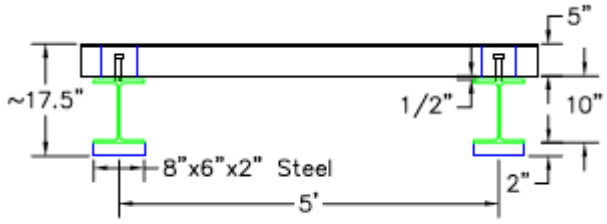

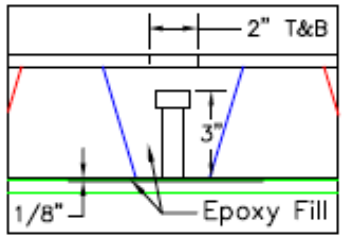

(b) (c)

Figure 5.4 Test Setup, (a) Elevation View Including Loading Plan, (b) Cross-Section View of the Test Setup, and (c) Detail A

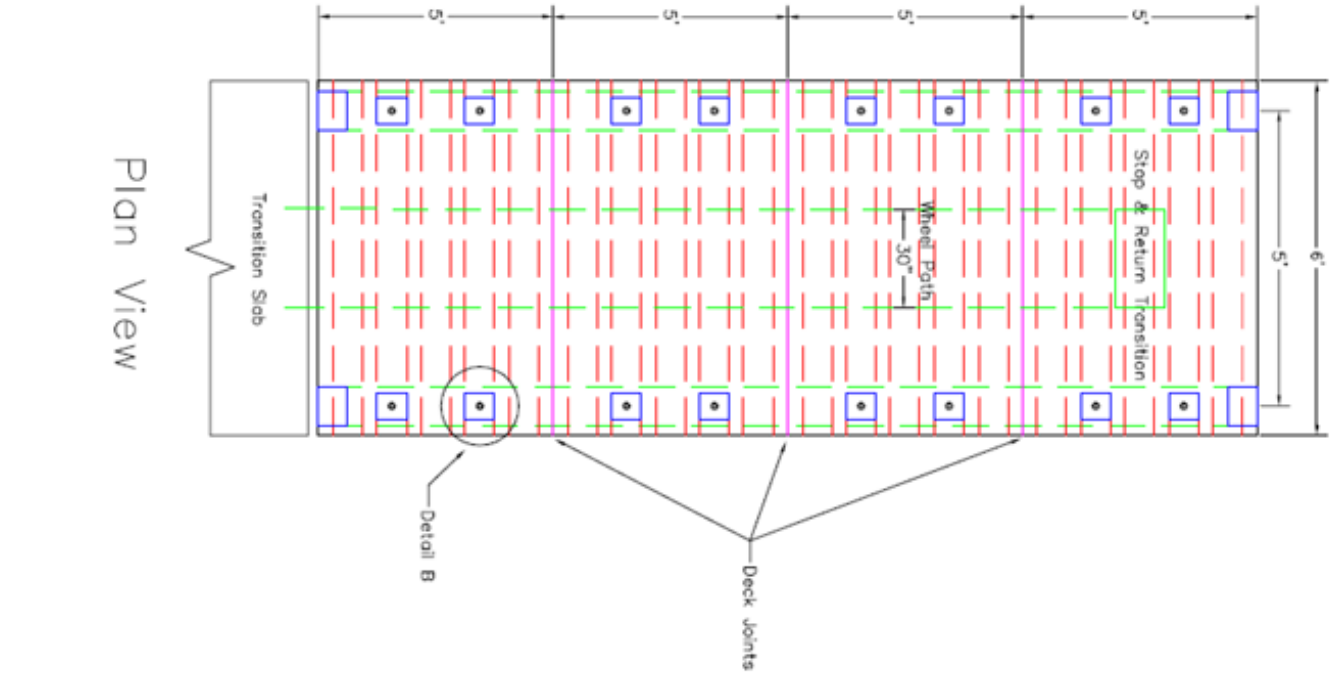

(a)

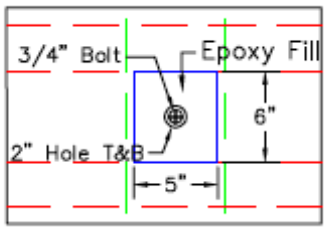

(b)

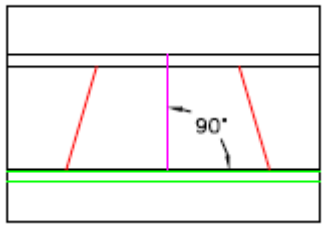

(c)

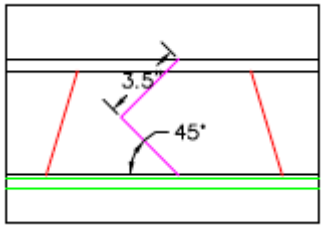

(d)

Figure 5.5 (a) Loading Path Plan, (b) Detail B, (c) Butted Epoxy, and (d) Chevron Epoxy

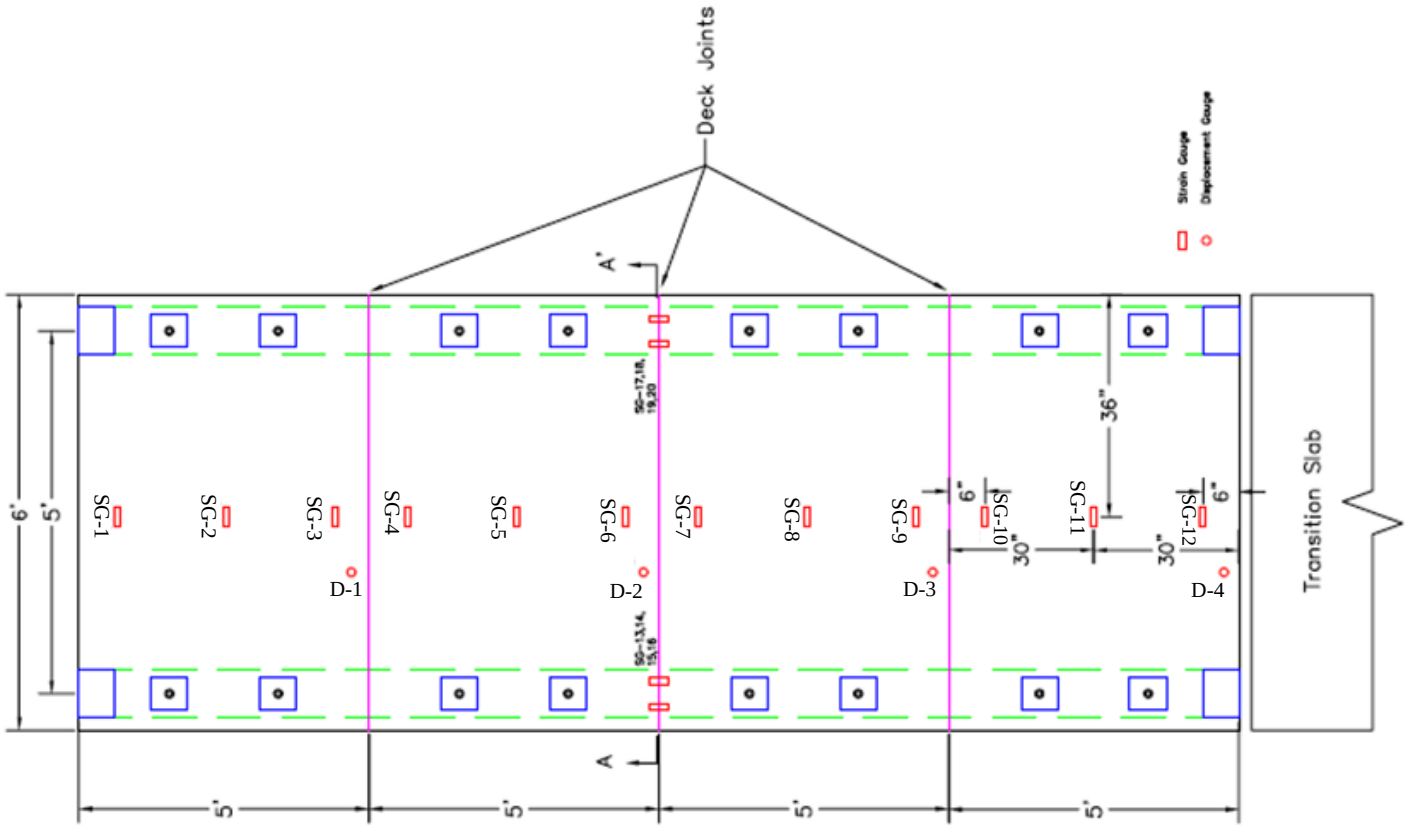

Figure 5.6 Instrumentation Plan on Decks and Support Beam

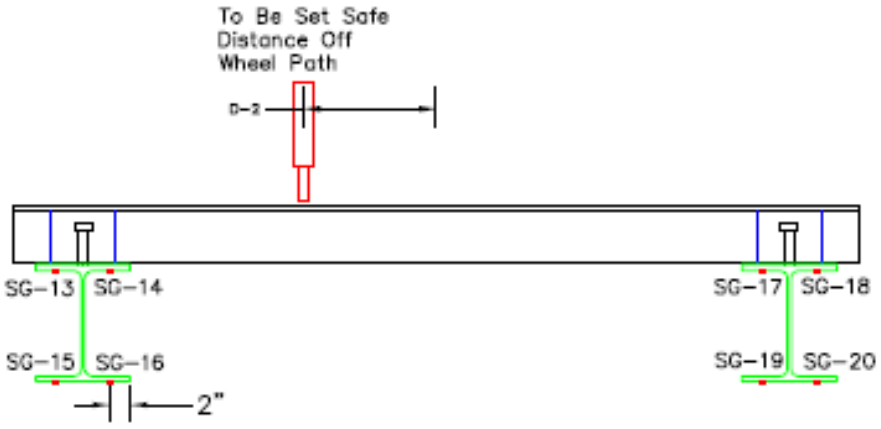

(a)

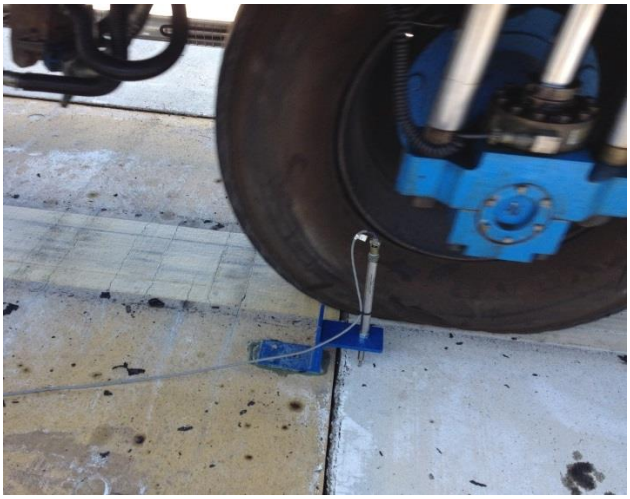

(b)

Figure 5.7 Instrumentation Plan on Decks and Support Beam (a) Strain Gauges on Support Beams, and (b) Relative Deflection Recording Device

5.3. Test Results and Discussions

Figure 5.8a shows the cracks appeared on the deck top surface. These cracks may be related to the wearing surface cracks at the early stages of the testing. Such cracks appeared at the top edge of each diagonal layer as a sign of local bending which affected the top layer. The relative deflection at the connection of the panels is shown in Figure 5.8b.

(a) (b)

Figure 5.8 Cracks (a) at Mid-Span, and (b) at the connection

Defection curves versus the number of truck passage are compared in Figure 5.9 for four panels. As seen in the figure, the deflection was constant during the test except for the beginning which may be attributed to the seating of the panels and support beams. String pot 2 shows a significant change at 150,000 passes. The shifting and significant changes in the data can be attributed to issues with the mounting of the deflection gages. The gages had to be adjusted due to the movement and method of mounting. The deflection is the edge deflection over the stringer. Deflection at the centerline of panel could not be monitored. The measured deflections for Panels 1 to 4 at the constant points are 0.51 in., 0.35 in., 0.21 in., and 0.48 in., respectively.

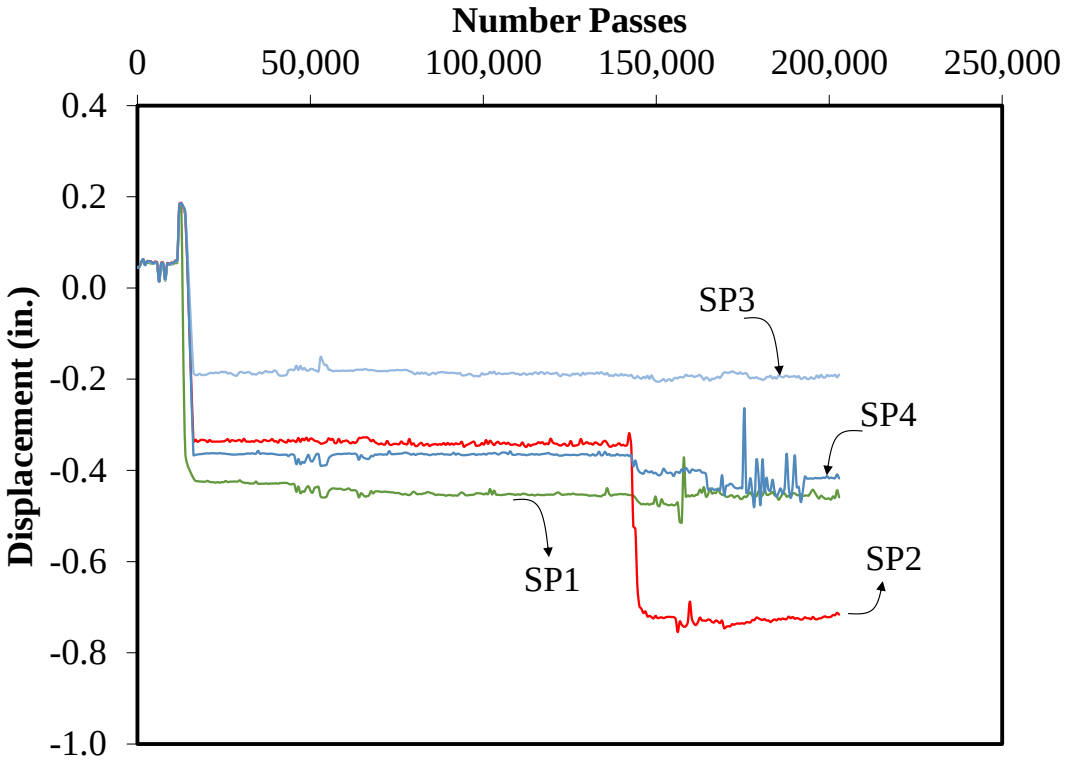

Figure 5.9 Deflections of Panels vs. the Number of Truck Passages

Surface-mounted strain gauges were installed at critical points to capture the strains. Figure 5.10 shows the strain response of the deck panels at mid-span of each panel (corresponding to SG2, SG5, SG8, and SG11 in Figure 5.6). The maximum strain recorded for SG2, SG5, SG8, and SG11 are 0.008, 0.008, 0.008, and 0.007, respectively.

Figure 5.11 shows the strain response for the instruments attached to next to the connections which recorded the same results as the strain gauges at mid-span (corresponding to SG3, SG4, SG6, SG7, SG 9 and SG11 in Figure 5.6). SG1 and SG12 and the strain gauges on the top and bottom flanges did not show any reasonable results. The responses curves are shown in Appendix C.

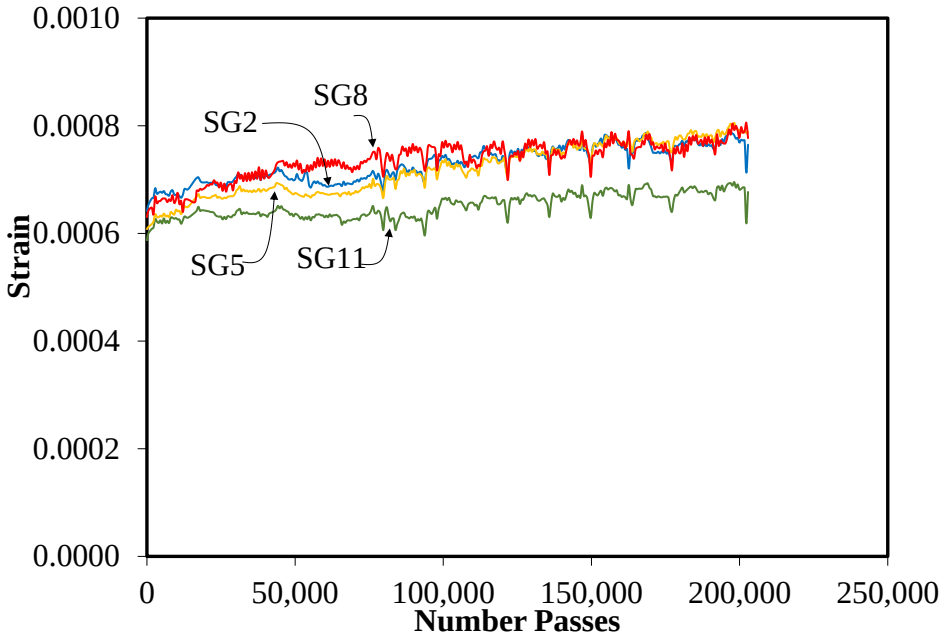

Figure 5.10 Strain Responses at Mid-Span of Each Panel

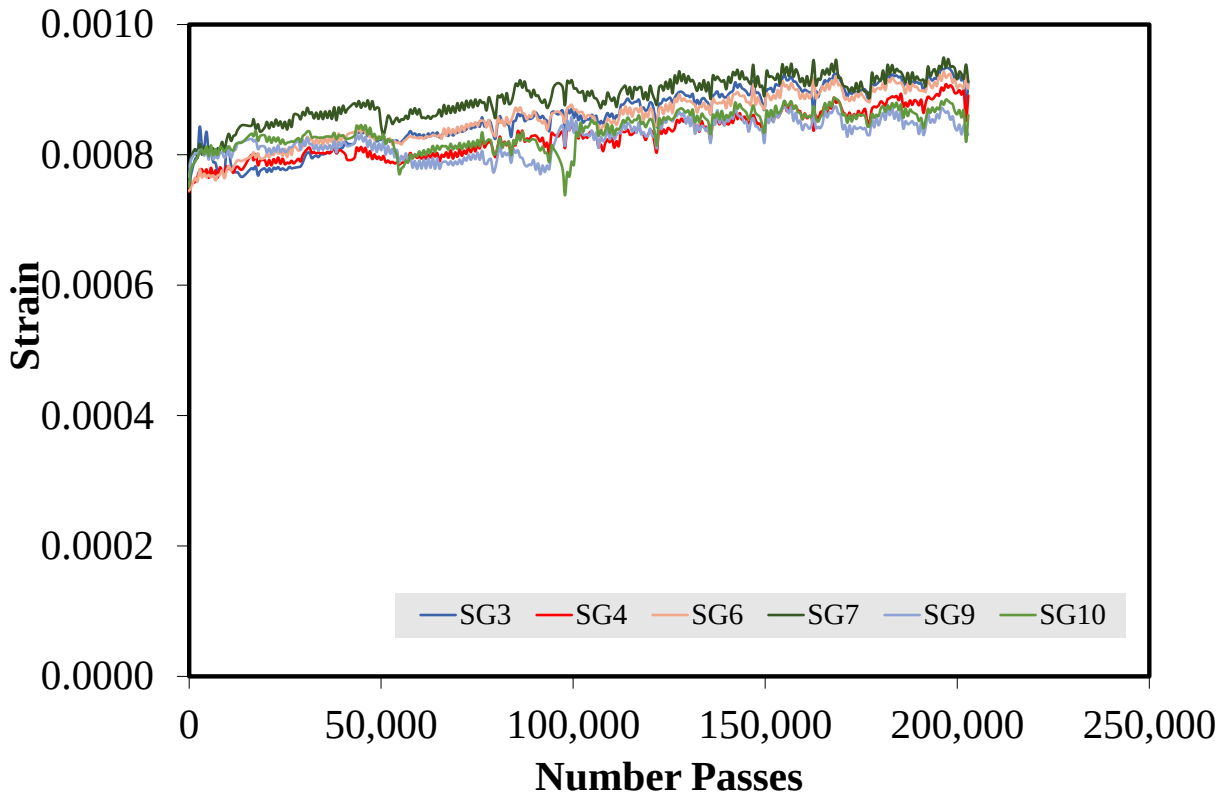

Figure 5.11 Strain Responses next to the Connection Sections

Figure 5.12 shows the maximum and minimum temperature of the top and bottom of the bridge decks. As seen in the Figures the mean temperatures at all locations were steady during the testing period, except for the minimum temperature at the bottom of the deck on Day 10, which could be attributed to a faulty gage given the magnitude of the values.

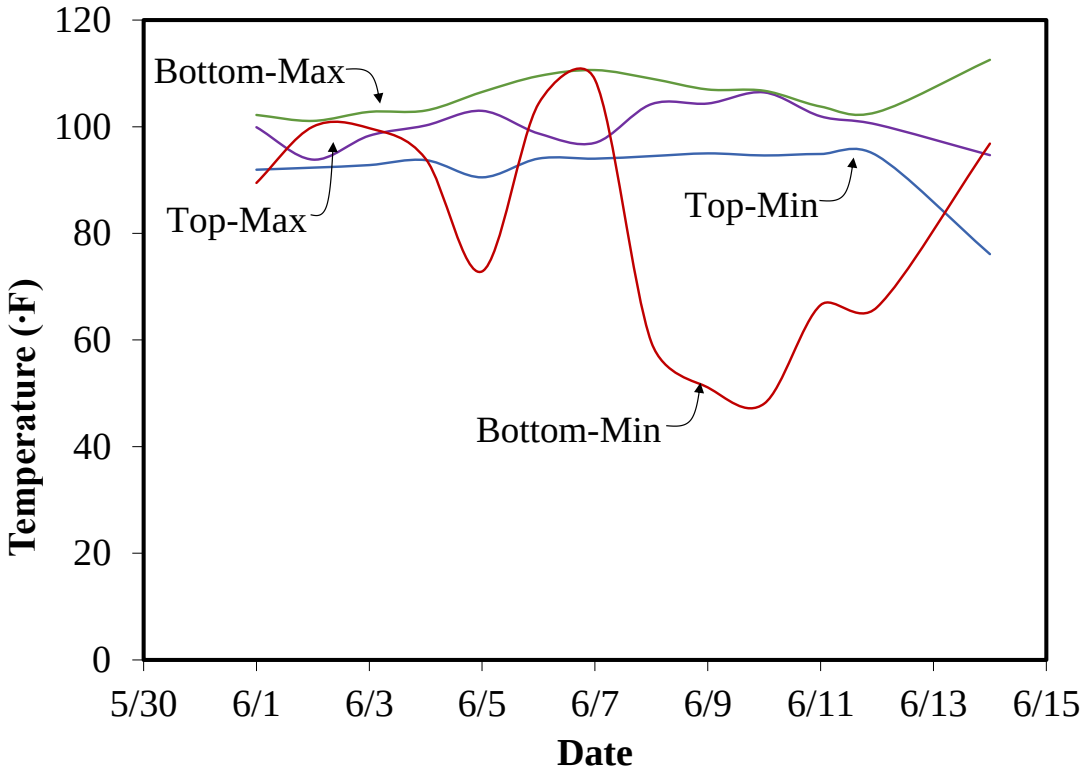

Figure 5.12 Maximum and Minimum Temperature of the FRP Deck

5.4. Conclusions

A detailed evaluation on cyclic loading under HVS was conducted on FRP composite bridge deck. According to the test results, the FRP bridge decks met the AASHTO LRFD strength and loading requirement. However, according to previous studies, the deflection of the bridge deck turned out to be greater than the allowable deflection by standard (L/800) which suggests an improvement may be necessary for the deck system. Moreover, the cracks on the top of the panels create serious concerns such as wearing surface delamination, moisture intrusion, etc. The panel-to-panel and panel-to-stringer connections performed well under wheel load testing.

Chapter-6

Summary and Conclusion

The main objective of this research was to develop lightweight solid deck alternatives for movable bridges. The alternatives should meet the AASHTO LRFD loading and serviceability requirements while satisfying 21 psf self-weight requirements. Five different bridge deck systems were considered for this purpose, including UHPC waffle deck with HSS reinforcement, UHPC waffle deck with CFRP reinforcement, UHPC-FRP hybrid deck, and FRP composite deck. Detailed experimental and analytical evaluation of these systems led to the following conclusions and recommendations.

6.1. UHPC-HSS Bridge Deck System

Detailed component and ancillary tests were carried out to evaluated UHPC waffle deck with HSS reinforcement in three phases. The results led to the following conclusions:

1. The system showed viability to serve as an alternative for light-weight bridge decks. It was shown by the experimental and analytical evaluations that the system meets the load requirements.
2. The dominant mode of failure was beam shear cracks. The cracks initiated on the web near the supports and propagated toward the slab which eventually resulted in load drop and final failure.
3. The main bar in the longitudinal ribs yielded in the single-rib simple-span specimens, but not in the two-span or multi-rib specimens.
4. No sign of punching shear failure was observed in any of the optimized deck panels for the 4-ft. spacing of the stringers. The punching observed in the panels with a 5-ft. span was addressed by increasing the thickness of the flange.
5. In regards to load distribution among primary ribs, the middle rib takes 33% of the load, while each of the adjacent ribs take 22% and 11% of the load.

6.2. UHPC-CFRP Bridge Deck System

Similar studies were carried out on UHPC-CFRP bridge deck system in three phases. The results can be summarized as follows:

1. The system showed its capability to work as an alternative for light-weight bridge decks by satisfying load requirements. Additional work is needed to address the displacement control for the UHPC-CFRP bridge deck system.
2. The dominant mode of failure for all but the first four specimens was beam shear cracks. The cracks started on the web next to the supports and widened and propagated toward the slab; resulting the eventual failure and significant load drops. In the first four specimens, the anchorage system was with GFRP wrap impregnated in epoxy resin, and did not provide adequate anchorage against bar slippage. As such, shear cracks in those specimens began at the mid-point between supports and edge of loading pad and propagated toward the loading pad.
3. Performance for punching shear was quite similar to the decks with HSS reinforcement.
4. Load distribution among primary ribs was similar to the decks with HSS reinforcement.
5. Test results of APT reveals that minor cracking in the top surface of the UHPC deck was observed. Except for the minor cracking, the UHPC deck panels performed well under the APT testing. The change in the strain and deflection was minor throughout the duration of testing and behaved within expected levels based on the prior static testing.

6.3. UHPC-FRP Hybrid Bridge Deck System

A lightweight UHPC-FRP hybrid system was fabricated using vacuum-VARTM infusion in two phases. Analytical and experimental test results can be summarized as below:

1. Except for the first three specimens, the system satisfied the load and displacement requirements. This substandard performance of the first three specimens was attributed to their fabrication process.
2. The dominant mode of failure was either at the interface of FRP and UHPC, or through buckling of the FRP web.
3. At the end of first phase, all specimens were cut to investigate the quality of the infusion. All fibers in web area were completely dry and resin only transferred through a short distance from the edge. The exception was for Specimen No. 6 due to the advantage of the chopped mat. This issue was solved in the second phase of the tests.

Although the UHPC-FRP composite system seems to be very promising, the following additional work is needed for improving the bond between the UHPC and top fibers layers:

1. Additional indentations are needed in the UHPC slab to accommodate a better bond with FRP.
2. Different types of connections such as mechanical, FRP connectors, and resin beads need to be considered.

6.4. FRP Composite Bridge Deck System

Similar to the results obtained from static and fatigue tests on FRP composite deck system in the previous phases of this research study, the deck system satisfied the AASHTO LRFD loading requirements, but in the previous study failed the deflection criteria. Cracking was observed above the webs in the wearing surface of the panels. However, as mentioned earlier, these cracks are related to the wearing surface weaknesses. The panel-to-panel and panel–to-stringer connections performed well.

REFERENCES

Aaleti, S., and Sritharan, S. (2014). Design of ultrahigh-performance concrete waffle deck for accelerated bridge construction. *Transportation Research Record: Journal of the Transportation Research Board*, *2406*(1), 12-22.

Aaleti, S., Sritharan, S., Bierwagen, D., and Wipf, T. (2011). Structural Behavior of Waffle Bridge Deck Panels and Connections of Precast Ultra-High-Performance Concrete: Experimental Evaluation. *Transportation Research Record: Journal of the Transportation Research Board*, (2251), 82-92.

AASHTO. (2013). *Bridge design specifications*. American Association of State Highway and Transportation Officials. Washington, D.C.

ACI 408-R03. (2003). Bond and development of straight reinforcing bars in tension. *American concrete institute*. Farmington Hills, MI.

Ahlborn, T. M., Peuse, E. J., & Misson, D. L. (2008). Ultra-high-performance-concrete for michigan bridges material performance–phase I.

Alagusundaramoorthy, P., Harik, I., & Choo, C. (2006). Structural behavior of FRP composite bridge deck panels. *Journal of Bridge Engineering*, *11*(4), 384-393.

Alnahhal, W. I., Chiewanichakorn, M., Aref, A. J., & Alampalli, S. (2006). Temporal thermal behavior and damage simulations of FRP deck. *Journal of Bridge Engineering*, *11*(4), 452-464.

ASCE. (2013). Report card for America's infrastructure. American society of civil engineers. Reston, VA.

ASTM Standard D7205/D7205M. (2011). *Standard test method for tensile properties of fiber reinforced polymer matrix composite bars*. ASTM International, West Conshohocken, PA.

Blais, P. Y., and Couture, M. (1999). Precast, prestressed pedestrian bridge-world's first reactive powder concrete structure. *PCI Journal*, *44*, 60-71.

Chajes, M. J., Finch Jr, W. W., Januszka, T. F., and Thomson Jr, T. A. (1996). Bond and force transfer of composite-material plates bonded to concrete. *ACI Structural Journal*, *93*(2).

Chakrabortty, A., Khennane, A., Kayali, O., & Morozov, E. (2011). Performance of outside filament-wound hybrid FRP-concrete beams. *Composites Part B: Engineering*, *42*(4), 907-915.

Chen, D., and El-Hacha, R. (2011). Behaviour of hybrid FRP–UHPC beams in flexure under fatigue loading. *Composite Structures*, *94*(1), 253-266.

Cole, T. A., Lopez, M., and Ziehl, P. H. (2006). Fatigue behavior and nondestructive evaluation of full-scale FRP honeycomb bridge specimen. *Journal of Bridge Engineering*, *11*(4), 420-429.

Culmo, M. P. (2011). Accelerated Bridge Construction-Experience in Design, Fabrication and Erection of Prefabricated Bridge Elements and Systems (No. FHWA-HIF-12-013).

Davalos, J. F., Chen, A., and Zou, B. (2010). Stiffness and strength evaluations of a shear connection system for FRP bridge decks to steel girders. *Journal of Composites for Construction*, *15*(3), 441-450.

Davalos, J. F., and Chen, A. (2005). Buckling behavior of honeycomb FRP core with partially restrained loaded edges under out-of-plane compression. *Journal of Composite Materials*, *39*(16), 1465-1485.

Davalos, J. F., Qiao, P., Xu, X. F., Robinson, J., and Barth, K. E. (2001). Modeling and characterization of fiber-reinforced plastic honeycomb sandwich panels for highway bridge applications. *Composite Structures*, *52*(3), 441-452.

Elmahdy, A., El-Hacha, R., and Shrive, N. (2007). Bonding of CFRP and SRP to Ultra-High Performance Concrete. *Proceedings of the First Asia-Pacific Conference on FRP in Structures (APFIS 2007)*.

Frostlechner, F.X. (2012). Composite Structures Made of Ultra-High Performance Concrete and Fiber-Reinforced Polymers. *Proceedings of the 9th fib International PhD Symposium in Civil Engineering*, Karlsruhe Institute of Technology (KIT), Karlsruhe, Germany

Ghasemi, S., Mirmiran, A., Xiao, Y., and Mackie, K. (2015). Novel UHPC-CFRP Waffle Deck Panel System for Accelerated Bridge Construction. *Journal of Composites for Construction*, 04015042.

Ghasemi, S. (2015). Innovative Modular High Performance Lightweight Decks for Accelerated Bridge Construction. PhD Dissertation, Florida International University.

Graybeal, B. (2011). *Ultra-high performance concrete* (No. FHWA-HRT-11-038).

Graybeal, B. A. (2007). Compressive behavior of ultra-high-performance fiber-reinforced concrete. *ACI Materials Journal*, *104*(2).

Graybeal, B. A. (2006). *Structural behavior of ultra-high performance concrete prestressed I-girders* (No. FHWA–HRT–06–115).

Graybeal, B. A. (2005). Characterization of the behavior of ultra-high performance concrete. PhD Dissertation. University of Maryland.

Graybeal, B. A., & Hartmann, J. L. (2003, October). Strength and durability of ultra-high performance concrete. In *Concrete Bridge Conference, Portland Cement Association.*

Habel, K., Viviani, M., Denarié, E., and Brühwiler, E. (2006). Development of the mechanical properties of an ultra-high performance fiber reinforced concrete (UHPFRC). *Cement and Concrete Research*, *36*(7), 1362-1370.

Hajar, Z.; Simon, A.; Lecointre, D.; and Petitjean, J. (2004) Design and Construction of the world first Ultra-High Performance road bridges. *Proceedings of the International Symposium on Ultra High Performance Concrete*, Kassel University Press, Kassel, Germany, pp 39-48

Harris, D. K., and Roberts-Wollmann, C. L. (2005). *Characterization of the punching shear capacity of thin ultra-high performance concrete slabs* (Virginia Department of Transportation. Report VTRC 05-CR26) Virginia Tech, Blacksburg, Virginia.

Heimann, J. (2013). *The Implementation of Full Depth UHPC Waffle Bridge Deck Panels*: Final Report (No. FHWA-HIF-13-031).

Horiguchi, T., and Saeki, N. (1997). Effect of test methods and quality of concrete on bond strength of CFRP sheet. *Non-Metallic (FRP) Reinforcement for Concrete Structures*, *1*, 265-270.

Hughes Brothers. (2011). Carbon fiber reinforced polymers (CFRP) bar - Aslan™ 200 Series. Seward, NE. http://www.hughesbros.com/

Kahl, S. (2007). Corrosion Resistant Alloy Steel (MMFX) Reinforcing Bar in Bridge Decks. Transportation Research Board (Vol. 1499).

Keierleber, B., Phares, B., Bierwagen, D., Couture, I., and Fanous, F. (2007). *Design of Buchanan County, Iowa, Bridge Using Ultra High Performance Concrete and PI Girders.* Proceedings of the 2007 Mid-Continent Transportation Research Symposium, Ames, IA.

Keller, T., and Gürtler, H. (2005). Composite action and adhesive bond between fiber-reinforced polymer bridge decks and main girders. *Journal of Composites for Construction*, *9*(4), 360-368.

Kumar, P., Chandrashekhara, K., and Nanni, A. (2004). Structural performance of a FRP bridge deck. *Construction and Building Materials*, *18*(1), 35-47.

Mirmiran, A., Mackie, K., Saleem, M. A., Xia, J., Zohrevand, P., and Xiao, Y. (2012). *Alternatives to Steel Grid Decks-Phase II* (Florida Department of Transportation Research) Florida International University, Miami, Florida.

Mirmiran, A., Saleem, M. A., Mackie, K., and Xia, J. (2009). *Alternatives to steel grid decks.* (Florida Department of Transportation Research) Florida International University, Miami, Florida.

Mu, B., Wu, H., Yan, A., Warnemuende, K., Fu, G., Gibson, R. F., et al. (2006). FEA of complex bridge system with FRP composite deck. *Journal of Composites for Construction*, *10*(1), 79-86.

Nakaba, K., Kanakubo, T., Furuta, T., and Yoshizawa, H. (2001). Bond behavior between fiber-reinforced polymer laminates and concrete. *ACI Structural Journal*, *98*(3).

Righman, J., Barth, K., and Davalos, J. (2004). Development of an efficient connector system for fiber reinforced polymer bridge decks to steel girders. *Journal of Composites for Construction*, *8*(4), 279-288.

Rizkalla, S., El-Hacha, R., and Elagroudy, H. (2006). Bond characteristics of high-strength steel reinforcement. *ACI Structural Journal*, *103*(6).

Robinson, M., and Kosmatka, J. (2008). Light-weight fiber-reinforced polymer composite deck panels for extreme applications. *Journal of Composites for Construction*, *12*(3), 344-354.

Schesser, D., Yang, Q., Nanni, A., and Giancaspro, J. (2013). Expansive Grout-Based Gripping Systems for Tensile Testing of Large-Diameter Composite Bars. *Journal of Materials in Civil Engineering*, *26*(2), 250-258.

Saleem, M. A., Mirmiran, A., Xia, J., and Mackie, K. (2012). Development length of high-strength steel rebar in ultrahigh performance concrete. *Journal of Materials in Civil Engineering*, *25*(8), 991-998.

Saleem, M. A. (2011). *Alternatives to steel grid bridge decks*. PhD. Dissertation, Florida International University.

Saleem, M. A., Mirmiran, A., Xia, J., and Mackie, K. (2011). Ultra-high-performance concrete bridge deck reinforced with high-strength steel. *ACI Structural Journal*, *108*(5).

Scott, D. W., Lai, J. S., and Zureick, A. (1995). Creep behavior of fiber-reinforced polymeric composites: a review of the technical literature. *Journal of Reinforced Plastics and Composites*, *14*(6), 588-617.

Shann, S. V. (2012). Application of ultra high performance concrete (UHPC) as a thin-bonded overlay for concrete bridge decks. Master Dissertation, Michigan tech.

Williams, B., Shehata, E., and Rizkalla, S. H. (2003). Filament-wound glass fiber reinforced polymer bridge deck modules. *Journal of Composites for Construction*, *7*(3), 266-273.

Wu, H., Mu, B., and Warnemuende, K. (2003). Failure analysis of FRP sandwich bus panels by finite element method. *Composites Part B: Engineering*, *34*(1), 51-58.

Wu, Z., Mirmiran, A., and Swanson, J. (2004). Fatigue behavior of prestressed tubular bridge deck of fiber-reinforced polymer. *Transportation Research Record: Journal of the Transportation Research Board*, (1892), 246-255.

Xia, J., Mackie, K. R., Saleem, M. A., and Mirmiran, A. (2011). Shear failure analysis on ultra-high performance concrete beams reinforced with high strength steel. *Engineering Structures*, *33*(12), 3597-3609.

Yoshizawa, H., Myojo, T., Okoshi, M., Mizukoshi, M., & Kliger, H. S. (1996, November). Effect of sheet bonding condition on concrete members having externally bonded carbon fiber sheet. In *Materials for the New Millennium*(pp. 1608-1616). ASCE.

Appendix A. Additional Test Results for UHPC-HSS Deck System

Figure A.1 Strain Gauge Attached to the Top Surface of the UHPC (Specimen 1T1S)

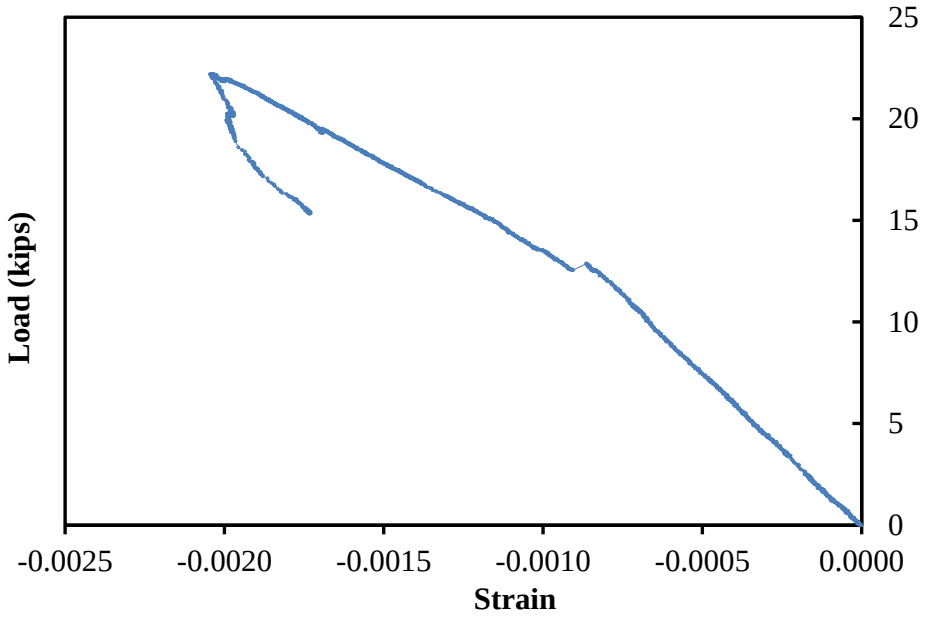

Figure A.2 Load-Strain Responses of Strain Attached to the Top Surface (Specimen 1T1S)

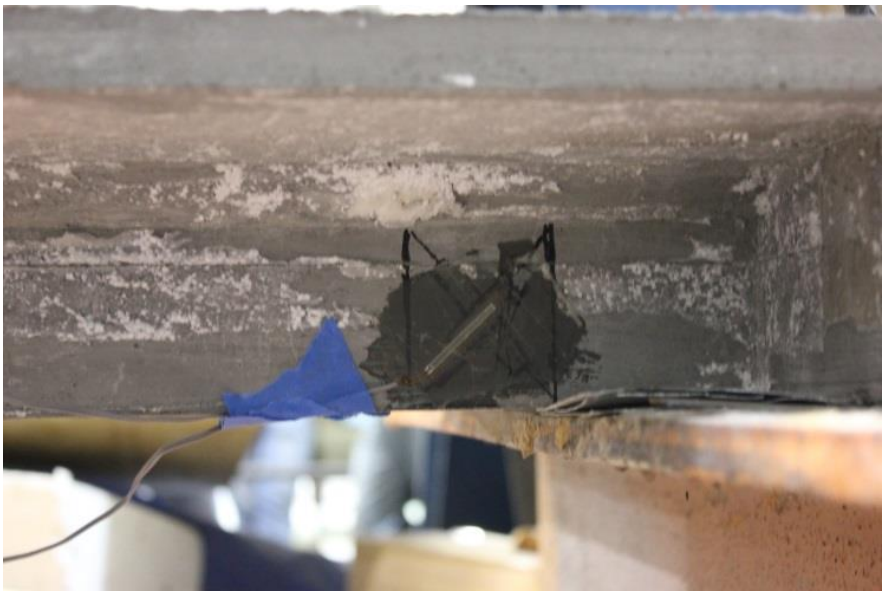

Figure A.3 Strain Gauge Attached to the Web (Specimen 1T1S)

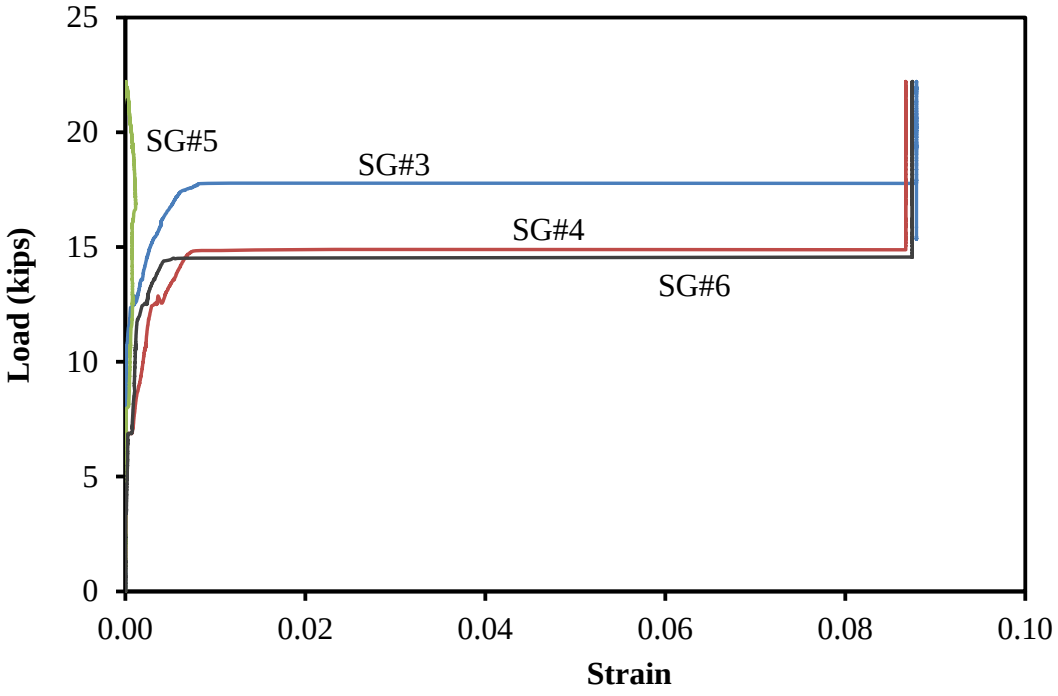

Figure A.4 Load-Strain Responses of Strain Attached to the Web (Specimen 1T1S

Appendix B. Additional Test Results for UHPC-CFRP Deck System

Figure B.1 Strain Gauge Attached to the Web (Specimen 1T1S)

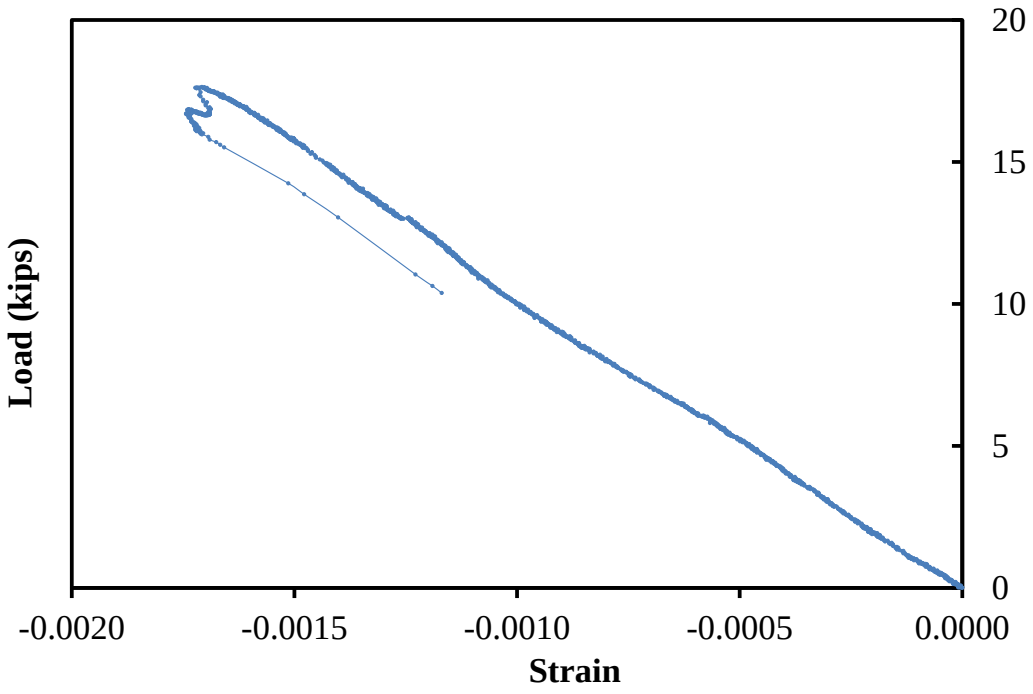

Figure B.2 Load-Strain Responses of Strain Attached to the Web (Specimen 1T1S)

Appendix C. Additional HVS Test Results for FRP Composite Deck

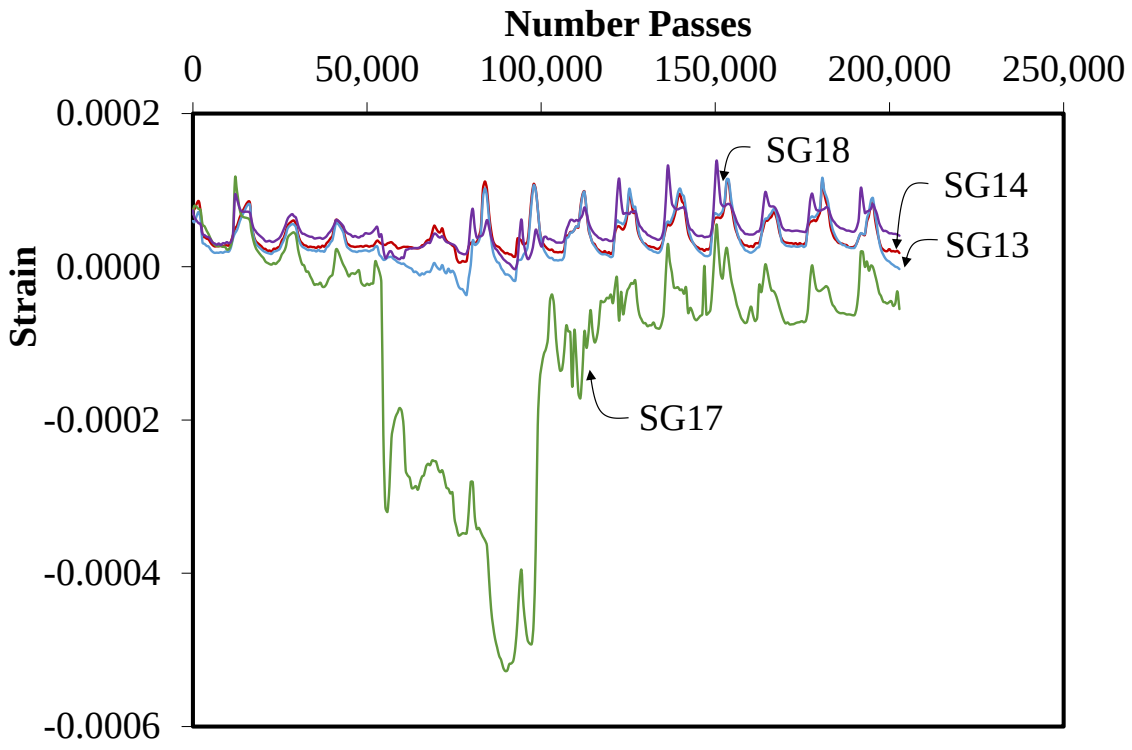

Figure C.1 Strain Responses of the Strain Gauges Attached to Top Flange

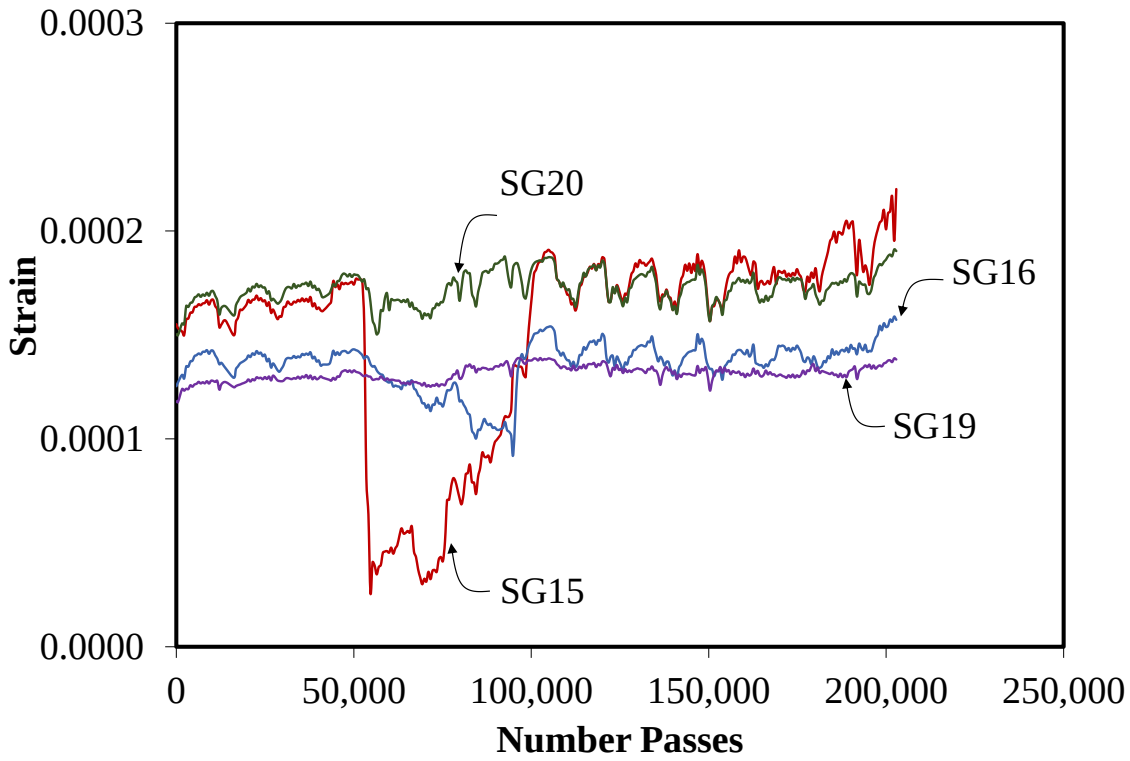

Figure C.2 Strain Responses of the Strain Gauges Attached to Bottom Flange

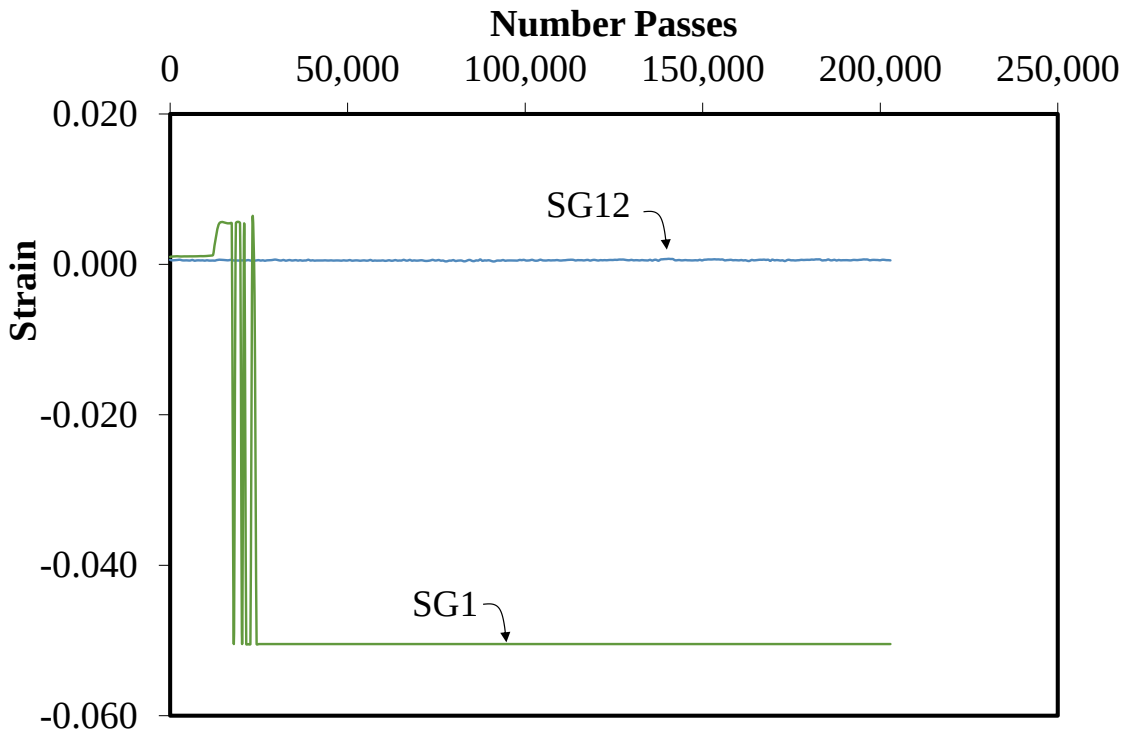

Figure C.3 Strain Responses for SG1 and SG12